Sorptive Removal of Per- and Polyfluoroalkyl Substances (PFAS) from Water by Biochars

by

Samuel Allen Krebsbach

A thesis submitted to the Graduate Faculty of
Auburn University
in partial fulfillment of
the requirements for the degree of
Master of Science

Auburn, Alabama
May 6, 2023

Keywords: Per- and polyfluoroalkyl substances (PFAS), biochars, physiochemical properties, structural equation modeling, groundwater, environmental factors

Approved by

Dr. Dengjun Wang, Chair, Assistant Professor, School of Fisheries, Aquaculture and Aquatic Sciences, Auburn University.

Dr. Ann Ojeda, Committee Member, Assistant Professor, Department of Geosciences, Auburn University.

Dr. Dongye Zhao, Committee Member, Professor, Department of Civil, Construction and Environmental Engineering, San Diego State University.

Abstract

This thesis aims to employ biochar (a carbonaceous material) as a cost-effective sorbent to remove per- and polyfluoroalkyl substance (PFAS) from water by two case studies. Study 1 seeks to identify which biochars perform better for the sorption of perfluorooctane sulfonate (PFOS) from water, and which physicochemical properties of biochars control PFOS sorption. The biochars with higher sorptive capacity of PFOS are further tested in Study 2 to investigate how these biochars perform at environmentally relevant conditions (e.g., pH, salt, and natural organic matter) for the sorption of PFOS and other C4-C8 PFAS compounds. Biochars produced from Douglas fir and poplar feedstocks exhibit high PFOS sorption efficiency. Biochar properties such as specific surface area, pore diameter, pore diameter/pore volume ratio, and hydrophobicity play important roles for PFOS sorption. Salt promotes PFAS sorption, while natural organic matter decreases PFAS sorption mainly due to the competition of sorption sites of biochars.

Acknowledgments

I would like to thank my advisor Dr. Dengjun Wang for his long-term guidance and support of this thesis over the past two years. I would also like to thank my committee members Dr. Ann Ojeda and Dr. Dongye (Don) Zhao for their support and feedback on the guidance of this thesis, along with data discussion during various committee meetings. The friends and colleagues I met during my time here at Auburn were important for the timely completion of this thesis. Lab experiments would not have been possible without the lab mates and friends at the School of Fisheries, Aquaculture and Aquatic Sciences (Ansley Hamid, Matthew Gladfelter, Hannah Zinnert, and Suzanne Tenison), and the Chemical Engineering Department (Farshad Feyzbar and Ehsan Hassani). I want to thank Dr. Alan Wilson, Dr. Sushil Adhikari, Dr. Tae-Sik Oh, Dr. William Ashurst, Dr. Todd Steury, and Dr. Yaniv Olshansky for their help and access to various lab instruments/equipment and statistical analyses for this thesis. Sample analysis could not have been completed without the help from Dr. Joel Hayworth, Dr. Vanisree Mulabagal, and Danyang Wang at the Environmental Engineering Department as well as Dr. Melissa Boersma in the Mass Spectrometry Center. A special thank you to Dr. Jianzhou He for his invaluable guidance in experimental design, PFAS sample analysis, and data analysis. Another special thank you to undergraduate student (Leonard Cole Davis at East Central University) for helping with data acquisition, as well as all other friends and family members for their long-term continuous support and encouragement along the way. Financial support was provided by the Department of Defense (DoD) Strategic Environmental Research and Development Program (ER22-3150); U.S. Geological Survey (USGS), Alabama Water Resource Research Institute (G21AS00517); U.S. Department of Agriculture (USDA), National Institute of Food and Agriculture (NIFA), Hatch Program, Alabama Agricultural Experiment Station (ALA016-1-

19123); and National Science Foundation-Research Experiences for Undergraduates (REU) for Warm-Water Aquatic Ecology (DBI-1658694).

Table of Contents

List of Tables

List of Figures

List of Abbreviations

AC	Activated carbon
AFFF	Aqueous film-forming foam
AGC	Automatic gain control
AIC	Akaike Information Criterion
BET	Brunauer-Emmett-Teller
BJH	Barrett-Joyner-Halenda
$CaCl_2$	Calcium chloride
CAS	Chemical abstracts service
DI	Deionized
DRIFT	Diffuse reflectance infrared Fourier transform
ECF	Electrochemical fluorination
EIS	Extracted internal standard
EPA	Environmental Protection Agency
ePFTE	Expanded polytetrafluoroethylene
FT	Fluorotelomerization
FT-IR	Fourier-transform infrared
GAC	Granular activated carbon
GenX	Hexafluoropropylene oxide dimer acid
HAL	Health advisory level
HI	Hazard index
HPLC	High-performance liquid chromatography
HRMS	High-resolution mass spectrometry

IHSS	International Humic Substances Society
KBr	Potassium bromide
LC	Liquid chromatography
LOQ	Limit of quantification
MCL	Maximum contaminant level
$MgSO_4$	Magnesium sulfate
MS/MS	Tandem mass spectrometry
NaCl	Sodium chloride
$NaHCO_3$	Sodium bicarbonate
NIS	Non-extracted internal standard
PAC	Powdered activated carbon
PFAS	Per- and polyfluoroalkyl substances
PFBA	Perfluorobutanoic acid
PFBS	Perfluorobutane sulfonate
PFHxA	Perfluorohexanoic acid
PFHxS	Perfluorohexane sulfonate
PFNA	Perfluorononanoic acid
PFOA	Perfluorooctanoic acid
PFOS	Perfluorooctane sulfonate
PFPeA	Perfluoropentanoic acid
PFPeS	Perfluoropentane sulfonate
PFTE	Polytetrafluoroethylene
RO	Reverse osmosis

SEM	Structural equation modeling
SPE	Solid phase extraction
SSA	Specific surface area
UPLC	Ultrahigh performance liquid chromatography
WWTP	Wastewater Treatment Plant
XRD	X-ray Diffraction

Chapter 1. Introduction

1.1 PFAS History and Production

On April 6th, 1938, Dr. Roy J. Plunkett and his research associates at DuPont were working with chlorofluorocarbon refrigerants in an attempt to make a refrigerant safer than those on the market [1]. Upon checking a compressed frozen sample of tetrafluoroethylene, they found a new material that had spontaneously polymerized into a waxy white solid substance and named it as polytetrafluoroethylene (PFTE) [2]. PFTE is uniquely special since it is inert to most chemicals and is one of the most slippery materials in nature, making it useful in aerospace, communications, electronics, architecture, and virtually all other industrial processes [2]. In 1945, PFTE was trademarked as Teflon™ and commercially sold in 1946, becoming the first generation of many per- and polyfluoroalkyl substances (PFAS) on the market [2]. In the same year, 3M licensed the Simons electrochemical fluorination (ECF) method, a method for synthesizing organofluoride molecules invented by Dr. Joseph Simons at Penn State University [3]. This ECF process yielded 30–45% perfluorooctane sulfonyl fluoride (a precursor of perfluorooctane sulfonate; PFOS) as the main product and a wide range of other perfluorinated carboxylic acids (precursors to perfluorooctanoic acid; PFOA) as byproducts [4]. In 1949, 3M built their first pilot scale manufacturing ECF process in Cottage Grove, MN, and continuously developed the ECF method for fluorochemical products until 2002 [3]. It has been estimated that 80–90% of global PFOA manufacturing from the 1950s to 2002 was done by 3M plants in Antwerp, Belgium; Cottage Grove, MN; Cordova, IL; and Decatur in Alabama [5]. In 2000, 3M began voluntarily phasing out of the ECF perfluorooctyl chemistries for long-chain PFAS production, but continues to use it for short-chain PFAS [6]. Although it is not entirely clear, this phase out action was likely due to pressure from the regulatory agencies such as the U.S.

Environmental Protection Agency (EPA) [7]. The large-scale production of PFOA continued under a new process called fluorotelomerization (FT) developed by DuPont in the 1970s [8]. PFAS isomers created from FT approach differ from those derived from ECF, since produced isomers are pure, and typically have linear geometry (i.e., $CF_3(CF_2)_xC_2H_4R$) [5, 8]. This process is estimated to account for 10–20% of PFOA production globally from 1975 to 2004; however, it is currently the dominant method for making perfluorinated carboxylic acids and other fluorotelomer products in North America [5, 9]. Although 3M ceased the use of ECF method, both ECF and FT approaches are still being used to produce other PFAS compounds today [10, 11].

PFAS is a broad family of chemicals, with over 4,700 different compounds identified [6, 12]. These compounds can either be classified as polymer or nonpolymer, which can be further categorized as perfluoroalkyl or polyfluoroalkyl substances, depending on the structure of the carbons and fluorine within the compound (**Fig. 1.1)** [12]. However, a large area of concern surrounding environmental contamination and health effects is focused on the C4–C8 perfluoroalkyl acids (i.e., compounds have four to eight carbons in the structure; **Fig. 1.1**). For example, C8 PFOA and PFOS, and C4 perfluorobutanoic acid (PFOA) and perfluorobutane sulfonate (PFBS) (**Fig. 1.2**) have been widely detected in the subsurface environment, including soil, sediment, surface water, groundwater, and biota [13-16].

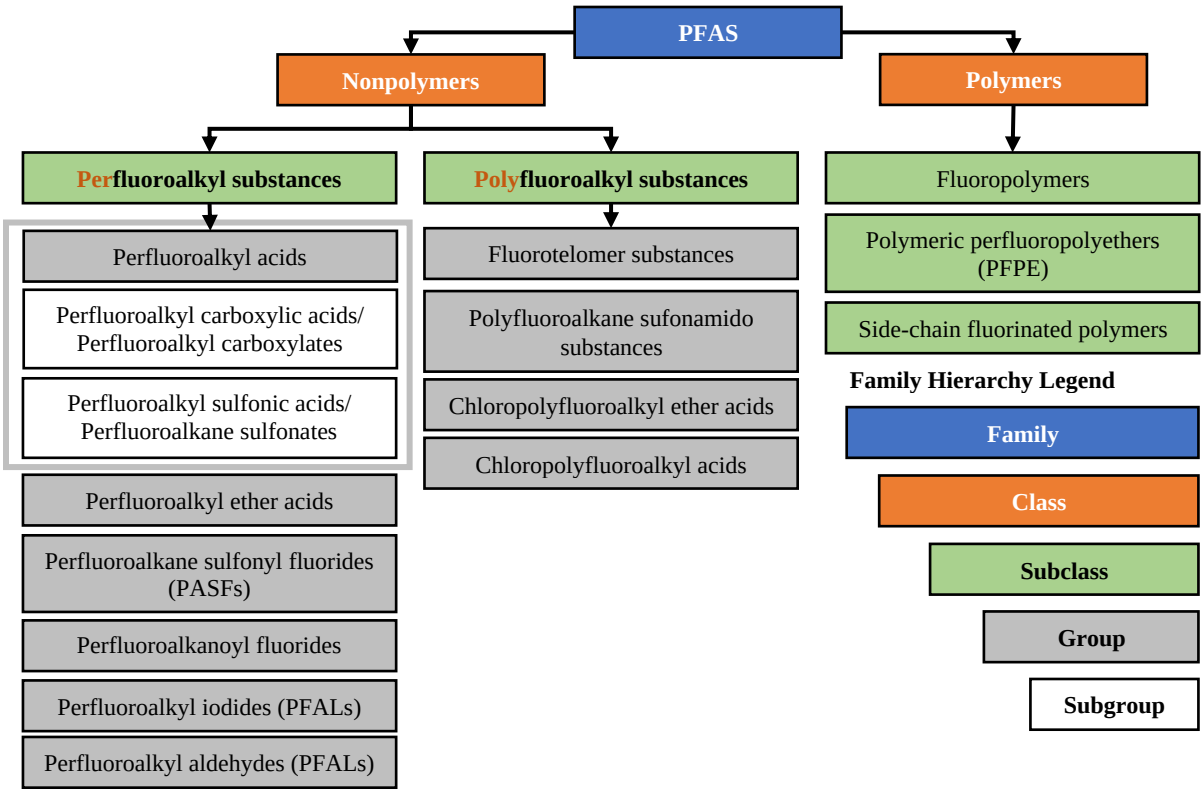

Fig. 1.1. Flowchart for PFAS classification, adapted from the IRTC Naming Convention for PFAS [12]. The family of PFAS chemicals can be easily expanded to cover over 4,700 chemical abstracts service (CAS) registered chemicals with so many different categories and functional groups in their structures. This thesis focuses on the perfluoroalkyl acids subgroup. Adapted from IRTC's Naming Conventions for PFAS.

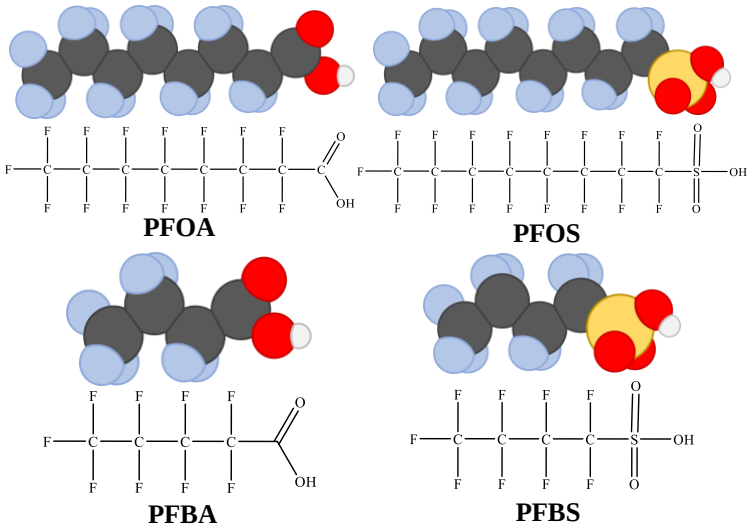

Fig 1.2. Four common PFAS compounds widely detected in the environment are also included in this thesis: PFOS, PFOS, PFBS, and PFBS. These PFAS fall under the perfluoroalkyl acid subgroup, have a carbon chain length of four to eight and either a carboxylate or sulfonate group attached.

1.2 PFAS Use

During the initial PFAS production, the synthesis process of PFOA and PFOS was still had uses in stain and water resistant products and protective coatings by the mid-1950s [6]. By the 1960s, PFOS was being implemented in the production of firefighting foams, also known as aqueous film-forming foams (AFFFs) [6]. AFFFs are effective in suppressing fires on highly flammable and hazardous liquids; however, they are one of the major sources for PFAS contamination to soil and groundwater (e.g., widely used by the Department of Defense; DoD) [17]. Firefighting foams are grouped into two major classes: class A and class B [17]. The Class A foams were developed in the 1980s and can be used for wild and structure fires [17]. These foams do not contain PFAS [18]. In contrast, the Class B foams are specifically designed to extinguish flammable and combustible liquids and gasses such as grease, tars, oil, gasoline, solvents, and alcohols [17]. Most of the class B foams used in the U.S. contain PFAS [17]. In 1976, Gore-Tex™ began making waterproof jackets from expanded PTFE (ePTFE), which then was also used to make space suits for astronauts on the apollo missions, water resistant footwear and other outdoor clothing [19]. Production and synthesis of other fluorotelomers and long-chain (≥ C8) PFAS compounds also began in the 1970s for use in architectural resins and firefighting foams. By 2000, fluorotelomers (precursors to many types of PFAS) were the primary form of firefighting foams [6]. PFAS have many unique physiochemical properties such as hydrophobicity, water solubility, corrosion/heat resistance, ability to lower surface tension, and acidity that make them a useful chemical in many every day and industrial products [20, 21]. Glüge et al. (2020) found that PFAS were used in 64 different areas of industry and other use categories with 210 different ways that PFAS are directly employed in industry and consumer products [21]. PFAS long production history and use in so many areas have led to a present-day worldwide contamination crisis in the environment [22].

1.3 PFAS Contamination and Health Effects

PFAS are released into the environment from primary and secondary industries, AFFF applications, and many others since they are present in so many products [23]. Primary industrial facilities that produce PFAS release large amounts of them into the environment through air, wastewater, and stormwater emissions [23]. Secondary facilities refer to all other industrial facilities that may use fluoropolymers or other PFAS-based products as part of their specific industrial processes [23]. Examples of secondary industries include building and construction, cable and wiring, metal finishing and plating, paper products and packaging, semiconductors, textiles, apparel, and many others [9, 21, 23-27]. These industries inherently contaminate many forms of environmental media in some ways through direct discharge of industrial waste into air and waterways, AFFF applications contaminate soil and groundwater, or through the transport of PFAS in the environment [23]. PFAS can volatilize via stack emissions from industries, resulting in direct aerial contamination, long range air transport, and finally deposition to soil and surface water [28, 29].

AFFF is a large and highly concentrated source of PFAS for soil contamination, which further transports to surface water and groundwater through runoff and percolation [23]. Class B firefighting foams have been, and continue to be, stored and used at military installations, civilian facilities, airports, petroleum refineries and bulk storage facilities, and chemical manufacturing plants and storage facilities [4, 30]. Solid waste management facilities such as landfills are the final repository of PFAS from solid waste sources [23]. Landfill leachates contain high concentrations of PFAS from the consumer and industrial PFAS-containing solid waste they hold [31, 32]. The leachates are collected and sent to wastewater treatment plants (WWTPs) for treatment [23]. Contamination of WWTP effluent comes from a large variety of

sources other than landfill leachates [23]. WWTP effluents are a major threat to surface water contamination, since PFAS cannot be efficiently removed by conventional treatment methods [33, 34]. Biosolids from WWTPs are also a source of PFAS contamination, when they are used as agricultural fertilizers for land applications [35, 36]. PFAS from this contamination source will either be taken up by crops or percolated back into the groundwater [37, 38].

Recently PFAS have been detected at levels above the U.S EPA's proposed Maximum Contaminant level (MCL) of 4 ng/L in various environmental media across the United States [39]. PFAS occurrence in a drinking water distribution system near primary PFAS production facilities has been reported at a concentration range of 1,500 to 7,200 ng/L, while other drinking water distribution systems that are not heavily affected by primary industry still have PFAS concentrations ranging from 5 to 29 ng/L [40]. Industrial wastewaters have been tested and found to have effluent concentrations ranging from 662 to 1,143 ng/L [41]. PFAS have been detected ubiquitously in WWTP effluent with concentrations reaching several hundred ng/L [42]. For the year 2013, the total volume of landfill leachate generated in the U.S. was estimated to be 61.1 million cubic meters, meaning the mass of measured PFAS from U.S. landfill leachate to WWTP was estimated to be between 563 and 638 kg in the year 2013 [43]. Soils adjacent to fire-training areas that use the class B AFFFs have had PFAS concentrations ranging from 0.3–65,000 µg/g, leading to contamination of the surrounding groundwater concentration at 22 µg/L ΣPFAS [44].

The first documentation of global contamination was reported on PFAS concentrations in wildlife by Giesy and Kannan in 2001 [14, 15]. A common focus for studying PFAS

toxicological effects is immunomodulation, or how PFAS affect the function of the organism's immune system [45]. A review published by Antoniou et al. (2022) reported the lowest observed adverse immunomodulation effect levels of PFOS in different small rodent species ranged from 0.002–3.5 mg/kg/day [45]. Another review by Boyd et al. (2022) showed that PFAS may have adverse cancer related health effects in low doses among animals; however, it is difficult to confidently describe the response for the cancer-related effects from a mechanistic standpoint [46]. Documentation of fluorochemical presence in plant workers has dated back to 1980, but there were no health effects reported at that time [47]. PFOA, PFOS, and other PFAS were later documented in human blood samples by Hansen et al. (2001) with samples purchased from biological supply companies [15, 48]. PFAS contamination in living organisms has been attributed to their ability to bind to blood proteins, giving them long half-lives within the body [6, 49-51].

Some of the most comprehensive evidence for PFAS toxicity in humans arises from a group of studies on the communities near the DuPont Washington Works fluorotelomer plant in West Virginia [52]. These studies found probable links between PFOA exposure and elevated levels of cholesterol, thyroid disease, pregnancy-induced hypertension, ulcerative colitis, and kidney and testicular cancer [52-56]. This group of studies was one of the largest PFAS exposure groups ever monitored, with over 69,000 participants [57]. Grandjean et al. (2012) observed that children with 2-folds higher concentrations of PFAS in their blood serum at age 5 exhibited a 50% decline in antibody concentrations two years later at age 7, supporting the hypothesis that PFAS impair immune system function for children [58]. Similarly, a study by Grandjean and Budtz-Jørgensen in 2013 had a benchmark dose of 1.3 ng/mL PFOS and 0.3 ng/mL PFOA

among children in the Faroe Islands and estimated that drinking water advisories are several hundred-folds high, based on dose response curves [59]. The 3M Decatur (AL) manufacturing workers had some of the highest PFAS concentrations in their blood, and so did the surrounding residents due to the contaminated water [60]. **Fig 1.3** shows what human populations in Alabama may be at risk of PFAS contamination, based on a recent PFAS concentration survey conducted by Viticoski et al. (2022).

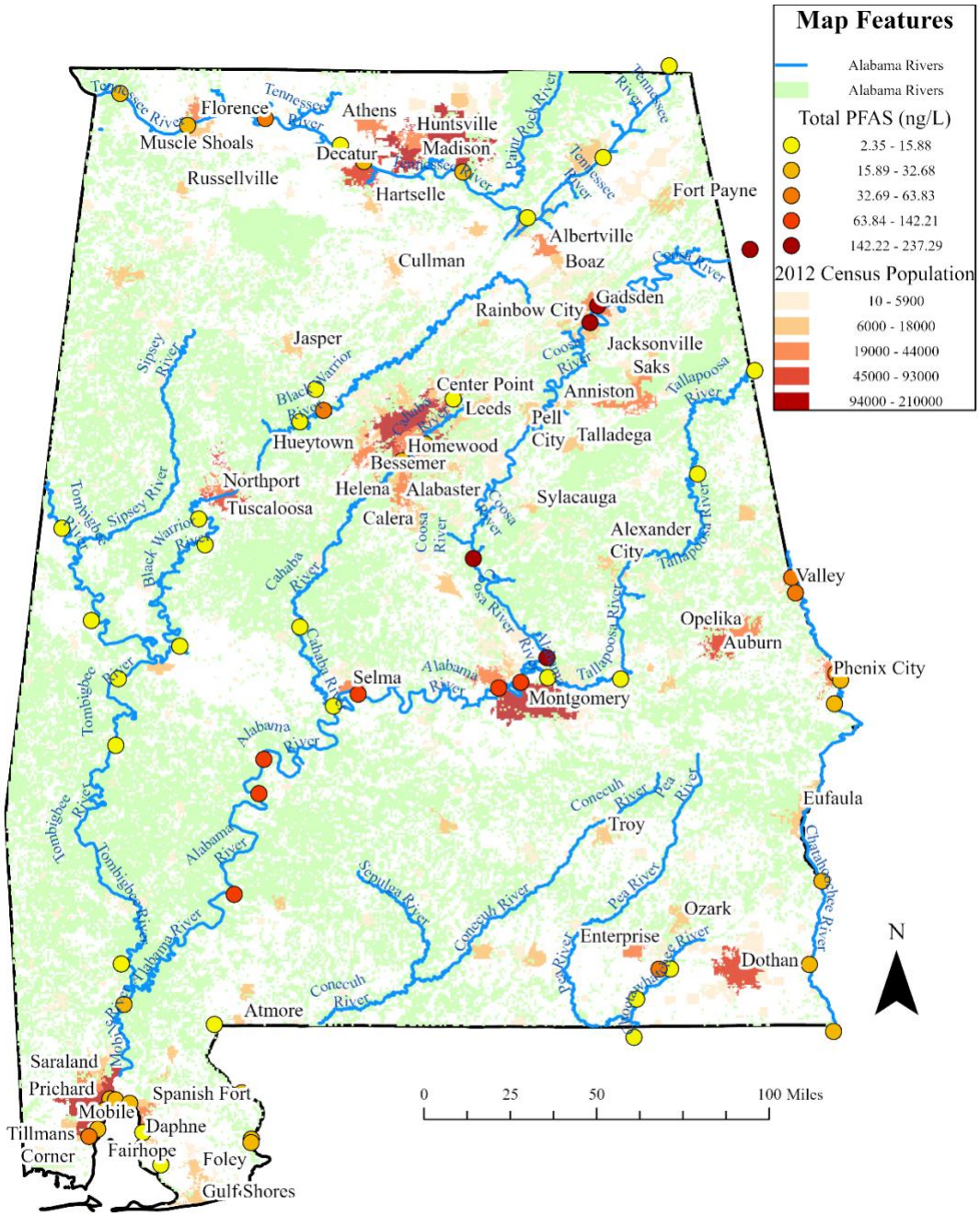

Fig. 1.3. This map contains the major rivers and populated areas of Alabama along with the total PFAS concentration from several locations within Alabama rivers sampled by Viticoski et al. (2022). PFAS analyzed included PFBS, PFPeA, PFHxA, PFOA and PFOS. Decatur is in north-central Alabama and is known for its high PFAS concentrations in residents and the surrounding water from years of PFAS manufacturing. However, residents that get their drinking water from the Coosa, Alabama, and Mobile rivers are at risk of high PFAS concentrations. Large populations along these rivers listed from northeast to southwest include Gadsden, Rainbow City, Pell City, Millbrook, Montgomery, Prattville, Selma, Pritchard, and Mobile. Residents in Valley, Phenix City, Eufaula may also be at risk due to PFAS levels in the Chattahoochee River.

1.4 PFAS Regulation

Regulation of PFAS compounds have not come until recent years, and original regulations have focused on long-chain PFAS compounds. In 2016, the U.S. EPA released a lifetime health advisory level (HAL) for the PFOA and PFOS, the two most widely detected PFAS, at 70 ng/L combined in drinking water [61]. In June 2022, the U.S. EPA released significantly more stringent HALs for PFOA and PFOS at 0.004 ng/L and 0.02 ng/L, respectively, while adding two new PFAS compounds, PFBS and hexafluoropropylene oxide dimer acid (GenX), at HALs of 2,000 ng/L and 10 ng/L respectively [62]. The most recent U.S. EPA proposal on PFAS regulation was announced on March 14th, 2023, where enforceable maximum contaminant levels (MCLs) of 4 ng/L for PFOA and PFOS (individual concentrations) were proposed, as well as Hazard Index (HI) for perfluorononanoic acid (PFNA), perfluorohexane sulfonate (PFHxS), PFBS, and GenX [63]. This HI is a tool used to determine the toxicity of a mixture of chemicals based on their combined concentrations [63, 64]. The calculation for the proposed HI is as follows:

$$\text{Hazard Index (HI)} = \left(\frac{[\text{GenXwater}]}{[10\text{ ppt}]}\right) + \left(\frac{[\text{PFBSwater}]}{[2000\text{ ppt}]}\right) + \left(\frac{[\text{PFNAwater}]}{[10\text{ ppt}]}\right) + \left(\frac{[\text{PFHxSwater}]}{[9.0\text{ ppt}]}\right) \quad (1.1)$$

where the sum of the measured concentration of each chemical cannot be above a value of 1.0 (unitless). Some states have their own PFAS regulations in drinking water, and Michigan, Minnesota, New Hampshire, New Jersey, New York, Ohio, and Vermont have sued PFAS manufacturers for threats to public health and the environment [65]. In 2021 alone, state legislatures considered a combined 196 bills related to PFAS, that range from regulating production to drinking water standards [65]. The PFAS studied in thesis along with their physical and chemical properties can be found in **Table 1.1**.

Table 1.1. Physical and chemical properties of the C4-C8 PFAS used in this thesis.

Acronym	Full Name	CAS No.	MW (g/mol)	Chemical Formula	Density (g/cm^3) at 20-40°C	Melting Point (°C)	Boiling Point (°C)	Solubility (mg/L) at 25°C	Vapor Pressure (Pa)	Henry's Constant (K_{aw})	CMC (mg/L)	pK_a
PFBA	Perfluorobutanoic acid	375-22-4	214	C_3F_7COOH	1.61 to 1.65	-17.5	120	327 to 5.60×10^6	0.22 to 4.48×10^3	6.40×10^4 to 2.0	1.35×10^5 to 1.62×10^5	0.20 to 1.60
PFBS	Perfluorobutane sulfonate	375-75-5	300.10	$C_4F_9SO_3H$	1.81 to 1.85	20.4 to 70.4	80 to 214	107 to 1.60×10^5	1.60×10^{-6} to 631	1.20×10^{-8} to 10.5	n/a	0.14 to 0.30
PFPeA	Perfluoropentanoic acid	2706-90-3	264.10	C_4F_9COOH	1.71	-13.2 to 25.3	139	61.0 to 4.90×10^5	1.10 to 2.72×10^3	1.30×10^{-8} to 7.20	5.27×10^4 to 6.05×10^4	-0.10 to 0.40
PFPeS	Perfluoropentane sulfonate	2706-91-4	350.10	$C_5F_{11}SO_3H$	1.81 to 1.84	10.7 to 78.4	198 to 225	8.10 to 4.20×10^6	3.80×10^5	8.90×10^{-9}	n/a	n/a
PFHxA	Perfluorohexanoic acid	307-24-4	314.10	$C_5F_{11}COOH$	1.76	7.8 to 14.0	136 to 157	5.00 to 6.90×10^5	5.10 to 562	1.00×10^{-8} to 26.90	2.22×10^4 to 4.34×10^4	-0.16 to 1.60
PFHxS	Perfluorohexane sulfonate	355-46-4	400.10	$C_6F_{13}SO_3H$	1.84	26.7 to 190	95 to 238	0.60 to 3.40×10^5	1.10×10^{-6} to 47.9	8.00×10^{-9} to 140	7.28×10^3	0.14 to 0.30
PFOA	Perfluorooctanoic acid	335-67-1	414.10	$C_7F_{15}COOH$	1.80	-8.69 to 65.7	188 to 204	0.01 to 1.20×10^6	0.03 to 1.72×10^3	8.30×10^{-9} to 370	1.65×10^3 to 1.57×10^4	-0.50 to 3.70
PFOS	Perfluorooctane sulfonate	1763-23-1	500.10	$C_8F_{17}SO_3H$	1.84 to 1.85	15.2 to 185	133 to 249	2.40 to 1.10×10^6	3.30×10^{-4} to 34	7.60×10^{-10} to 1.90 $x10^3$	536 to 4.57×10^4	0.14 to 0.30

MW: Molecular weight.

CMC: Critical micelle concentration.

pK_a: Acid dissociation constant.

n/a: Not available.

1.5 PFAS treatment technologies

Ultimately, PFAS remediation must lead to a destruction process to stop their persistence in the environmental cycles. Therefore, PFAS remediation consists of to two main technologies: (I) PFAS removal from environmental media; and (II) PFAS destruction [66]. The techniques currently employed in PFAS removal include physical, chemical, biological, and treatment train techniques combining different removal techniques [67]. More specifically, these techniques include conventional flocculation and coagulation, sedimentation, filtration, sorption, ion exchange resins, polymers, nanomaterials, foam fractionation, ozone fractionation, and soil stabilization [66, 68]. Conventional water treatment methods use coagulation and flocculation approaches that are not successful at removing PFAS due to their chemical properties such as high water solubility and are therefore unsuccessful [66, 69, 70]. Modern technologies have given birth to many more advanced water treatment options. One common solution to address environmental contaminant issues is via sorptive removal [71]. Some of the more advanced sorption technologies such as resins offer short equilibrium times and high sorption efficiencies of PFAS, reaching capacities as high as 2,390 mg/g for PFOS [72, 73]. Anion exchange resins contain ethanol groups, giving them a more favorable surface structure for PFAS sorption than other sorbents [72, 74]. Wu et al. (2018) also employed sorptive tactics, fabricating a layered porous graphite structure that displayed sorption capacities as high as 1,240 mg/g for PFOS and 366 mg/g for PFBS [75]. Nanomaterials such as carbon nanotubes and nanosized iron oxides are also potential PFAS sorbents being tested [72]. These nanomaterials have reported equilibrium times less than two hours and capacities as high as 700 mg/g [76]. However, some of the most successful sorption materials to date are polymers [72, 77-80]. For example, Liu et al. (2022) found that positive aromatic framework polymers with an N,N-dimethyl-butylamine amendment

had a sorption capacity of over 2,000 mg/g and removed 99.99% of PFOA (1,000 ng/L initial concentration) in less than 2 min [80]. There have also been studies that show natural materials such as minerals possess surface characteristics suitable for PFAS sorption [72, 81, 82]. Although minerals tend to have a much lower sorption capacity compared to other sorbents, modifications can drastically improve their results [72, 83]. Surface modification of sorbents is a strategy for many materials towards enhanced sorption of PFAS [84, 85]. Since PFAS are hydrophobic and typically have a negatively charged functional group, sorbent surface modifications typically attempt to improve hydrophobicity and/or make negative charges positive to promote hydrophobic interactions and electrostatic interactions [84, 86].

Activated carbon (AC) has been widely used to treat a variety of environmental contaminants due to its relatively easy production process and high sorption capacity for many contaminants [72, 87]. AC is a carbonaceous material pyrolyzed from substances with high carbon and low inorganic contents, which is also commonly referred to as granular activated carbon (GAC) or powdered activated carbon (PAC) [88, 89]. AC has been used for potable water treatment since 1862, and performs well at removing a wide variety of contaminants [90, 91]. The sorption capacity of AC has been reported to reach up to 120 and 290 mg/g for PFOA and PFOS respectively [72]. It is generally agreed that AC is effective at removing long-chain PFAS, while showing poor performance for short-chain compounds [72, 92, 93]. AC performance is also greatly reduced for waters with presence of other organic contaminants or natural organic matter (NOM) [72, 94]. Some studies have also had success in stabilizing PFAS in the sub surface with AC both at the lab and field scales [95-97]. Although AC is not the most efficient adsorbent, it is cost effective compared to other options and already widely implemented in many water

treatment scenarios [66]. Both GAC and PAC have been successfully implemented in WWTPs and shown promising removal performance for long-chain PFAS compounds [98-104]. Generally, specific surface area (SSA) and hydrophobicity are the two main properties for the efficient removal of PFAS by AC.

1.6 Biochar Production, History, Qualities, and Use in Water Treatment.

Similar to AC, biochar is defined by the International Biochar Initiative as a solid material obtained from the thermochemical conversion of biomass in an oxygen-limited environment [105].

Biochar is deemed as the precursor of activated carbon (AC) in that both can be derived from similar materials (AC can also be made from coal), but biochar is generally produced at lower pyrolysis temperatures (normally less than 1,000 °C). However, there are some types of AC made at lower pyrolysis temperatures, and many ACs have been known to be made from feedstocks such as coconut and palm shells [106, 107]. Therefore, a clear definition separating biochars from ACs has not yet been reached. Herein, the carbonaceous material produced from biomass under oxygen-free (N2) conditions will be referred to as biochar in this thesis.

Biochar is also produced naturally by wildfires, but evidence of anthropogenic biochar production dates to over 2,000 years ago with links to tribes in the Amazon River basin [108-110]. These amazon soils known as Terra Preta, meaning “the black soils of the Indians”, were derived from slash and burn activities [108-112]. For most of its known existence, biochar has been used primarily as a soil amendment, due to its high surface area, increased biomass production, and ability to increase nutrient and water holding capacity [109, 113]. Areas of Asia, specifically Japan and Korea, also have a long history of biochar use as a soil amendment [108,

109]. During research on Terra Preta in the mid-1990s, it was discovered that biochar also had the potential to reduce atmospheric CO_2, and in the early 2000s, research on other biochar uses for environmental heath began [114]. Fast forward to present day, it has been found that biochar has uses in water and wastewater treatment, building materials, climate change mitigation, carbon sequestration, as well as many other environmental uses that are still being explored [109, 115, 116]. Although biochars historical use in water treatment is short lived it has proven successful in removing heavy metals, organic and inorganic contaminants, nitrogen, phosphorus, pesticides, and antibiotics [117-122].

Biochar has richer surface functional groups than AC, due to the lower pyrolysis temperatures during production [123, 124]. A lower pyrolysis temperature coupled with the waste derived feedstocks inherently makes biochar more cost-effective, tunable, and energy-efficient compared to AC. For example, the energy demand, average greenhouse gas emission, and price tag between biochar and AC are reported at 6.1 vs. 97 MJ/kg, 0.9 vs. 6.6 kg CO_2 eq/kg, and $350–1,200/tonne vs. $1,100–1,700/tonne, respectively [89, 125]. Furthermore, biochar has also shown to offer carbon sequestration and energy production benefits during pyrolysis, compared to AC [89]. Additionally, biochar sorptive removal of PFAS is expected to be promising, due to high SSA, rich functional groups, hydrophobicity, and tunable surface functionalities [76]. Biochar also converts wastes from agriculture and forestry into useful materials, creating a circular economy and keeping the biochar production cost low. All these benefits clearly suggest biochar holds the high promise to remove PFAS from water.

1.7 Biochar for PFAS Removal and Scope of This Thesis

Recent studies have shown that biochar derived from many feedstocks is an effective way for the sorptive removal of PFAS from water [126-130]. However, these studies lack fundamental knowledge on what mechanisms likely play a key role in PFAS sorption with respect to which physicochemical properties of biochars, as well as what and the extent to which environmental factors affect PFAS sorption performance. Therefore, two case studies were conducted in this thesis. Study 1 screened out which biochars perform better for PFAS sorption and which biochar physicochemical properties influence the sorption efficiency of PFAS. In total, 15 biochars pyrolyzed in the lab plus one commercially produced biochar were used in batch sorption experiments for PFOS. Physiochemical properties of all biochars were systematically analyzed, including elemental content, pH, SSA, pore volume, pore diameter, hydrophobicity, surface charge, functional groups, and surface crystallography. PFOS was used as a representative PFAS compound in batch sorption experiments. Structural equation modeling (SEM) was used to narrow down what physiochemical properties most influence biochars sorption efficiency. It was hypothesized that SSA, hydrophobicity, and functional groups will be the key players for PFOS sorption.

Based on the PFOS batch sorption data from Study 1, the biochars with higher PFOS sorption capacity were used in Study 2 with several sets of experiments. First, a screening experiment containing C4-C8 PFAS compounds in a cocktail solution was conducted using these biochars in a relatively clean background media. These selected biochars were also used to sorb C4-C8 PFAS from water under different environmental conditions varying in pH, salt, and natural organic matter (NOM) concentrations. Specifically, different solution pHs, concentrations of salts and NOM were investigated to quantify biochars sorptive performance under different

environmental conditions. Ultimately, an artificial groundwater solution was utilized to assess how environmental conditions affect biochars performance for all C4-C8 PFAS. It was hypothesized that high solution pH and addition of NOM will negatively impact biochars sorption performance. However, salts may improve sorption due to cations decreasing the effective charge and increasing PFAS aggregation. Data gathered from the two case studies in the thesis will provide insights into how to further improve biochars sorptive abilities for future research as well as needed information about biochars sorptive efficiency for PFAS in real world scenarios.

Chapter 2: Mechanistic Understanding of Perfluorooctane Sulfonate Sorption by Biochars

2.1 Abstract

Biochar has recently emerged as a cost-effective solution to combat PFAS pollution in water, but mechanistic understanding of which physicochemical properties of biochars affect PFAS sorptive removal from water remains elusive. Herein, 15 biochars were pyrolyzed from 5 feedstocks (corn, Douglas fir, eucalyptus, poplar, and switchgrass) at 3 pyrolysis temperatures (500, 700, and 900°C) to investigate their removal efficiency and mechanisms of PFOS from water. A commercial biochar was also included for comparison. Biochar physiochemical properties, including elemental composition, pH, specific surface area (SSA), pore structure, hydrophobicity, surface charge, surface functional groups, and crystalline structure were systematically characterized. Batch sorption data showed that the Douglas fir 900, poplar 900, and commercial biochars removed over 95% of PFOS from water. Structural equation modeling (SEM) was used to unravel which biochar properties affect PFOS sorption. Interestingly, biochar pore diameter was identified as the most critical factor controlling PFOS removal, but pore diameter/pore volume ratio, SSA, pyrolysis temperature, hydrophobicity, and elemental composition all played variable roles. It has been hypothesized that biochars with small pore diameters and large pore volumes have a narrow yet deep pore structure that traps PFOS inside once already sorbed, resulting in an enhanced PFOS sorption. Biochars with small pore diameter, low nitrogen content, and high pyrolysis temperature were favorable for enhanced PFOS sorption. Our findings mechanistically advance the understanding of using biochars with optimized properties to remove PFOS and possibly other similar PFAS compounds from water.

2.2 Introduction

PFAS have been extensively used in a wide spectrum of products such AFFF for fire training purposes, surfactants, paints, and adhesives since the early 1940s [2, 6, 19, 20]. On March 14th 2023, the U.S. EPA proposed setting MCLs for PFOA and PFOS at 4 ng/L and a HI for PFNA PFHxS, PFBS, and GenX [63]. PFAS remediation cost is ultimately paid for by tax dollars so a cost-effective, efficient, and sustainable treatment technique for PFAS removal is critical [131]. GAC is efficient at removing long-chain PFAS compounds, but high production and operation costs in WWTPs make it an undesirable option [89, 125]. Biochar is similar to AC in that it is a low-density carbonaceous material, produced by the pyrolysis of agricultural and forestry wastes in an oxygen-limited environment, and can be thought of as a pre-cursor to activated carbon [132-135]. The lower energy demand, average greenhouse gas emission, and price tag of biochar make it a more lucrative and eco-friendlier alternative [89, 125]. Additionally, biochar sorptive removal of PFAS is expected to be promising, due to high SSA, rich functional groups, hydrophobicity, and tunable surface functionalities [76]. All these benefits clearly suggest biochar holds the highest promise to remove PFAS from water.

Recent studies back this hypothesis, showing that biochar derived from many feedstocks is an effective tool for PFAS sorption [126-130]. However, these studies lack key information about what biochar properties promote or inhibit sorption efficiency. Thus, the current knowledge on which biochar types, what physicochemical properties, and what environmental factors affect sorptive performance remain unclear. This research aims to provide an in-depth investigation into biochar physiochemical properties for PFOS removal from water. The findings from this

study will shed light on the mechanistic understanding for the development of next generation biochars for effective and efficient removal of PFAS from water.

2.3 Materials and Methods

2.3.1 Chemicals and Reagents

Potassium perfluorooctane sulfonate (PFOSK at 95% purity) was purchased from Matrix Laboratories (Mount Prospect, IL). The physiochemical properties of PFOS were shown in **Table 1.1**. Sodium chloride (NaCl) was purchased from Acros Organics. ACS-grade methanol was purchased from VWR. Deionized (DI) water and Milli-Q water were produced using a Milli-Q Ultrapure water system (Darmstadt, Germany).

2.3.2 Feedstocks for Biochar Production

Five feedstocks, i.e., corn cob (*Zea mays)*, Douglas fir (*Pseudotsuga menziesii***)**, eucalyptus (*Eucalyptus benthamii*), poplar (*poplus spp.)*, and switchgrass (*Panicum virgatum*) were used to produce biochars (one commercial biochar was also included for comparison). These five feedstocks include two grasses (corn and switchgrass), two hardwoods (eucalyptus and poplar), and one softwood (Douglas fir). Although corn is not actually a grass feedstock, its properties are more similar to grass than to wood feedstocks and will be referred to as a grass feedstock for the remainder of study. Detailed descriptions of feedstocks are shown in **Table 2.1**.

Table 2.1. Basic descriptions of the 5 feedstocks used for biochar production.

Feedstock	Details
Corn Cob	Obtained from the Auburn University Variety Testing Program. Ears of corn were shelled and ground on site at the seed station in Auburn. Sizes ranged approximately 0.5–10 mm.
Douglas Fir	Obtained from Forestconcepts™ Precision Feedstocks® (Sample ID; 2015.04.06.01.6A.B). Douglas Fir chips were processed by cascading to 0.8 mm Lab Crumbler®. Chip sizes ranged 0.51–1.14 mm.
Eucalyptus	Obtained from Forestconcepts™ Precision Feedstocks® (Sample ID; 2015.02.23.001.A). The Eucalyptus chips were processed by cascading to 0.8 mm Lab Crumbler®. Chip sizes ranged 0.51–1.14 mm.
Poplar	Obtained from Forestconcepts™ Precision Feedstocks® (Sample ID; 2015.06.18.01.A.E). The poplar chips were run by a hammer mill to pass though mesh 30 (but not mesh 60).
Switchgrass	Obtained from the University of Tennessee Biofuels Initiative (UTBI) program.
Commercial [a]	Rouge Biochar™ was obtained from Oregon Biochar Solutions produced at ~1,000°C from softwood feedstocks and powdered from a roller mill.

[a] *Commercially produced biochar was donated by Oregon Biochar Solutions.*

2.3.3 Biochar Production

The slow pyrolysis process of feedstocks was used to produce biochars at three targeted temperatures of 500, 700, and 900°C using an MTI 1100X furnace (MTI Corporation Richmond, CA). The heating gradient started at a rate of 8.5°C/min from 25°C to 200°C, where it was held for 30 min, allowing the furnace to purge any moisture and precisely reach the desired temperature. The same rate of 8.5°C/min was then used to reach the targeted pyrolysis temperatures (500, 700, and 900°C) and held there for 30 min to ensure even and complete pyrolysis of the feedstocks. The furnace was then cooled down to 200°C at a rate of 8.5°C/min. Then the biochar was allowed to cool down on its own within the sealed furnace. A detailed depiction of biochar production was shown in **Fig. 2.1**. Biochar samples were stored in beakers covered by foil inside a desiccator. The commercial biochar donated by Oregon Biochar

Solutions was produced in an oxygen limited environment at 1,000°C, but a detailed production method was not provided due to intellectual property rights. In total, 16 biochars (15 biochars produced from 5 feedstocks at 3 pyrolysis temperatures and one commercially produced biochar) were used for PFOS removal from water (described below).

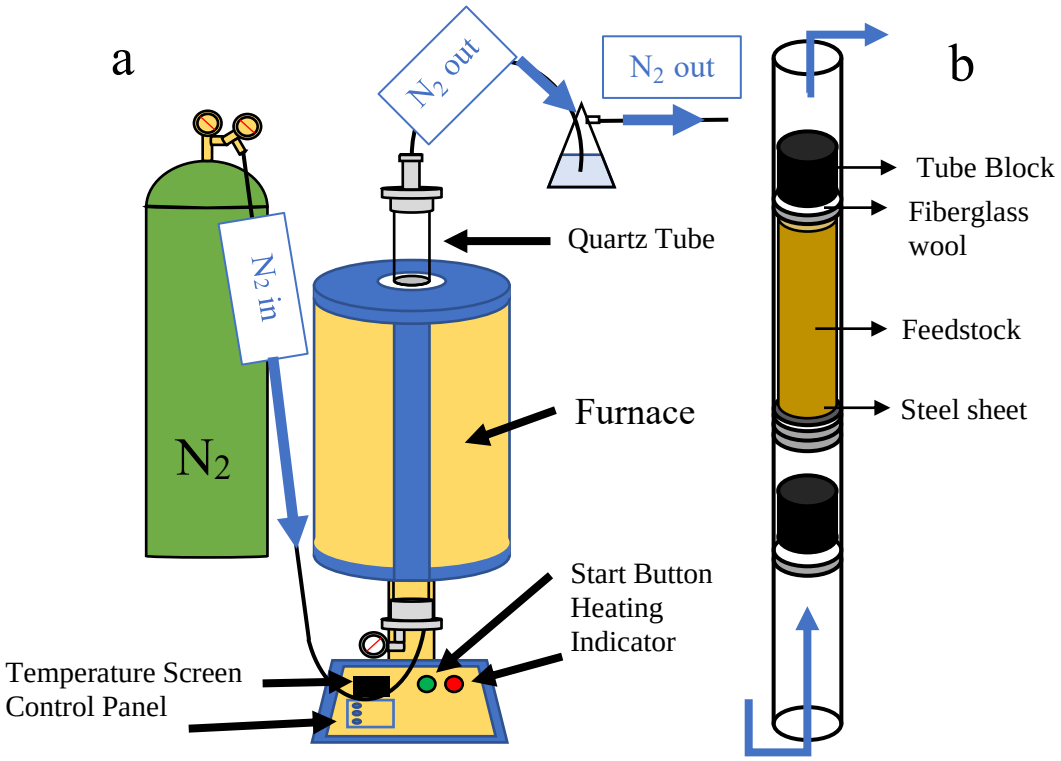

Figure 2.1 (a) Schematic showing the pyrolysis of biochar in a furnace under N_2 condition. **(b)** quartz tube holding the feedstock inside the furnace for biochar production.

An easy way to increase biochar SSA for better PFOS sorption is to reduce particle size. This was done by ball milling in an MTI planetary ball mill (4 × 500 mL capacity; MTI Corporation Richmond, CA). All biochar samples were ball milled at 500 rpm for 3 h, in which 10 mL of methanol was added to the milling jar to facilitate particle breakup. After ball milling, biochar was saturated with methanol and transferred to 50 mL polypropylene centrifuge tubes. The biochar samples were then centrifuged at 9,500 rpm for 30 min, and the methanol supernatant

was discarded. The remaining biochar/methanol slurry left over was dried for 24 h at 70°C to ensure all methanol was evaporated. This drying process caused coagulation between biochar particles so the biochars are re-ground with a pestle and mortar and stored in a desiccator for later use.

2.3.4 Detailed Characterization of Physicochemical Properties of the Biochars

The physicochemical properties of biochars, including elemental composition, pH, SSA, pore structure, hydrophobicity, surface charge, surface functional groups, and crystallinity were systematically characterized. Briefly, elemental composition of biochars was analyzed on a Vario MICRO, Elementar (Ronkonkoma, NY) using the ASTM D5373-21 method [136]. This analysis was performed using 1.01–1.33 g of biochar, and samples were run in duplicate. The pH of biochar suspensions (0.1 g/L) was measured on an Orion star pH meter (Thermo Fischer Scientific Waltham, MA) in triplicate. The nitrogen adsorption/desorption isotherms were measured at 77 K using a micrometrics MicroActive for ASAP 2460 2.02 (Anton-Paar, Ashland, Virginia) to determine biochar SSA and pore structure. The SSA was obtained according to the Brunauer-Emmett-Teller (BET) equation and total pore volume was calculated by N_2 adsorbed amount at a relative pressure of 0.99. Both pore size and pore size distribution were calculated from N_2 desorption via the Barrett-Joyner-Halenda (BJH) method, assuming that all pore shapes are cylindrical and the absorbed amount is from both physical adsorption onto the pore walls and capillary condensation in mesopores [137].

The contact angle of water droplets was used to assess the hydrophobicity of biochars on a ramé-hart Contact Angle Goniometer (Succasunna, NJ) equipped with the DROPimage software (**Fig.**

2.2). Biochar hydrophobicity was determined using a modified sessile drop method [138]. Briefly, a double-sided tape was adhered to a microscope slide and a small amount (<0.005 g) of each biochar was spread to form a thin homogeneous layer on the double-sided tape. Contact angles on either side of the water droplets were measured at a contrast above 80% and a tilt of less than 0.2°. A blank measurement of the double-sided tape was found to have a contact angle of approximately 90° (±2° to account for instrument error), meaning the tape was neither hydrophobic nor hydrophilic.

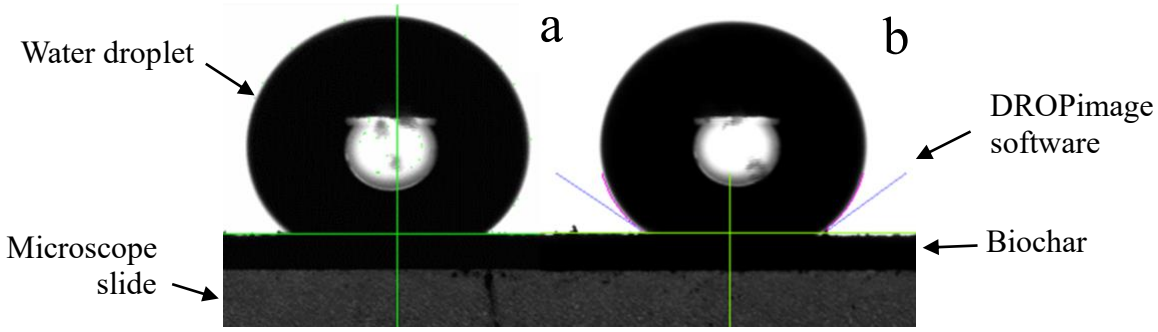

Figure 2.2. (a) Image of water droplet on biochar through the lens of the goniometer and **(b)** an image of the water droplet being measured with DROPimage software.

Surface charge and particle size of biochar suspension (0.1 g/L in 1 mM NaCl) were measured in a DTS1070 disposable folded capillary cells on a Malvern Pro Blue Zetasizer Particle size analyzer (Malvern Panalytical Ltd, U.K.). Surface functional groups of biochars were measured on a Jasco Fourier-transform infrared (FT-IR-6600) (Jasco Inc., Easton, MD) spectrometer using the FT-IR Diffuse reflectance infrared Fourier transform (DRIFT) method. Biochar samples were mixed with potassium bromide (KBr) at a mass ratio of ~300: 1 (KBr: biochar), and infrared absorbance was measured between wavenumbers 600 and 4000 cm^{-1} at a scanning rate of 4 cm/s. After obtaining the raw data, the obtained curves were smoothed and zero corrected using the Jasco Spectra Manager Program. Proto manufacturing XRD (X-ray diffraction) powder

diffraction system (Proto Manufacturing, Taylor, MI) was used to analyze the crystallographic structure of biochars. Biochar samples were prepared by spreading the fine biochar powders uniformly across a small shallow magnetic dish. The dish was then adhered to a magnetic holder on the instrument for analysis. Biochar samples were scanned at a rate of 2.2°/min at 30 mA and 40 kV with 2-theta of 10° and dwelling time of 5 seconds.

2.3.5 Batch Sorption Experiments of PFOS by Biochars and PFOS Concentration Analysis

Batch sorption experiments were conducted to determine the removal efficiency (%) of PFOS by the 16 biochars. Experiments were performed in triplicate using 50-mL polypropylene centrifuge tubes in a total volume of 40 mL. All stock solutions of PFOS, biochar, and NaCl were made with Milli-Q water and stored in 1 L polypropylene bottles. For the experiment, biochar and NaCl were diluted to 0.1 g/L and 1 mM, respectively. Biochar suspensions were sonicated and shaken vigorously before spiking to break apart any coagulation that may have occurred. PFOS was spiked last at a concentration of 500 µg/L and samples were placed on an orbital shaker for 48 h (sorption equilibrium was achieved within 48 h). Samples were then centrifuged at 9,500 rpm for 30 min, and 25 mL of supernatant was pipetted out by passing through 2 sequentially stacked 0.22 µm polypropylene filters to remove any excess biochar particles. The first 5 mL of supernatant was discarded to eliminate the interference of PFAS loss, due to membrane filtration. Then, 0.9 mL of supernatant was transferred to a 2 mL polypropylene microcentrifuge tube and spiked with 0.1 mL internal standard in methanol. Final internal standard concentration was 20 µg/L in a 90% water 10% methanol solution. Samples were then vortexed and 300 µL was transferred to a polypropylene autosampler vial. Samples were stored at 4°C until analysis (within 2 weeks).

PFOS concentrations in the samples were analyzed on the Vanquish Binary ultrahigh performance liquid chromatography (UPLC), quadrupole-orbitrap tandem mass spectrometer (MS/MS; Exploris 120, ThermoScienific), based on the retention time (RT) and the exact mass of $[M–H]^-$, which was further verified via tandem MS, when needed. The limit of quantification (LOQ) of PFOS was estimated to be around 10 parts per trillion (ppt). The instrument had a delay column between pump and autosampler (HypersilGOLD, 1.9 µm, 175 Å, 3 × 50 mm) to separate any PFAS in the liquid chromatography (LC) system and solvents from the analytes. An Accucore RP-MS, 2.6 µm, 2.1 × 100 mm C18 column was used for UPLC separation of PFOS analytes. Mobile phase composition consisted of 2 mM ammonium acetate in high performance liquid chromatography (HPLC)-grade water and HPLC-grade acetonitrile. Sample injection volume was 10 µL. A constant flow of 0.2 mL/min was maintained in the column at 40 °C. The gradient began at 20% 2 mM ammonium acetate for the first 1.8 min then to 95% at 13.4 min, held at 95% for 0.5 min, back to 20% at 14.5 min, and then re-equilibrated at 3.5 min. The UPLC-HRMS/MS system was interfaced with a heated electrospray ionization source. The MS scan range was 100–1000 m/z with a resolution of 60,000, standard automatic gain control (AGC) target, 70% radiofrequency (RF) lens, maximum injection time auto, with EASY-IC run-start on. The spray voltage was 2,200 V, ion transfer tube temperature was 250°C, vaporizer temperature was 175 °C, and mild trapping was on. The sheath gas was 30 and aux gas 5 (arbitrary units). A targeted inclusion mass list with retention time windows was used for comparing the standard and sample fragmentation pattern with a 5-ppm mass tolerance. Raw UPLC-MS/MS data was analyzed by Xcalibur 4.4, TraceFinder 5.1 EFS, and Compound Discoverer 3.2 software.

2.3.6 Statistical Analyses

Linear regression models in R [139], were used to unravel potential relationships between feedstock type, pyrolysis temperature, and biochar physiochemical properties with PFOS removal. Gathered information from these linear regression models were used to build SEMs for determining which biochar physicochemical properties are most important in controlling PFOS sorption [140]. This SEM package in R has been widely used in ecology and natural resource fields to explain complex causal relationships among various variables [141-143], which is the scenario in our study involving 5 feedstock types, 3 pyrolysis temperature, and diverse physicochemical properties (section 2.4). Particularly, SEM enables us to generalize the considered properties and efficiency of all biochars to filter out which physiochemical properties of biochars may affect PFOS sorption. Like other multivariable analyses, SEM works the best when the variables of interest are normalized, so direct comparisons can be made. This was achieved by log transforming all data, including pyrolysis temperature and PFOS removal. To this end, biochar properties and performance can be compared using standard deviation rather than respective units, allowing direct comparison of which properties carry more weights for PFOS sorption. Three different SEMs were created to find the most likely influence of sorption between physiochemical properties, while the best model was discussed in depth. Explanation on PFOS removal, lowest Akaike Information Criterion (AIC) weight score, and strongest influence from pore structure were considered when choosing the best model.

2.4 Results and Discussion

2.4.1. Physicochemical Properties of Biochars

As expected, biochar was mostly comprised of carbon, with a carbon content ranging from 74.1% (switchgrass 700) to 95.6% (Douglas fir 900) (**Table 2.2 and Fig. 2.3**). Higher contents of nitrogen were observed in biochars produced from grass feedstocks compared to soft and hardwood feedstocks ($p < 0.05$) (**Table 2.2 and Fig. 2.3**). It is hypothesized this increased nitrogen content comes from the naturally higher nitrogen content of grass feedstocks compared to wood materials. For example, Bransby et al. (1998) found that switchgrass had nitrogen contents as high as 1.26% while Özcan et al. (2020) found that poplar only had 0.65% nitrogen. Except for the hardwood feedstocks, the hydrogen content exhibited an inverse relationship with pyrolysis temperature **(Table 2.2**) [144, 145]. The linear regression model analyses showed that there was no consistent statistical trend between pyrolysis temperature and feedstock type with contents of other elements (e.g., S).

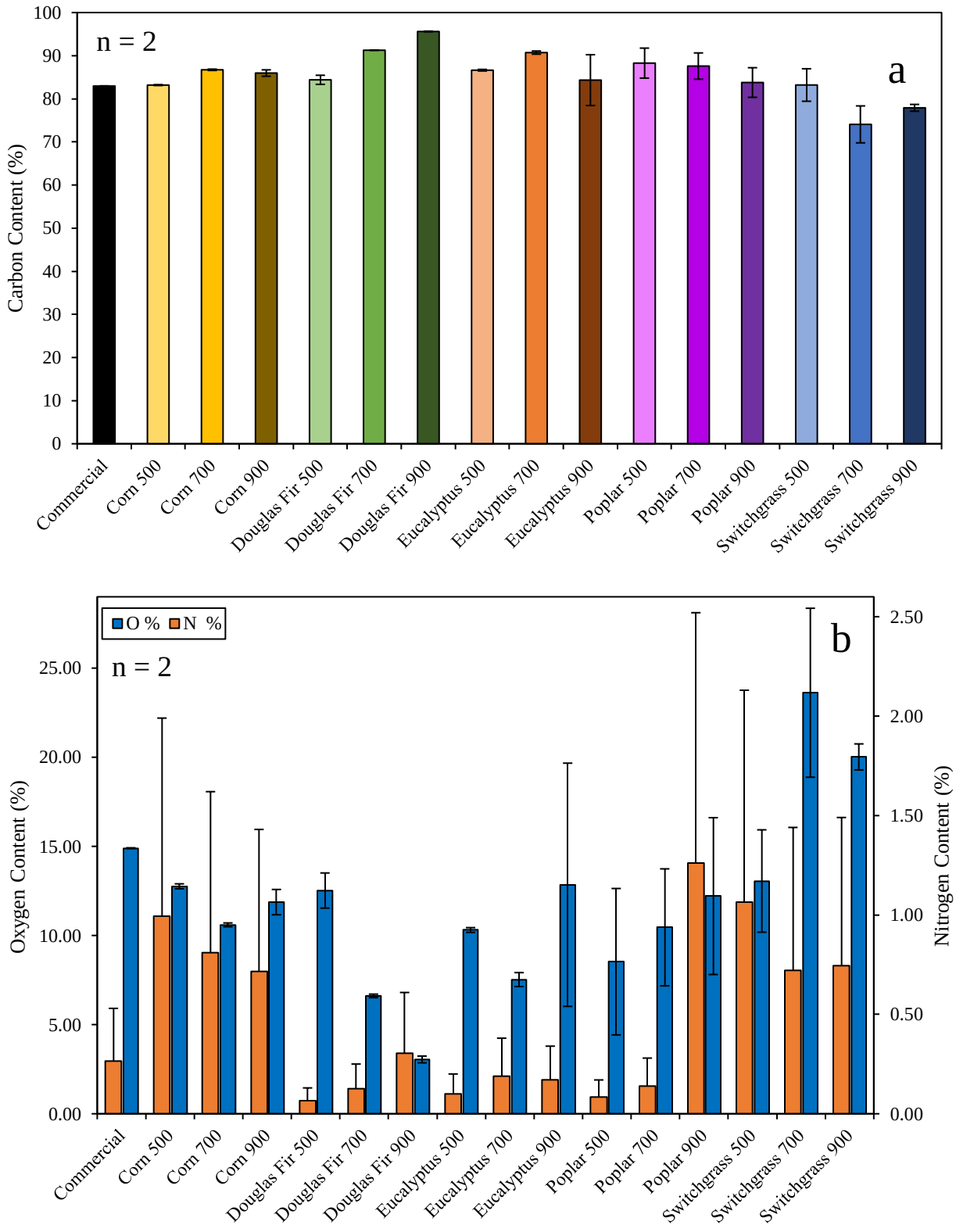

Figure 2.3. Elemental composition of the 16 biochars used in this study, including **(a)** carbon content (%) and **(b)** hydrogen, nitrogen, sulfur, and oxygen contents (%). The error bars represent the standard deviations from duplicate analysis of each biochar sample.

Table 2.2. The production yield, pH, SSA, pore volume, pore diameter, pore diameter/pore volume ratio, and carbon (C), hydrogen (H), nitrogen (N), and sulfur (S) contents of the 16 biochars used in this study.

Biochar sample	PT (°C) [a]	PY (%) [b]	pH	SSA (m^2/g) [c]	PV (cm^3/g) [d]	PD (nm) [e]	PD/PV ($nm/cm^3/g$) [f]	C (%)	H (%)	N (%)	S (%)
Corn 500	500	40.8 ± 7.3	6.82 ± 0.03	56.7	0.117	9.18	78.8	83.2	3.02	1.00	0.04
Corn 700	700	33.8 ± 8.1	6.78 ± 0.05	112	0.119	4.00	33.7	86.7	1.83	0.81	0.03
Corn 900	900	21.8 ± 4.4	6.85 ± 0.15	33.6	0.070	33.5	476	86.0	1.36	0.72	0.07
Douglas fir 500	500	38.1 ± 5.3	5.91 ± 0.00	163	0.122	2.70	22.2	84.4	2.99	0.07	0.02
Douglas fir 700	700	27.9 ± 9.0	6.00 ± 0.08	453	0.107	12.8	120	91.3	1.98	0.13	0.01
Douglas fir 900	900	24.1 ± 13	6.09 ± 0.11	410	0.124	10.7	86.2	95.6	0.98	0.31	0.06
Eucalyptus 500	500	51.0 ± 13	6.16 ± 0.01	379	0.117	8.35	71.3	86.6	2.94	0.10	0.01
Eucalyptus 700	700	34.0 ± 5.1	6.7 ± 0.07	134	0.090	7.83	86.9	90.7	1.55	0.19	0.02
Eucalyptus 900	900	19.9 ± 9.5	6.61 ± 0.09	429	0.099	12.0	122	84.3	2.63	0.17	0.02
Poplar 500	500	34.8 ± 16	6.47 ± 0.05	292	0.238	2.59	10.9	88.3	3.09	0.09	0.02
Poplar 700	700	27.1 ± 15	6.51 ± 0.06	393	0.129	14.6	114	87.6	1.79	0.14	0.02
Poplar 900	900	20.9 ± 8.8	6.72 ± 0.09	60.9	0.073	8.02	110	83.8	2.68	1.26	0.07
Switchgrass 500	500	41.6 ± 10	7.03 ± 0.07	121	0.087	16.6	191	83.2	2.59	1.07	0.09
Switchgrass 700	700	30.8 ± 8.9	7.02 ± 0.04	232	0.099	18.8	190	74.1	1.53	0.72	0.06
Switchgrass 900	900	22.4 ± 8.8	5.92 ± 0.12	60.9	0.082	22.7	276	77.9	1.25	0.75	0.07
Commercial	1,000	n/a	8.60 ± 0.01	471	0.184	8.94	48.5	83.0	1.71	0.27	0.17

[a] Pyrolysis temperature. [b] Production yield. [c] BET specific surface area (SSA). [d] BJH pore volume (PV). [e] BJH pore diameter (PD). [f] pore diameter/pore volume ratio.

Interestingly, all biochar suspensions were measured neutral or slightly acidic, except for the commercial biochar with an unknown production method. Ball milling of biochar is hypothesized to enhance CO_2 exposure, making the biochars more acidic. However, this hypothesis was ruled out since there was no significant difference of pH (ΔpH = 0.01; n = 3) for the Douglas fir 700 biochar with vs. without ball milling. Similar pH results were reported for other biochars produced from Douglas fir feedstock [146]. Linear regression model results indicated there was no significant difference of biochar pH with pyrolysis temperature and feedstock type in this study.

SSA and pore structure of biochar are important properties affecting PFAS sorption. A biochar with higher SSA has more sites for PFOS sorption, but other surface features such as pore diameter and pore volume are also important. As shown in **Table 2.2**, most biochars produced at 700°C exhibited the highest SSA, which is inconsistent with the notion that higher pyrolysis (e.g., 900°C) produces biochars with higher SSA. We speculate that ball milling did not proportionally increase the SSA of biochar as a function of pyrolysis temperature, rather feedstock property (**Table 2.1**), pyrolysis temperature, and ball milling co-determined the SSA of biochars (**Table 2.2**). Nevertheless, woody feedstocks (e.g., Douglas fir and poplar) generally produced biochars with a much higher SSA, compared to biochars produced from other feedstocks (i.e., corn cob and switchgrass) (**Table 2.2**).

Biochar hydrophobicity is thought to be influenced by several factors such as porosity, particle size, alkalinity, pyrolysis conditions, feedstock type, O/C molar ratio, and functional groups present. [147-152]. All biochars had a contact angle greater than 90° (**Fig. 2.4**), meaning their

surfaces are overall hydrophobic. The Douglas fir biochars were significantly more hydrophobic, while the corn biochars were significantly less hydrophobic at the $p < 0.05$ level. Biochars produced at 700°C had a significantly lower contact angle than biochars produced at 500 and 900°C ($p < 0.05$). Overall, the hydrophobic propensity of biochar surfaces is expected to sorb hydrophobic PFAS molecules (C–C backbone) via hydrophobic interactions [153].

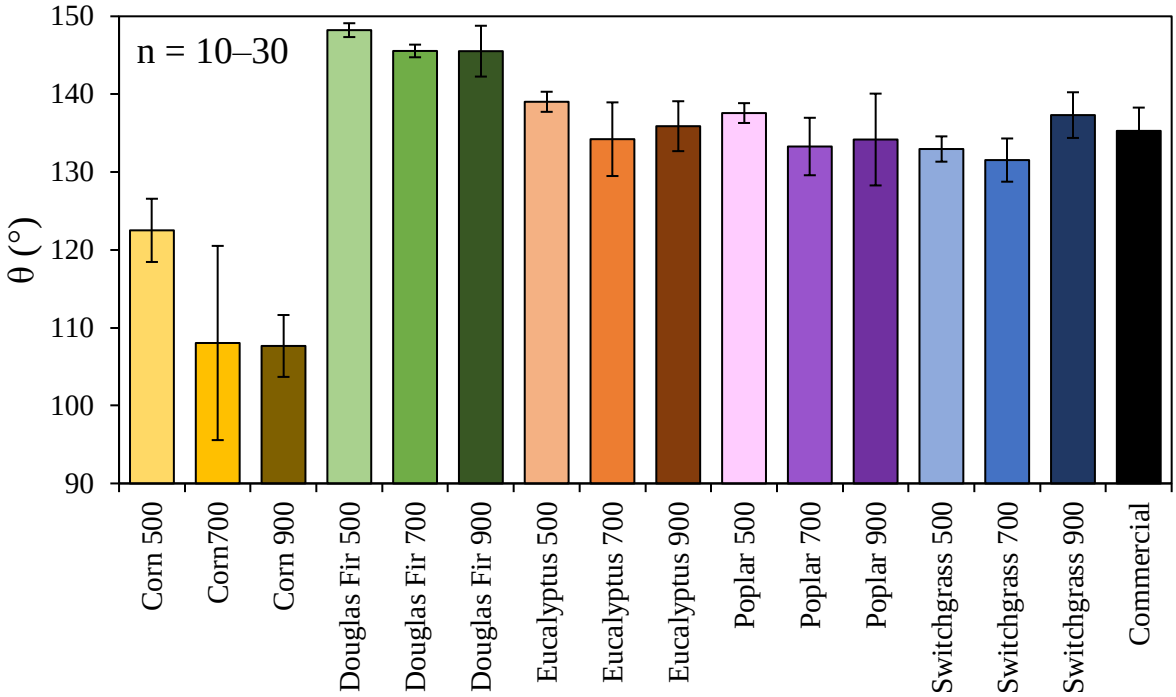

Figure 2.4. The contact angle (θ) of 16 biochars. A contact angle above 90° indicates hydrophobicity. The error bars represent the standard deviations between samples and the number (n) indicates total effective measurements.

All biochars have a point of zero charge (pH_{PZC}) ranging from pH 2–4 (**Fig. 2.5**). At environmentally relevant pH conditions (e.g., 5–9), the biochars were negatively charged (e.g., –25.0 to –58.1 mV), indicative of electrostatic repulsions between negatively charged biochars and anionic PFOS **(Fig. 2.5)**. The Douglas fir, switchgrass, and commercial biochars were less negatively charged compared to corn and poplar-derived biochars ($p < 0.05$), suggesting a less electrostatic repulsion between these three biochars with PFOS. However, the differences of zeta

potential among the biochars did not exhibit a significant effect on PFOS (e.g., no significant relationship between zeta potential and PFOS removal at $p > 0.05$). Therefore, zeta potential was not considered in the SEM analysis. Similarly, feedstock type and pyrolysis temperature were found to have a negligible impact on the zeta potential of biochars ($p > 0.05$), further suggesting that zeta potential should be ruled out during the SEM analysis.

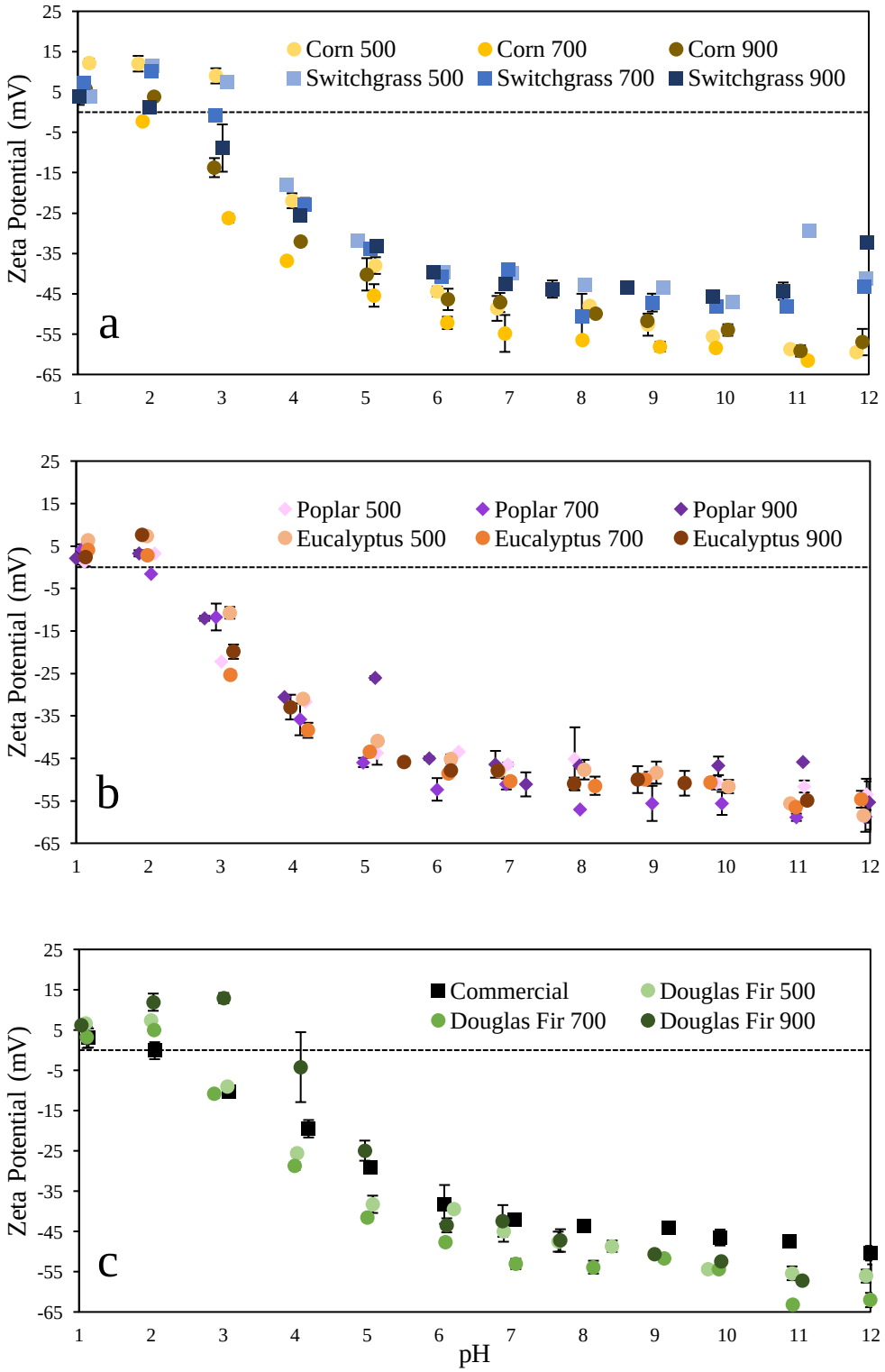

Figure 2.5. Zeta potential of (**a**) grass-, (**b**) hardwood-, and (**c**) softwood-derived biochars used in this study. The error bars represent the standard deviations from duplicate experiments.

The surface functional groups of biochars after pyrolysis were comprised of carbon, oxygen, and hydrogen. Similar to Keiluweit et al. (2010), we found an increasing degree of condensation across the three pyrolysis temperatures in this study [154]. Approximately 10 different characteristic peaks were identified for the produced biochars (**Fig. 2.6** and **Table 2.3**). These 10 characteristic peaks were at 3650-3600 cm^{-1} (free O–H stretching of phenolic and alcoholic –OH); 3500-3100 cm^{-1} (water, H-bonded hydroxyl (-OH) groups); 3100-3000 cm^{-1} (C–H stretching of substituted of aromatic C); 3000-2900 cm^{-1} (asymmetric C–H stretching of aliphatic CH_x); 1750-1700 cm^{-1} (C=O stretching of ketones and carboxylic acids); 1600-1550 cm^{-1} (C=C and C=O stretching of carboxylic carbon); 1350-1100 cm^{-1} (O-H and α-CH_2 bending); 1257 cm^{-1} (C-O-C groups and aryl ethers); 1350-1100 cm^{-1} (C–O–C symmetric stretch in ester groups of cellulose and hemicellulose); and 881–683 cm^{-1} (various types of substituted C-H bending) [154-157]. More importantly, biochars produced at low pyrolysis temperatures, particularly at 500°C, retained most of these functional groups (**Fig. 2.6** and **Table 2.3**). Only two characteristic peaks were identified on the surfaces of the commercial biochar at 1584 cm^{-1} (C=C stretching of aromatic components and C=O stretching of conjugated ketones and chinons) and 1212 cm^{-1} (C-O stretching of alkyl aryl ether) [155, 156] (**Fig. 2.6**). This could be due to the high pyrolysis temperature (1,000°C) for producing the commercial biochar. Biochars negative surface charge can be attributed to surface functional groups. Specifically, phenolic and carboxylic groups on the biochars surface are regarded as major contributors responsible for the negative surface charges of biochars observed in this thesis. Carboxylic functional groups are the dominant functional groups on biochars surface **(Table 2.3 and Fig 2.6)**.

Table 2.3. Surface functional groups of biochars determined by the Fourier-transform infrared (FT-IR) spectroscopy analysis.

Wavenumber (cm^{-1})	Characteristic Vibration	Functionality	Structure
3650-3600	'free' O-H stretching	alcoholic and phenolic -OH, not hydrogen bonded [154, 158]	
3500-3100	phenolic H-bonded hydroxyl -OH	water, H-bonded hydroxyl (-OH) groups [154, 158]	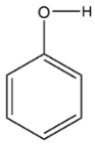
3100-3000	substituted aromatic C	[154, 159]	
3000-2900	symmetric C-H stretching	aliphatic CH_x [154, 160]	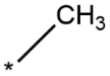
1750-1700	C=O stretching	mainly carboxyl with traces of aldehydes, ketones, and esters [154, 161-163]	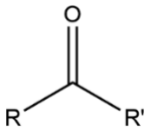
1600-1550	C=O and C=C stretching	C=O and C=C stretching of carboxylic [155, 156]	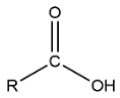
1500-1250	α-C-H_2 bending	alphatic -CH_3 deformations [158, 164]	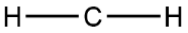
1350-1100	N-H bending	N-H stretching of amine groups [86]	
1350-1100	C-O-C symmetric esters	C-O stretching of esters [155, 156]	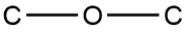
881-683	C-H deformation	aeromatic CH out-of-plane deformation and less substituted rings at lower wavenumbers [165, 166]	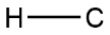

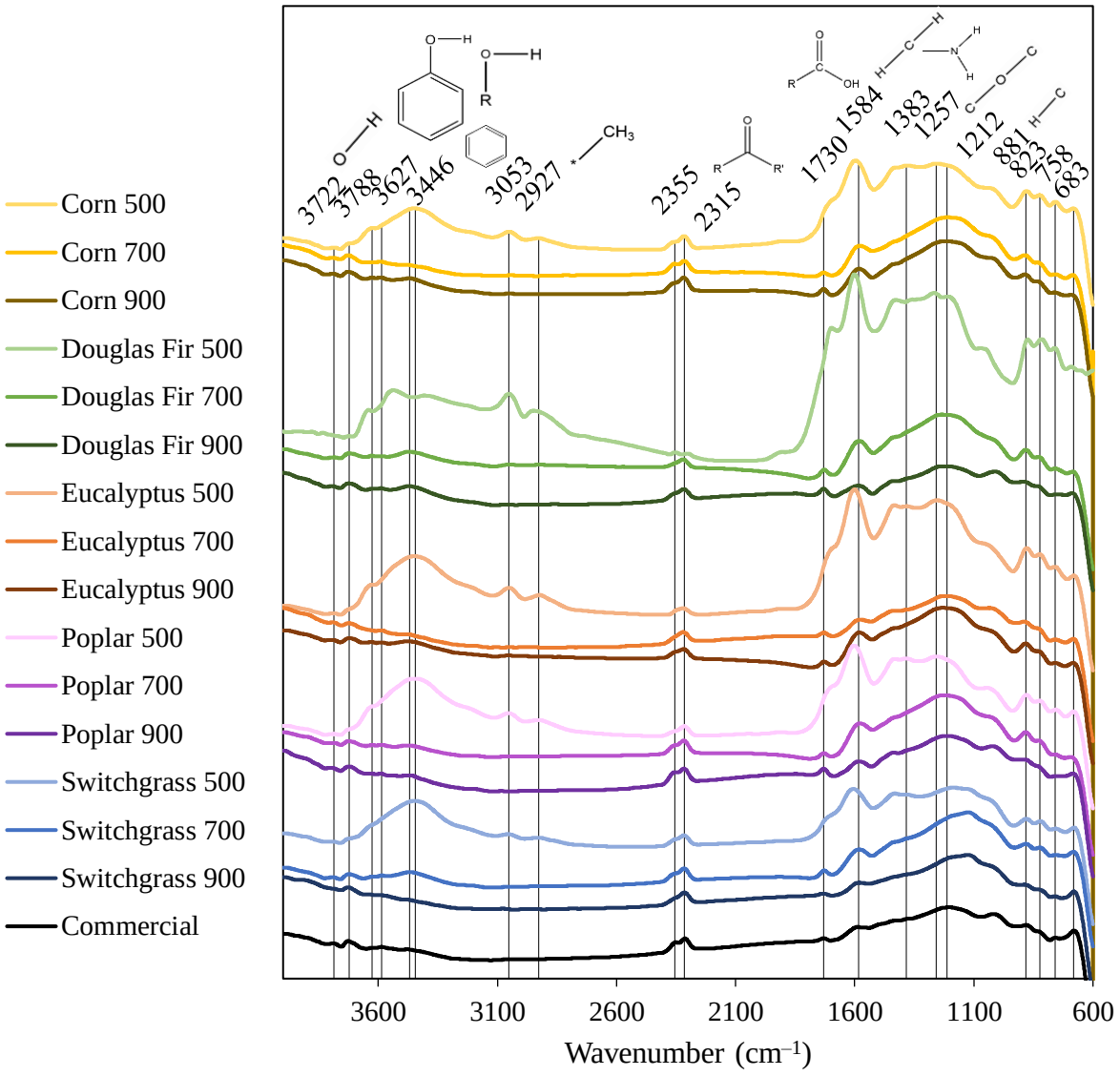

Figure 2.6. Fourier-transform infrared (FT-IR) spectra of the 16 biochars. Triplicate experiments were conducted for each biochar sample.

The XRD spectra showed that five different peaks were identified for the 16 biochars (**Fig. 2.7**). The first peak around 9° is representative of oxygen atoms that may intercalate into interlayer space, which is bonded to the graphite planar surface during the pyrolysis process [167]. A wide peak near 25° is indicative of tridymite and graphitic platelets [168]. Peaks on the downslope of the broad tridymite graphitic peak (26–28°) represent the (0, 0, 2) plane of biochar's graphitic

structure and the last broad peak at 45° signifies short-ranged order in graphene oxide layers [167, 169]. Overall, the intensity of the broad peak around 45° (graphitic platelets and short ranged order in graphene oxide layers) increased as the pyrolysis temperature was increased (**Fig. 2.7**). This suggests that the carbonaceous structure in biochars became more ordered at higher pyrolysis temperatures.

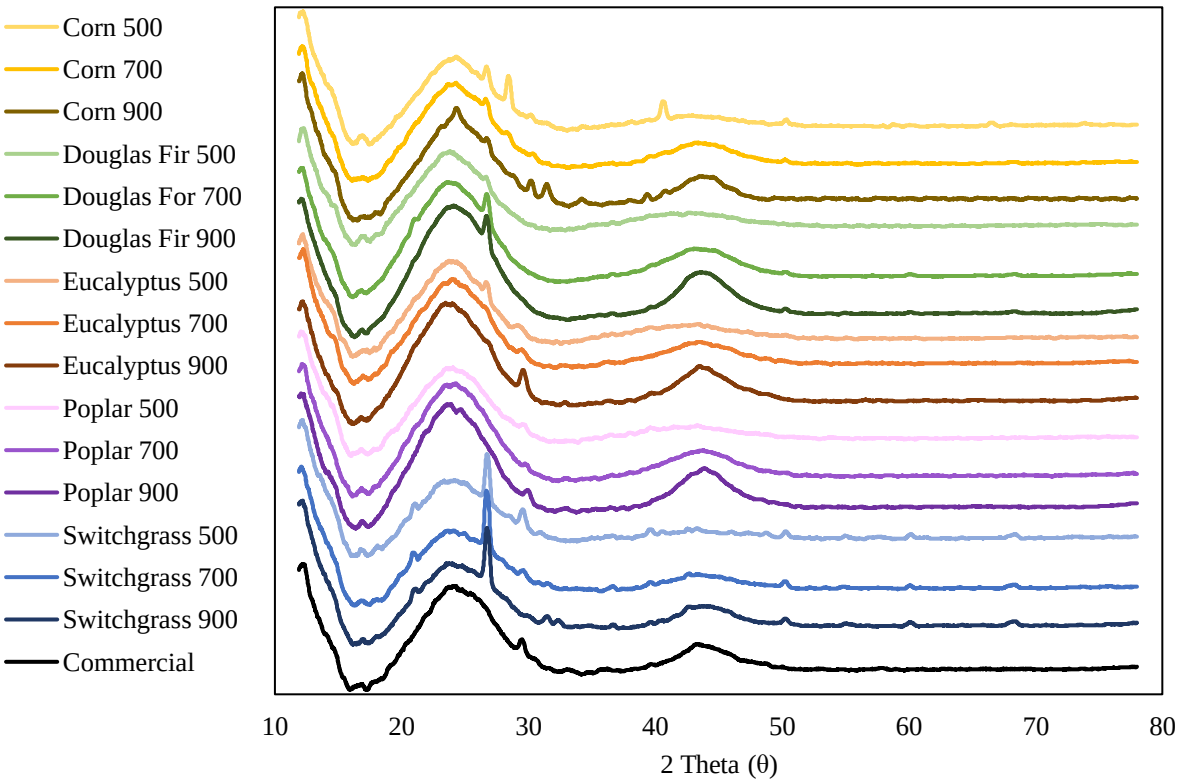

Figure 2.7. X-ray diffraction (XRD) spectra of the 16 biochars used in this study. With increasing pyrolysis temperature (from 500 to 900°C), the aromatic carbon became more ordered, which is reflected by the increased intensity at higher pyrolysis temperatures.

Overall, different feedstocks and pyrolysis temperatures tended to produce a wide variety of biochars with different physicochemical properties. All biochars were rich in carbon (74.1–95.6%), but nitrogen content in grass-derived biochars were higher than that of biochars derived from woody feedstocks (**Table 2.2**). The pH of biochars was neutral or slightly acidic, while the commercial biochar was alkaline (**Table 2.2**). SSA is a function of pyrolysis temperature,

feedstock properties, and ball milling but woody feedstocks produce biochars with higher SSA than grass feedstocks. All produced biochars were hydrophobic, with corn feedstocks producing the biochars with the lowest hydrophobicity while Douglas fir biochars having the greatest hydrophobicity. Surface charge of biochars ranged from –25.0 to –58.1 mV at environmentally relevant pH conditions, suggesting electrostatic repulsions between biochars and PFOS. All biochars shared similar characteristic peaks based on FT-IR and XRD spectra, while peak intensities are reduced as a function of pyrolysis temperatures.

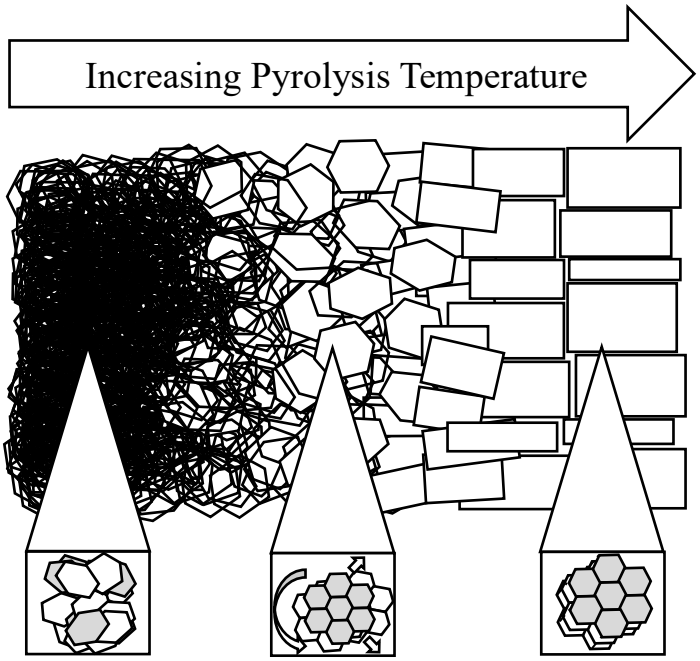

Figure 2.8. Proposed schematic showing how increasing pyrolysis temperature affects the ordering of carbon and graphite sheets of the biochars.

2.4.2. PFOS sorption by Biochars

Batch sorption experiments were used to investigate the removal efficiency (%) of PFOS by the 16 biochars. The Douglas fir 900, poplar 900, and commercial biochars removed >95% of the added 500 µg/L PFOS from solution (**Fig. 2.9**). The linear regression model analyses showed that pyrolysis temperature was a significant factor for PFOS removal. For example, for every

1°C increase in the pyrolysis temperature, we found a 0.052% (±0.051%; 95% CI) increase in PFOS removal ($p < 0.05$; $r^2 = 0.29$). However, biochar produced at one pyrolysis temperature did not significantly outperform another in terms of PFOS removal and there was not one feedstock type that systematically outperformed other feedstock types for PFOS removal. While biochars derived from woody feedstocks at 900°C did perform significantly better than other biochars, removing 28.24% (±13.99%; 95% CI) more PFOS than other biochars in this study ($p < 0.05$; $r^2 = 0.59$) (**Fig. 2.9**).

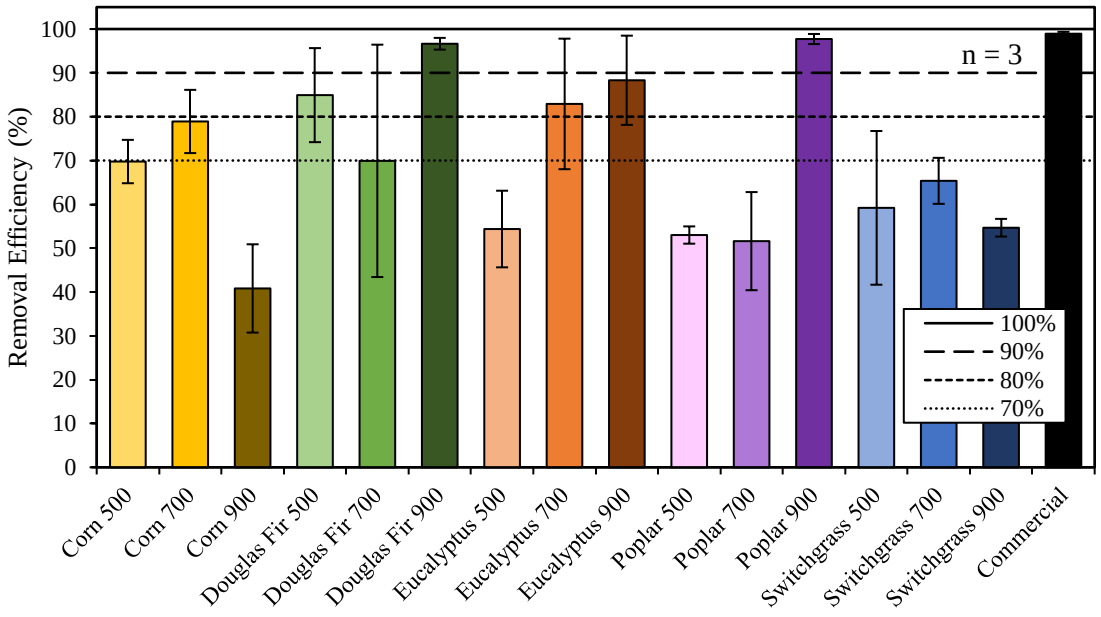

Figure 2.9. PFOS removal efficiency (%) by the 16 biochars. Experimental conditions include 500 µg/L PFOS, 100 µg/L biochar, and 1 mM NaCl. The error bars represent the standard deviations among triplicate experiments.

2.4.3 PFOS Sorption Mechanisms

Biochar properties vary significantly due to the diversity of their respective feedstocks and pyrolysis temperatures, making trend analysis difficult. The corn 900 biochar was found to be an extreme outlier in several physiochemical properties analyzed (e.g., SSA, pore diameter, pore volume, and pore diameter/pore volume ratio) and poplar 500 biochar was also an extreme

outlier with respect to pore volume and pore diameter/pore volume ratio, so both biochars were removed from the dataset before SEM construction. Removing these two biochars allowed for better trend analyses among dependent variables (e.g., when corn 900 and poplar 500 were removed, the r^2 comparing PFOS removal to pore diameter/pore volume ratio was increased from 0.12 to 0.27).

Feedstock type and pyrolysis temperature are two independent variables in this study, meaning that the selection of a given feedstock at a pyrolysis temperature dictates the outcome of all other dependent variables (e.g., physicochemical properties like SSA, hydrophobicity, and thus PFOS removal ability). However, categorical variables would not have worked in this SEM due to the small sample size, so feedstock type was also removed from the model construction. Given that pyrolysis temperature is an independent variable, it does not have a direct impact on PFOS removal. Rather, it affects the individual biochar properties, which in turn affect PFOS sorption. A path coefficient connecting pyrolysis temperature and PFOS removal enables us to capture the unexplained variables in the model (e.g., zeta potential and pH), which helps us to explain the holistic influence of pyrolysis temperature on PFOS removal, as shown in **Fig. 2.10**.

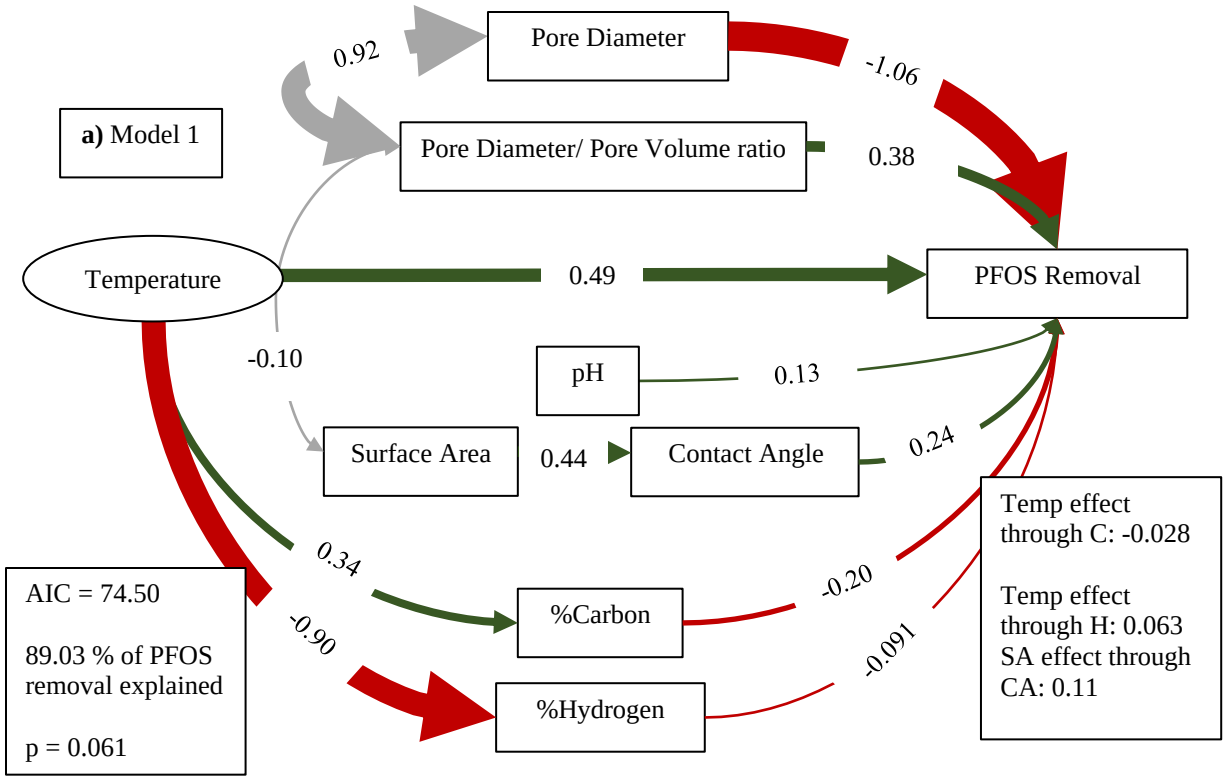
a) Model 1
Pore Diameter
Pore Diameter/ Pore Volume ratio
Temperature
PFOS Removal
pH
Surface Area
Contact Angle
%Carbon
%Hydrogen
0.92
-1.06
0.38
0.49
-0.10
0.13
0.44
0.24
0.34
-0.90
-0.20
-0.091
AIC = 74.50
89.03 % of PFOS removal explained
p = 0.061
Temp effect through C: -0.028
Temp effect through H: 0.063
SA effect through CA: 0.11

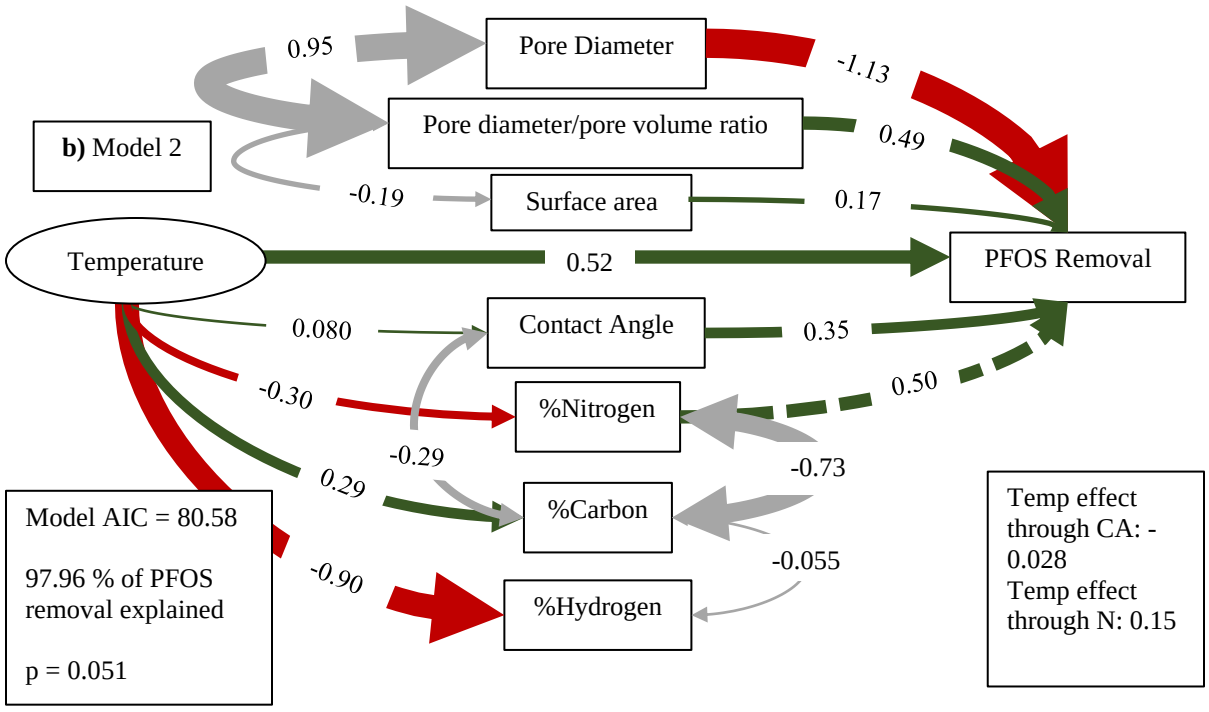
b) Model 2
Pore Diameter
Pore diameter/pore volume ratio
Surface area
Temperature
PFOS Removal
Contact Angle
%Nitrogen
%Carbon
%Hydrogen
0.95
-1.13
0.49
-0.19
0.17
0.52
0.080
0.35
0.50
-0.30
-0.29
-0.73
0.29
-0.90
-0.055
Model AIC = 80.58
97.96 % of PFOS removal explained
p = 0.051
Temp effect through CA: -0.028
Temp effect through N: 0.15

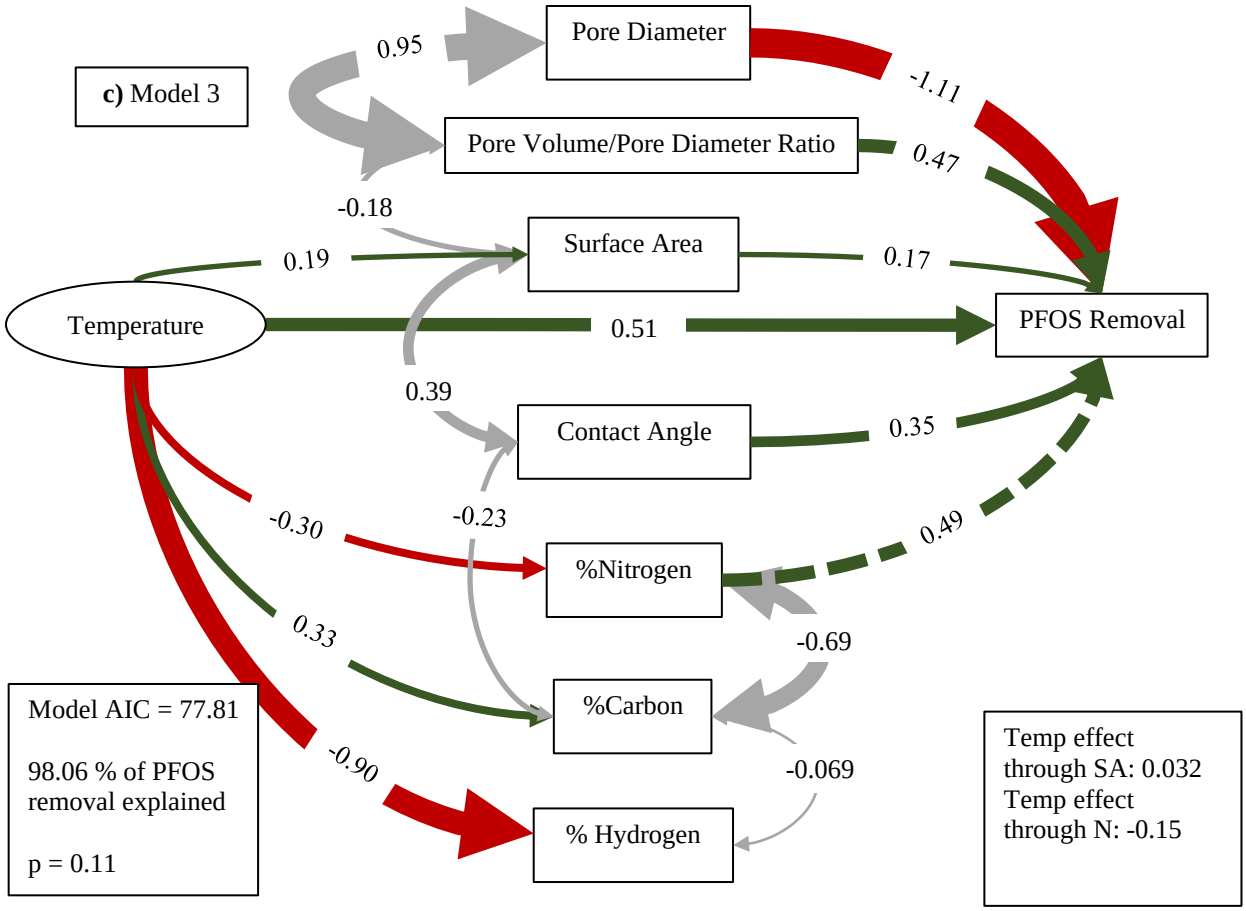

Figure 2.10. SEM is a form of multivariable analysis, showing the impact of biochars physiochemical properties on PFOS sorption. Green arrows indicate a positive relationship between biochar properties and PFOS sorption, while the red arrows indicate a negative relationship and gray arrows indicate correlations between biochar properties. Numbers on the arrows represent values of each standardized path coefficient, and the arrow width is proportional to the relationship strength (thicker arrow = stronger relationship). Models were constructed based on hypothesized relationships between physiochemical properties and PFOS removal. Specifically, **a)** Model 1 was built based on the hypothesis that temperature had a minimal impact on biochar properties except for elemental contents. In this model, pH was also included since it was hypothesized to have a big impact on PFOS sorption. However, there was a weak influence by pH according to Model 1, therefore, pH was removed in the subsequent models. **b)** Model 2 was built under the hypothesis that temperature had a marked impact on all physiochemical properties except for surface morphology, since surface morphology is drastically changed after ball milling. This model did have a higher AIC score than Model 1, but also had a much higher explanation for PFOS removal, increasing from 89.03% to 97.96%. In Model 2, temperature was not found to have a strong influence on contact angle, so this relationship was removed in the final model. **c)** The final model was based heavily off Model 2, but rather than temperature weakly influencing contact angle, it was hypothesized that temperature influenced surface area, which was then correlated with biochars hydrophobicity. This model was determined to be the best model overall since it had the highest explanation for

PFOS removal at 98.06%, and an acceptable AIC score of 77.81. All models had non-significant p-values (the null hypothesis of an SEM is a model with a better fit cannot be produced), meaning we fail to reject the null-hypothesis, and a better model is not likely to be produced. However, Model 3 had the most non-significant value, further justifying it is the best produced model. The dashed green line between pyrolysis temperature and PFOS removal represents pyrolysis temperatures indirect effect on PFOS removal. The total effects of pyrolysis temperature through SSA and nitrogen content on PFOS removal can be found in the bottom right corner of the figure.

SEM construction in R is done manually based on results from various linear models. Theoretically, there is a countless number of SEMs that could be constructed, so linear models and physiochemical property-PFOS interaction hypothesis were used to determine the most likely scenario for sorption mechanisms. The overarching concept involves temperature influencing most if not all biochar properties which in turn influences how well a biochar performs for PFOS sorption. Thus, you will notice paths on all models flow from left to right except for paths representing correlations. For example, temperature is the independent variable in this study, meaning no other variables can affect the pyrolysis temperature at which biochar is produced. Between all three SEMs constructed, you will notice all paths point away from temperature, influencing physiochemical properties which are dependent variables. Similarly, PFOS removal cannot affect the physiochemical properties of a biochar, so arrows point away from physiochemical properties and towards PFOS removal.

Generally, it is not hypothesized that biochar physiochemical properties influence one another, except for model **Fig. 2.10a**, where it was proposed that SSA influences biochars contact angle. However, linear models showed that many biochar properties were found to be relatively correlated with one another, so various correlations between physiochemical properties were explored in SEM construction. Here the best example can be found in the strong correlation

between pore diameter and pore diameter/pore volume ratio. It is clear these two properties would be correlated since pore diameter/pore volume ratio includes pore diameter in the calculation. Adding this correlation between variables allows the SEM package in R to determine path coefficients more precisely.

To some extent, all physiochemical properties likely have an influence on PFOS sorption, but some play a larger role than others. Again, linear models were used to help determine which physiochemical properties have had more influence than others and paths were constructed accordingly. For example, Hydrogen was found to be correlated with PFOS removal in a linear model but was found to have a weak influence on PFOS sorption when considered within the SEM **(Fig. 2.10a)** and was not included in the construction of other SEMs. However, hydrogen was still heavily influenced by pyrolysis temperature and weakly correlated with C (%) so it was crucial for model construction.

Although AIC is an important representation of how well a model fits, AIC values are highly relative depending on the data and the goal of this study is to explain PFOS removal. Pore structure was also found to be a key factor for PFOS sorption across all three SEMs, and therefore, model 3 (**Fig. 2.10c**) is likely still the best SEM constructed since it still has a relatively low AIC, a higher explanation for PFOS removal, and a high influence from pore structure. All three models exhibited a non-significant p-value (the null hypothesis of the model is the probability a model with a better fit could be produced) at $p < 0.05$ level.

Although some physiochemical properties of biochars carry more weight for PFOS sorption than others, it is ultimately a combination of properties that differentiates biochars with higher PFOS removal efficiency from the rest. Notably, pore diameter of biochars was found to be the most important factor for PFOS removal. Specifically, for every 1 standard deviation decrease in pore diameter, there is a 1.11 standard deviation increase in PFOS removal (**Fig. 2.10**), suggesting smaller pore diameters have greater PFOS removal efficiency. Another way to interpret the data further is to look at the pore diameter/pore volume ratio (**Fig. 2.10**). Specifically, for every 1 standard deviation increase in pore diameter/pore volume ratio, there was a 0.47 standard deviation increase in PFOS removal. These findings clearly suggest the importance of biochar pore structure in PFOS sorption. Logically, there should be a size threshold with respect to how small pore openings can be for a biochar to effectively sorb PFAS. Similarly, there also should be a size threshold in how large a pore diameter can be for effective sorption. PFOS have a size of about 1.32 nm [170], so pores on the smaller end of the observed data likely struggle to sorb PFOS within **(Table 2.2).** We propose that biochar having an ideal pore diameter range of approximately 7.5–11 nm can effectively sorb PFOS via the 'trapping' mechanism, making it difficult for PFOS to desorb once it is sorbed within the ideal pore structures, but protects the sorbed molecules from water turbulence unlike wider pores (**Fig. 2.11**).

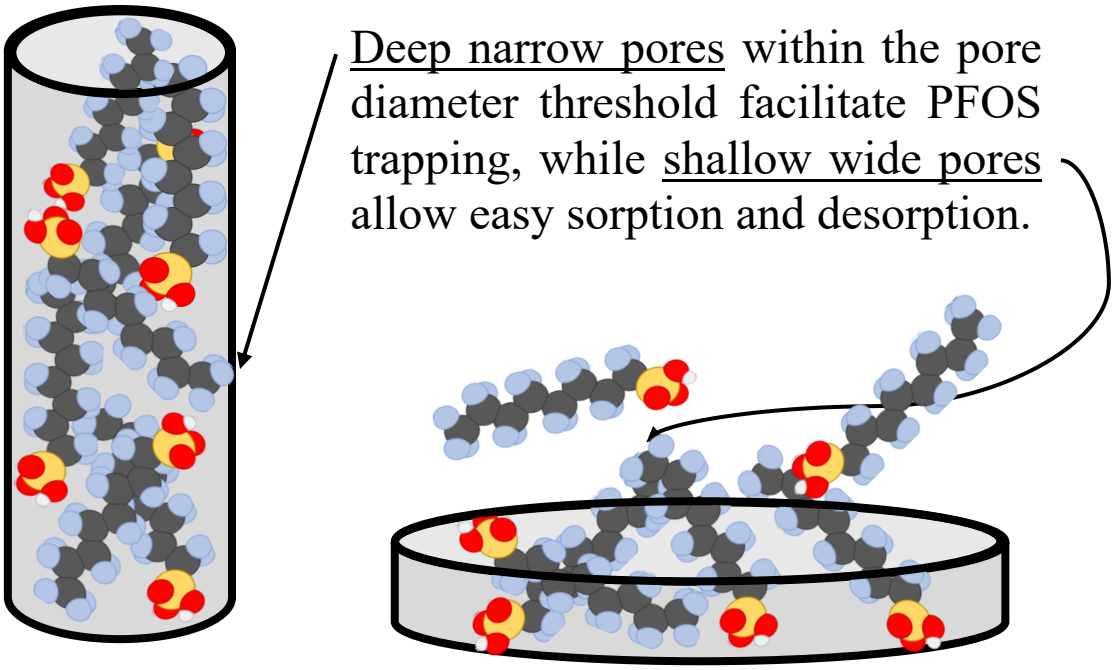

Figure 2.11. A schematic showing the ability of biochar pore structure to trap PFOS, preventing desorption once already sorbed. Biochars with a pore diameter that is too small cannot allow enough PFOS to percolate into pores while biochars with larger pore diameters do not have the ability to trap PFOS.

This 'trapping' effect for PFOS sorption is expected to be enhanced if the pore volume is larger, providing more space for PFOS molecules to sorb within the pore structures, i.e., the ideal pore diameter/pore volume ratio being approximately 50 to 150 ($nm/cm^3/g$). This hypothesis is supported by the data of pore diameters and pore diameter/pore volume ratios in **Table 2.2**, as well as the PFOS removal efficiency by biochars (**Fig. 2.9**). For example, the Douglas fir 900, poplar 900, and commercial biochars all fall within the proposed ideal pore structure range, that also exhibited the greatest removal efficiency for PFOS. The Douglas fir 500 and corn 700 biochars had smaller pores, while all three switchgrass-derived biochars had larger pores (**Table 2.2**). These five biochars showed less removal efficiency for PFOS, compared to the Douglas fir 900, poplar 900, and commercial biochars.

While pore structure of biochar is observed to play a crucial role for PFOS sorption, other physicochemical properties of biochars should be scrutinized as well. For example, both corn 500 and eucalyptus 500 biochars fall within the same ideal pore structure range (**Table 2.2**), but neither biochars showed high removal efficiency for PFOS, as compared to the Douglas fir 900 or commercial biochars (**Fig. 2.9**). However, the Douglas fir 900 and commercial biochars had the highest SSA of all biochars examined, while the corn 500 and eucalyptus 500 biochars showed relatively low SSA (**Table 2.2**), partially explaining the observed difference in PFOS removal efficiency (**Fig. 2.9**). For example, for every 1 standard deviation increase in biochar's SSA, there is a 0.17 standard deviation increase in PFOS removal (**Fig. 2.9**). Overall, the Douglas Fir 900 and commercial biochars fall within the proposed ideal pore structure range and had some of the highest SSA. These findings clearly suggest the importance of both pore structure and SSA for PFOS removal from water. Hydrophobicity also plays an appreciable role in PFOS sorption (**Fig. 2.4**). For every 1 standard deviation increase in biochar's contact angle, there is a 0.35 standard deviation increase in PFOS removal, again supporting the notion that PFOS is removed through hydrophobic interactions [153]. Given that all biochars were hydrophobic, it is likely that some biochars without the ideal pore structures but having high SSA still have the ability to effectively sorb PFOS through hydrophobic interactions (e.g., Douglas fir 500 biochar; **Fig. 2.4**).

Elemental composition of biochar varied greatly with pyrolysis temperature (**Table 2.2** and **Fig. 2.3**), but S and O contents were not included into the SEM analysis due to their low content (S) and high correlation with other variables (O), respectively. Interestingly, nitrogen (N) content was found to have the largest impact of all elements analyzed on PFOS removal (**Fig. 2.10**). The

positively charged N-containing groups (e.g., amine groups) of biochars can strongly sorb negatively charged PFOS via electrostatic attractions, accounting for a higher removal efficiency of PFOS by biochars with higher N contents (**Fig. 2.3** and **Table 2.3**) [86, 153]. While pyrolysis temperature did not have a direct impact on PFOS sorption, it can directly affect physiochemical properties of biochars that impact PFOS sorption. In the SEM analysis, the pyrolysis temperature arrow represents measured factors influencing sorption that were excluded from SEM (e.g., pH, zeta potential, and O content). Again, not all the measured physicochemical properties of biochars were included in the SEM analysis, due to small sample size and singularity errors during model creation. Similarly, surface functional groups and surface crystallography were precluded from the SEM analysis since they did not have quantitative results. However, biochars derived from woody feedstocks with less functional groups (**Fig. 2.6**) and higher carbon structure ordering (**Figs. 2.7–2.8**) exhibited high removal efficiency for PFOS (**Fig. 2.9**). Whereas PFOS removal by grass-derived biochars was favored from a lower pyrolysis temperature and a higher retention rate of N-containing functional groups. **(Figs. 2.6 and 2.7-2.9)**.

The SEM analysis with the highest explanation of PFOS removal (98.1%) and relatively low AIC score (77.8) was selected as the best model (**Figs. 2.9**). The other two SEM analyses showed 89.0% and 98.0% explanation of PFOS removal with AIC scores of 74.5 and 80.6, respectively (**Fig 2.9**). All the three SEMs showed high explanation for PFOS removal and acceptable AIC scores, but Model 3 in **Fig. 2.9** was the best since the correlation coefficients explained well how biochar physicochemical properties dictate PFOS removal, as elucidated above.

2.5 Conclusion

Our findings provide compelling evidence to support the notion of using biochar as a sorbent to remove PFOS from water. Mechanistically, pore diameter, pore diameter/pore volume ratio, contact angle, and nitrogen content were identified as key factors controlling PFOS removal. Moving forward, biochars that have pore diameters between 7.5 to 11 nm, pore diameter/pore volume ratios between 50 to 150 ($nm/cm^3/g$), large SSA, and high hydrophobicity may have high ability to remove PFOS from water. The Douglas fir 900, poplar 900, and commercial biochars can effectively remove >95% of PFOS at 500 µg/L under 1 mM NaCl. Moving forward, more research is needed to investigate how well biochars can perform to remove PFAS from environmentally relevant conditions (i.e., water matrices with organic matter, dissolved ions, and multiple PFAS compounds), but the current outlook for biochar as a potential PFAS sorbent appears promising and cost-effective.

Chapter 3. PFAS Sorption by Biochars Under Environmentally Relevant Conditions

3.1 Abstract

Our knowledge on how environmental factors affect PFAS sorption by biochars in water remains incomplete. In this study, four biochars pyrolyzed from Douglas Fir, Eucalyptus, Poplar, and Switchgrass feedstocks at two different temperatures (700 and 900 °C) were used to investigate the impacts of pH, and salt and humic acid concentrations on biochar sorptive performance of C4–C8 PFAS compounds. A commercial biochar was also included for comparison. An artificial groundwater solution was ultimately utilized to assess biochars ability for PFAS removal under real world water treatment scenario. Batch sorption experiments showed that PFAS sorptive efficiency by Douglas Fir 900 (Douglas Fir and 900 are the feedstock type and pyrolysis temperature, respectively) and commercial biochars were both negatively impacted by changes in pH and humic acid concentrations. However, the negative change degree was much less for commercial biochar (vs. Douglas fir 900 biochar). Salts were found to increase sorption due to their charge screening effect, increased PFOS aggregation, and ability to lower PFOS solubility [171]. PFAS sorptive efficiency by both Douglas Fir 900 and commercial biochars was lower in the simulated artificial groundwater solution (vs. simple solution chemistry tested previously). However, commercial biochar still removed over 70% of PFPeS, PFHxA, PFHxS, PFOA, and PFOS. Overall, this study showed that commercially produced biochar is a viable solution to PFAS contamination under environmentally relevant conditions.

3.2 Introduction

PFAS are a group of environmentally persistent chemicals that are known to have toxic effects for living organisms at low concentrations [15, 52]. These chemicals have been manufactured for over 70 years without production regulation or waste treatment techniques, leading to their contamination of environmental media globally [5, 6]. In recent years, the U.S. EPA has been lowering the recommended HALs for several PFAS compounds, while adding HALs for new PFAS compounds [61-63]. This regulatory trend is expected to continue due to the sheer size of the PFAS family of chemicals (**Fig. 1.1**) [12]. A subset of this large chemical family known as perfluoroalkyl acids has been a focus of remediation in recent years (**Fig. 1.3**) [172, 173]. PFAS global contamination, high toxicity, and increasing regulations show the need for an efficient and cost-effective remediation approach.

Biochar is a highly carbonaceous substance that has a low production cost, energy demand, and greenhouse gas emission potential during production [89, 125]. Additionally, biochar is also known as a useful carbon sequester and has unique physiochemical properties such as high specific surface area (SSA), rich functional groups, hydrophobicity, and tunable surface functionalities and even promising results in PFAS remediation [76, 89, 126-130]. However, it is not clear how biochars behave for PFOS sorption under environmentally relevant conditions, and to what extent environmental factors affect biochar performance. Three typical environmental parameters, i.e., solution pH, salt, and natural organic matter (NOM), were investigated using batch sorption experiments. Solution pH was observed to affect the zeta potentials of biochars as shown in **Fig 2.5c,** and the zeta potential became more negatively charged with increasing pH. Therefore, we hypothesize that biochar will have higher sorption

abilities under more acidic conditions, while the opposite trend will occur under alkaline conditions. We also hypothesize a negative relationship between PFAS sorption efficiency by biochar and NOM concentration, due to the competition of NOMs on the sorption sites from biochars. Increasing salt concentrations should screen the biochars negative charge and increase the aggregation of PFAS molecules, therefore increasing sorption. When salts are added to the solution with biochar, the free cation groups around the negatively charged biochar are expected to decrease the effective charge, which is known as the charge screening effect. Biochars properties can be further optimized for PFAS sorption to compensate for the negative effects environmental factors have on biochars performance. Together, these experiments will paint a clearer picture of how and to what extent environmental factors affect PFAS sorption by biochar in water.

3.3 Materials and Methods

3.3.1 Chemicals and reagents

Information on PFOS was stated previously in section 2.3.1. PFBA, PFBS, perfluoropentanoic acid (PFPeA), and perfluorohexanoic acid (PFHxA) were purchased from Matrix Scientific, Elgin, SC. Perfluoropentanesulfonic acid (PFPeS), PFHxS, and PFOA were obtained from SynQuest Laboratories, Alachua, FL. Physiochemical properties of each PFAS are shown in **Table 1.1**. Isotopically labeled internal standards for extracted internal standard (EIS) and non-extracted internal standards (NIS) for C4–C8 PFAS were purchased from Wellington Laboratories Guelph, ON, Canada (**Table 3.1**). Sodium chloride (NaCl) and sodium bicarbonate ($NaHCO_3$) were purchased from Acros Organics, Geel, Belgium. Calcium chloride ($CaCl_2$) and magnesium sulfate ($MgSO_4$) were purchased from VWR Chemical, Radnor, PA. The Suwanee

River humic acid, as a typical NOM, was purchased from the International Humic Substances Society (IHSS). HPLC-grade methanol was purchased from VWR Chemical, Radnor, PA. Oasis WAX cartridges (6 cc, 150 mg; Waters Corp., Milford, MA) were used for solid phase extraction (SPE). Deionized (DI) water and Milli-Q water were produced using a Milli-Q Ultrapure water system (Darmstadt, Germany).

Table 3.1. Target PFAS and associated isotopically labeled extracted internal standards (EISs) and non-extracted internal standards (NIS) used in this study.

Analyte Full Name	**Acronym**	**CAS Number**	**EIS**	**NIS**
Perfluorobutanoic acid	PFBA	375-22-4	^{13}C4-PFBA	^{13}C4-PFOA
Perfluorobutanesulfonic acid	PFBS	375-73-5	^{13}C3-PFBS	^{13}C4-PFOS
Perfluoropentanoic acid	PFPeA	2706-90-3	^{13}C5-PFPeA	^{13}C4-PFOA
Perfluoropentanesulfonic acid	PFPeS	2706-91-4	^{18}O2-PFHxS	^{13}C4-PFOS
Perfluorohexanoic acid	PFHxA	307-24-4	^{13}C5-PFHxA	^{13}C4-PFOA
Perfluorohexanesulfonic acid	PFHxS	355-46-4	^{13}C3-PFHxS	^{13}C4-PFOS
Perfluorooctanoic acid	PFOA	335-67-1	^{13}C2-PFOA	^{13}C4-PFOA
Perfluorooctanesulfonic acid	PFOS	1763-23-1	^{13}C8-PFOS	^{13}C4-PFOS

3.3.2 Biochars

The four best performing biochars with the highest sorption capacity for PFOS from **Chapter 2** were used here, including Douglas fir 900, eucalyptus 900, poplar 900, and switchgrass 700 biochars, along with the commercial biochar for comparison. In total, five biochars were used for the sorption of C4, C5, C6 and C8 PFAS compounds from water (described below).

3.3.3 PFAS batch sorption experiments

Several types of batch sorption experiments were conducted to determine the removal efficiency (%) of PFAS by the five biochars. All stock solutions of PFAS, biochar, salts, and humic acid

were made with Milli-Q water and stored in polypropylene bottles. With the exception of the kinetic experiments, all batch sorption experiments were performed in 50 mL polypropylene centrifuge tubes at a total volume of 40 mL. The kinetic experiments were performed in 1 L polypropylene bottles, and 40 mL of subsamples were taken at a specified time interval to investigate the sorption of PFAS by biochars as a function of time (sorption kinetics). Details of experimental parameters were given in **Table 3.2**.

Table 3.2. Concentrations and types of all biochars, PFAS, salts, and humic acid for all batch sorption experiments.

Experiment	Biochar Concentration (g/L)	PFAS Type	PFAS Concentration (µg/L)	Salt Type	Salt Concentration (mM)	Humic acid concentration (mg/L)
Screening	0.1	C4-C8 PFAS	0.2 µg /L each	NaCl	1mM	0 mg/L
Kinetics	0.1	C4-C8 PFAS	5 µg/L each	NaCl	1mM	0 mg/L
Isotherm	0.1	PFOS	10-4,000 ug/L	NaCl	1mM	0 mg/L
pH	0.1	PFOS	500 µg/L	NaCl	1mM	0 mg/L
Salt	0.1	PFOS	500 µg/L	NaCl, $CaCl_2$	0-10 mM and 0-2 mM respectively	0 mg/L
Humic Acid	0.1	PFOS	500 µg/L	NaCl	1mM	0-5 mg/L
Artificial groundwater	0.1	C4-C8 PFAS	0.2 µg/L	$NaHCO_3$, $CaCl_2$, $MgSO_4$	3.33 mM for each salt type	1mg/L

For batch sorption experiments, stock solutions for the five biochars, different PFAS compounds, salts, and organic matter (**Table 3.2**) were made and diluted into their respective concentrations at a final volume of 40 mL. All samples were allowed to equilibrate for 48 hours on an orbital rotator [127, 174]. Samples were centrifuged at 9,500 rpm for 1 hour, and 25 mL of the supernatant was extracted. The extracted supernatant was then passed through two sequentially stacked 0.22 µm polypropylene syringe filters (ThermoScientific) to remove any excess biochar particles. The first 5 mL of supernatant was discarded to eliminate the interference of PFAS loss, due to membrane filtration. The remaining 20 mL of supernatant was then spiked with 40 ng of

EIS (**Table 3.1**), loaded onto an Oasis WAX SPE cartridge (6 cc, 150 mg; Waters Corp., Milford MA), that was preconditioned with 4 mL of 0.1% ammonium hydroxide in methanol, 4 mL methanol, and 4 mL of LC grade water. After loading, cartridges were washed with 4 mL of a 25 mM ammonium acetate buffer in LC-grade water and gently dried under a vacuum. Analytes were then extracted from the cartridges with 4 mL of methanol followed by 4 mL of 0.1% ammonium hydroxide in methanol to achieve a final volume of 8 mL in a 15 mL polypropylene centrifuge tube. Samples were then transferred to LC vials and spiked with 10 ng of NIS (**Table 3.2**) for analysis. Samples from the pH experiment were not processed through SPE, due to their relatively clean background solution and risk of low internal standard recovery from pH adjustments.

3.3.6 PFAS sample analysis

PFAS sample analysis was performed between two instruments based on instrument availability at Auburn University. Most samples for the screening, kinetic, and isotherm experiments under different salt and NOM concentration, as well as in artificial groundwater solutions were analyzed using an ultrahigh-performance liquid chromatography-tandem mass spectrometry (UPLC-MS/MS). The UPLC-MS/MS comprises a 1290 Infinity II high speed pump (model G7120A) coupled to a triple quadrupoles mass spectrometry (model G6460C) and Jet Stream Electrospray Ionization (ESI) source (Agilent Technologies Inc., Santa Clara, CA, USA). Separation of PFAS was achieved on an Agilent C18 column (ZORBAXRRHD Eclips Plus C18, 2.1x100 mm, 1.8 µm). The binary mobile phases are Phase A of 5 mM ammonium formate in water/acetonitrile (95/5, v/v) and Phase B of water/acetonitrile (5/95, v/v). Sample injection volume was 10 µL. A constant flow of 0.2 mL/min was maintained at 40°C. The gradient began

at 20% mobile phase B for the first 2 min, then ramped up to 50% for 1 min. Mobile phase B was subsequently increased 10% every minute for 6 minutes where it was increased to 99%. It was held at 99% for 3.2 min and finally decreased to 20% and allowed to re-equilibrate for 1.8 min. The capillary voltage was 3,600 V, nozzle voltage was 1,500 V, sheath gas temperature was 350 °C at 11 L/min, and nebulizer was set to 45 psi.

The remaining PFAS samples for other experiments in this Chapter were analyzed using a Vanquish Binary UPLC, quadrupole-orbitrap high-resolution tandem MS (Exploris 120, ThermoScienific; UPLC-HRMS/MS). Details of instrument settings for this sample analysis were described above in Chapter 2 (**Section 2.3.5**). SPE for samples analyzed on this instrument followed a similar procedure described above but samples were diluted in an internal standard and Milli-Q water solution (1:1:8; sample/IS/Milli-Q; v/v/v) in a total volume of 1 mL for analysis.

3.3.7 Data Analyses

Biochar adsorption capabilities were calculated using equation 3.1:

$$Q_e = \frac{V(C_0 - C_e)}{M} \qquad (3.1)$$

Where C_0 and C_e are the initial and equilibrium PFAS concentrations, respectively, in µg/L, V is the experimental volume (L), and M is the total mass of the sorbent (g) in solution. Q_e represents the equilibrium capacity of biochar in (µg/g). Kinetics were calculated by pseudo first and second order kinetics, using equations 3.2 and 3.3, respectively:

$$Q_t = Q_e(1 - e^{-k_1 t}) \qquad (3.2)$$

$$Q_t = \frac{k_2 Q_e^2 t}{1 + k_2 Q_e t} \qquad (3.3)$$

Where *t* is the time Q_t is the amount sorbed onto biochar and time *t*, and k_1 and k_2 are the first and second order rate constants (g/µg/min), respectively. Adsorption isotherm values were calculated from the Langmuir and Freundlich models, using equations 3.4 and 3.5, respectively:

$$Q_e = \frac{Q_m k_L C_e}{1+k_L C_e} \qquad (3.4)$$

$$Q_e = k_F C_e^{1/n} \qquad (3.5)$$

Where Q_m is the theoretical maximum monolayer adsorption capacity (µg/g), C_e is the concentration at equilibrium (µg/L), and k_L and k_F are the are the rate constants for the Langmuir (L/µg) and Freundlich (µg/g)(L/µgL)^n models respectively, and 1/n is the adsorption intensity or surface heterogeneity.

3.3.8 *Statistical Analyses*

All statistical analyses were performed by linear regression models in R [139]. Statistics were calculated based on an individual experimental basis. For example, statistical significance on the sorption performance of biochar was tested for a change at pH 7. However, statistical significance on the effects of salt and humic acid concentrations were tested on a change from a humic acid concentration of zero.

3.4 Results and Discussion

3.4.1 C4-C8 PFAS screening experiment

The five best biochars for PFOS removal from chapter 2 were tested for removing C4-C8 compounds in a cocktail mixture solution. Overall, softwood (i.e., Douglas fir) and commercial biochars performed much better than the other types of biochars (**Fig. 3.1**).

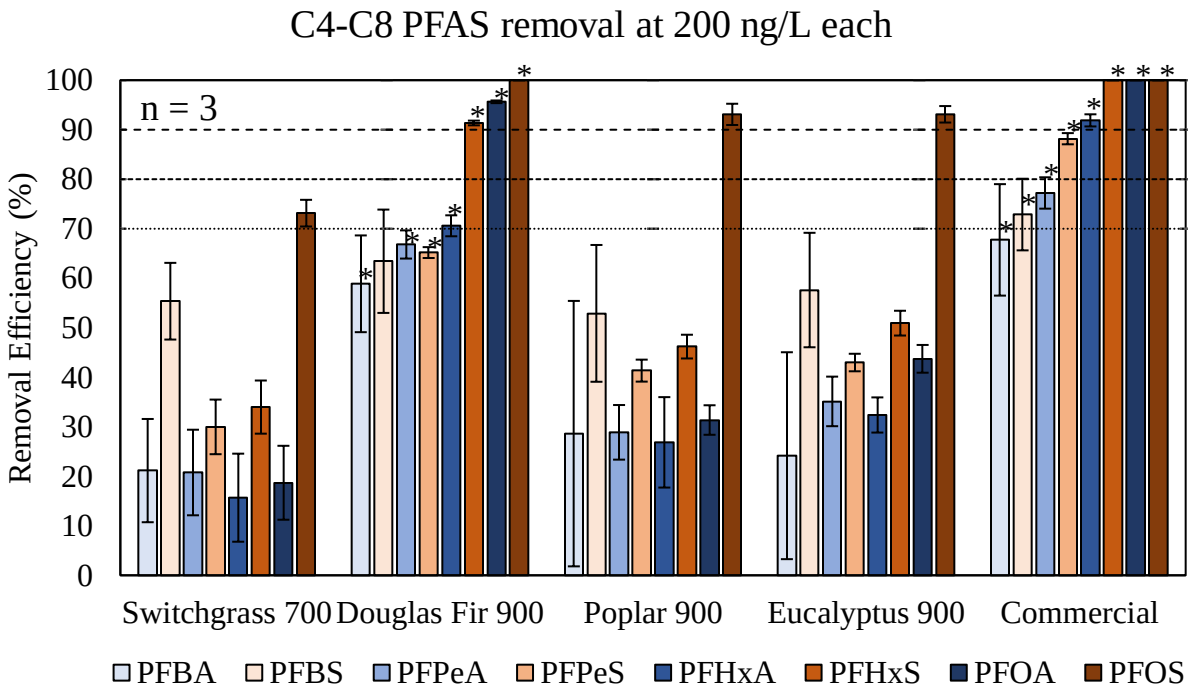

Fig 3.1. C4-C8 PFAS in a cocktail solution screening experiment for five biochars included in this study at an initial concentration of 200 ng/L. (*) indicates significant difference at the p = 0.05 level for commercial and Douglas fir 900 biochars at the respective PFAS carbon chain length. Error bars represent the standard deviations among triplicate samples.

Table 3.3. Biochar removal efficiency (%) for each C4-C8 PFAS analyzed at an initial PFAS concentration of 200 ng/L for each compound.

Removal efficiency (%)	Switchgrass 700	Douglas Fir 900	Poplar 900	Eucalyptus 900	Commercial biochar
PFBA	21.2 ± 10.4	58.9 ± 9.77	28.6 ± 26.8	24.2 ± 20.9	67.7 ± 11.3
PFBS	55.4 ± 7.74	63.4 ± 10.4	52.9 ± 13.9	57.6 ± 11.6	72.7 ± 7.23
PFPeA	20.8 ± 8.64	66.8 ± 2.85	28.8 ± 5.51	35.1 ± 5.00	77.2 ± 3.17
PFPeS	29.0 ± 5.52	65.2 ± 1.10	41.3 ± 2.22	43.0 ± 1.77	88.2 ± 1.13
PFHxA	15.7 ± 8.89	70.6 ± 2.12	26.9 ± 9.13	32.4 ± 3.55	91.9 ± 1.23
PFHxS	34.0 ± 5.37	91.4 ± 0.47	46.2 ± 2.40	50.9 ± 2.50	100 ± 0
PFOA	18.7 ± 7.46	95.6 ± 0.27	31.4 ± 2.98	43.7 ± 2.80	100 ± 0
PFOS	73.2 ± 2.69	100 ± 0	93.1 ± 2.15	93.1 ± 1.67	100 ± 0

The removal efficiency (%) biochars for C4-C8 PFAS sorption followed the order: Commercial > Douglas Fir 900 > Eucalyptus 900 > Poplar 900 > Switchgrass 700. Overall, wood feedstock biochars removed over 90% of PFOS from solution at an initial concentration of 200 ng/L.

Generally, sulfonate PFAS compounds are more readily removed, regardless of PFAS chain length, which is consistent with literature findings [127, 175]. Across all biochars, carboxylate PFAS were only removed more or equal to its respective same length sulfonate PFAS three times (i.e., Douglas Fir 900 removed more PFPeA than PFPeS) (**Fig 3.3 and Table 3.3**). Doulas Fir 900 biochar removed 66.8% PFPeA but only removed 65.2% PFPeS and PFOA and PFOS were almost completely removed by commercial biochar (i.e., below the detection limit of the instrument) (**Table 3.3**). Among all PFAS studied, PFOS is the most readily removed, but the hypothesized trend of longer chain PFAS being more readily removed is observed for Douglas Fir 900 and commercial biochars. Commercial biochar displayed the best performance, removing the highest percent of PFOS, PFOA, and PFHxS to the levels below detection limit of the instrument. The Douglas Fir 900 biochar was the second best in removing PFOS to levels below the detection limit and removing over 90% of PFOA and PFHxS. With the exception of PFBS sorption by Douglas Fir 900 biochar, both commercial and Douglas Fir 900 biochars removed significantly more PFAS than all other three biochars tested for the PFAS studied in this Chapter **(Fig. 3.3)**. Therefore, Douglas Fir 900 and commercial biochars were selected for the remaining batch sorption experiments in this study.

3.4.2 PFAS biochar kinetics

Kinetic experiments were performed for all C4-C8 PFAS to analyze the sorption characteristics of PFAS with different carbon chain lengths. Sorption equilibrium was achieved around 720 min (12 hr) for most PFAS sorbing to the Douglas Fir 900 and commercial biochars, except for PFPeA (**Fig. 3.2b**). PFBS, PFPeA, and PFHxA exhibited continuous sorption onto commercial biochar up until the 48 hr mark (**Fig. 3.2a**). Sorption of PFOS occurred very rapidly onto both

biochars, so effective data was not obtained before the first sampling point (i.e., taken at 10 min). Sample processing takes a minimum of about 10 minutes, so this was the earliest data we could achieve for kinetic experiments. Similarly, commercial biochar also removed PFHxS at a rapid rate and we were not able to obtain effective data due to sample processing restrictions (**Fig. 3.2**).

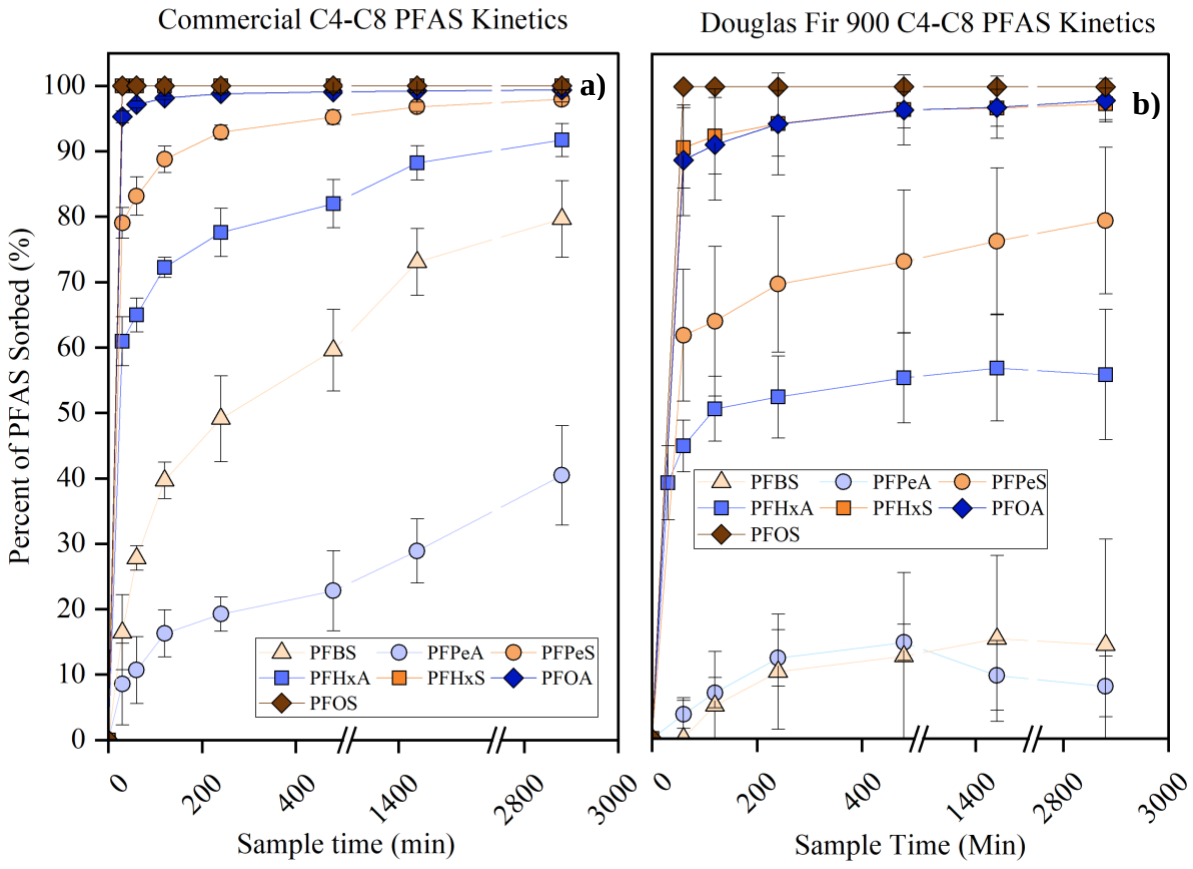

Fig 3.2. C4-C8 PFAS sorption kinetics for **a)** commercial and **b)** Douglas Fir 900 biochars. Douglas Fir 900 and commercial biochars were used since they were the best biochar performers in the screening experiment. Initial concentration was approximately 5 µg/L for each PFAS type with 0.1 g/L biochar and 1 mM NaCl.

Both pseudo first- and second-order kinetic models are commonly used to describe the sorption of contaminants onto sorbates [94]. Previous studies showed that the first-order kinetic model is

often used to describe physical sorption, while the second-order kinetic model is used to describe chemical sorption [94, 176]. However, physical and chemical sorption cannot be clearly differentiated based, only, on the underlying mathematics fitting the first and second order rate functions to the data [177]. Rather, the empirical fit of the model is justified by the underlying sorption mechanisms occurring between PFAS and biochar. According to the obtained r^2 values, the pseudo second order model described the sorption process better for most PFAS, except for PFBS and PFPeS onto Douglas Fir 900 biochar **(Fig 3.3 and Table 3.4).**

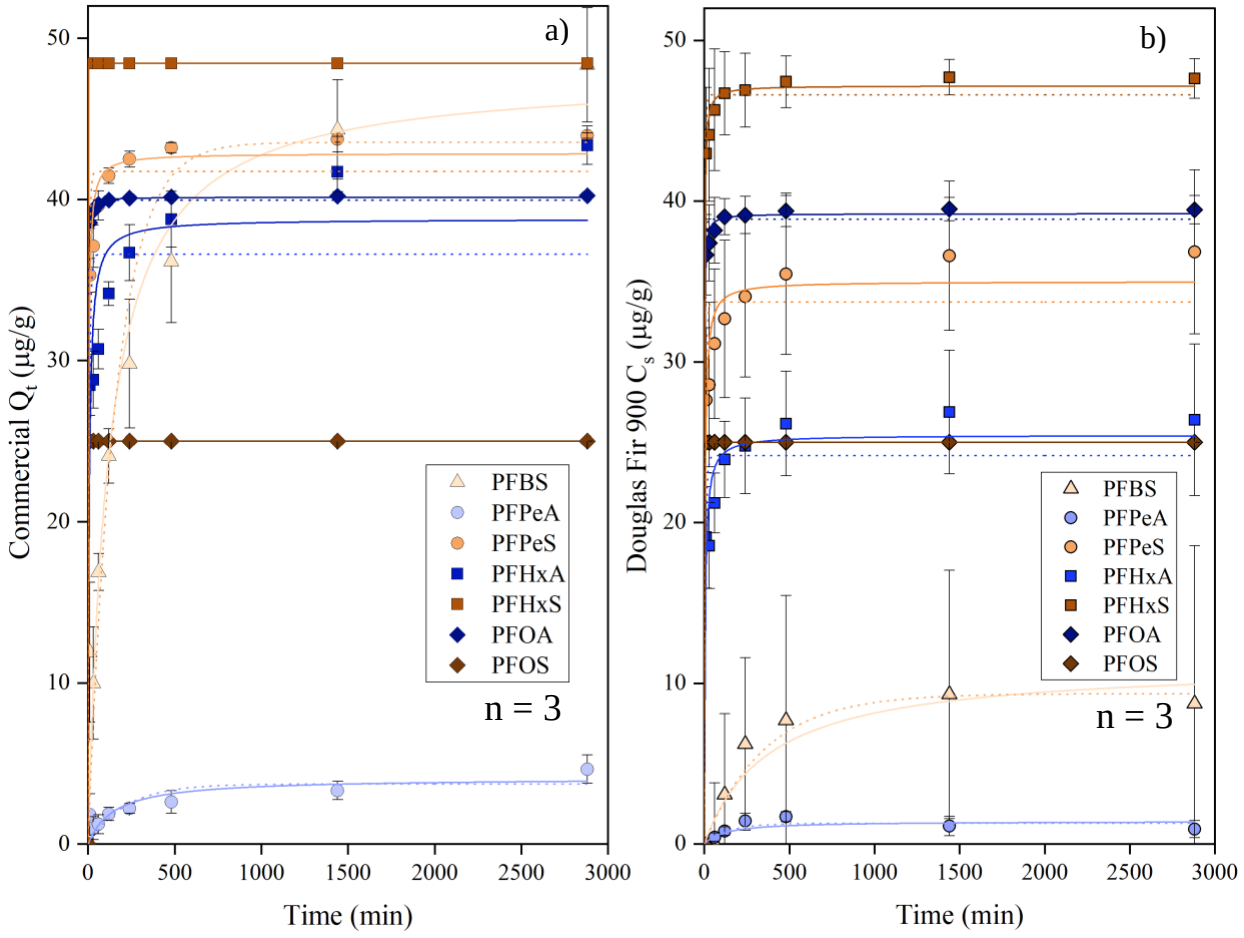

Fig. 3.3. Pseudo first (dashed line) and second (solid line) order kinetic models for C4–C8 PFAS sorbing to **(a)** commercial biochar and **(b)** Douglas Fir 900 biochar. Initial concentration was approximately 5 µg/L for each PFAS type with 0.1 g/L of biochar and 1 mM of NaCl.

Table 3.4. Equilibrium sorption capacity (Q_e), rate constants (k) and correlation (R^2) values for first and second order kinetics for C4-C8 PFAS sorbing to Douglas Fir 900 biochar.

	First Order				Second Order			
Biochar Type	PFAS type	Qe (µg/g)	K_1 (g/µg) min^{-1}	R^2	PFAS type	Qe (µg/g)	K_2 (g/µg) min^{-1}	R^2
Douglas Fir 900	PFBS	9.35 ± 2.63	0.003 ± 0.002	0.64	PFBS	11.2 ± 4.45	2.34E-4 ± 3.65E-4	0.62
	PFPeA	1.30 ± 0.30	0.007 ± 0.006	0.65	PFPeA	1.41 ± 0.43	0.006 ± 0.008	0.57
	PFPeS	33.7 ± 1.06	0.16 ± 0.043	0.94	PFPeS	35.0 ± 0.82	0.008 ± 0.002	0.98
	PFHxA	24.2 ± 1.07	0.14 ± 0.047	0.89	PFHxA	25.4 ± 0.86	0.007 ± 0.003	0.95
	PFHxS	46.6 ± 0.45	0.25 ± 0.034	0.99	PFHxS	47.2 ± 0.29	0.019 ± 0.003	0.99
	PFOA	38.9 ± 0.28	0.29 ± 0.035	0.99	PFOA	39.2 ± 0.18	0.032 ± 0.006	0.99
	PFOS	25.0 ± 0.00	3.76 ± 0.00	1.00	PFOS	25.0 ± 6.80E-14	2.73E11 ± 2.23E10	1.00
Commercial	PFBS	43.5 ± 3.11	0.006 ± 0.002	0.92	PFBS	47.8 ± 2.72	1.79E-4 ± 4.71E-5	0.96
	PFPeA	3.72 ± 0.55	0.005 ± 0.002	0.63	PFPeA	4.09 ± 0.61	0.002 ± 0.001	0.72
	PFPeS	41.7 ± 0.88	0.180 ± 0.035	0.97	PFPeS	42.9 ± 0.58	0.009 ± 0.002	0.99
	PFHxA	36.6 ± 1.91	0.133 ± 0.053	0.86	PFHxA	38.8 ± 1.68	0.004 ± 0.002	0.92
	PFHxS	n/a	n/a	n/a	PFHxS	48.4 ± 1.65E-13	2.51E11 ± 1.72E10	1.00
	PFOA	40.0 ± 0.12	0.330 ± 0.024	0.99	PFOA	40.2 ± 0.055	0.057 ± 0.005	0.99
	PFOS	25.0 ± 0.00	3.85 ± 0	1.00	PFOS	25.0 ± 6.81E-14	2.73E11 ± 2.23E10	1.00

This indicates that PFAS were sorbed to biochars mainly through chemical interactions rather that physical interactions (e.g., Van der Waals forces, hydrogen bonding, hydrophobic interactions), and is consistent with the findings of other studies reported in the literature [93, 94, 130, 178]**.** This is also justified by the sorption mechanisms previously described in **Chapter 2** of this thesis. Longer chain PFAS have faster sorption kinetics driven by their higher hydrophobicity and lower water solubility. The opposite trend was observed for shorter chain PFAS with higher solubility and lower hydrophilicity, creating a slower sorptive reaction. However, physical trapping of PFAS sorbed within biochars pores is also likely still occurring, meaning just chemical sorption mechanisms are not the only sorption phenomenon happening in solution.

3.4.3 *PFOS isotherm*

Different concentrations of PFOS were evaluated at constant temperature, pH, and adsorbent dosage to evaluate the sorptive process of Douglas Fir 900 and commercial biochars in a process known as sorption isotherms [179]. PFOS was selected for this experiment due to its high sorption affinity from the previous experiments. Langmuir and Freundlich models are two-parameter models commonly used to describe this sorption data [179]. The Langmuir model assumes a monolayer adsorption of molecules onto a homogeneous adsorbate surface. In comparison, the Freundlich model assumes multilayer or bilayer adsorption across heterogeneous active sites on the sorbent [170, 180, 181]. Both Langmuir (R^2 = 0.98 and 0.95 for commercial and Douglas Fir 900 biochars respectively) and Freundlich (R^2 = 0.95 and 0.96 for commercial and Douglas Fir biochars respectively) models fit the data well (**Fig. 3.4**).

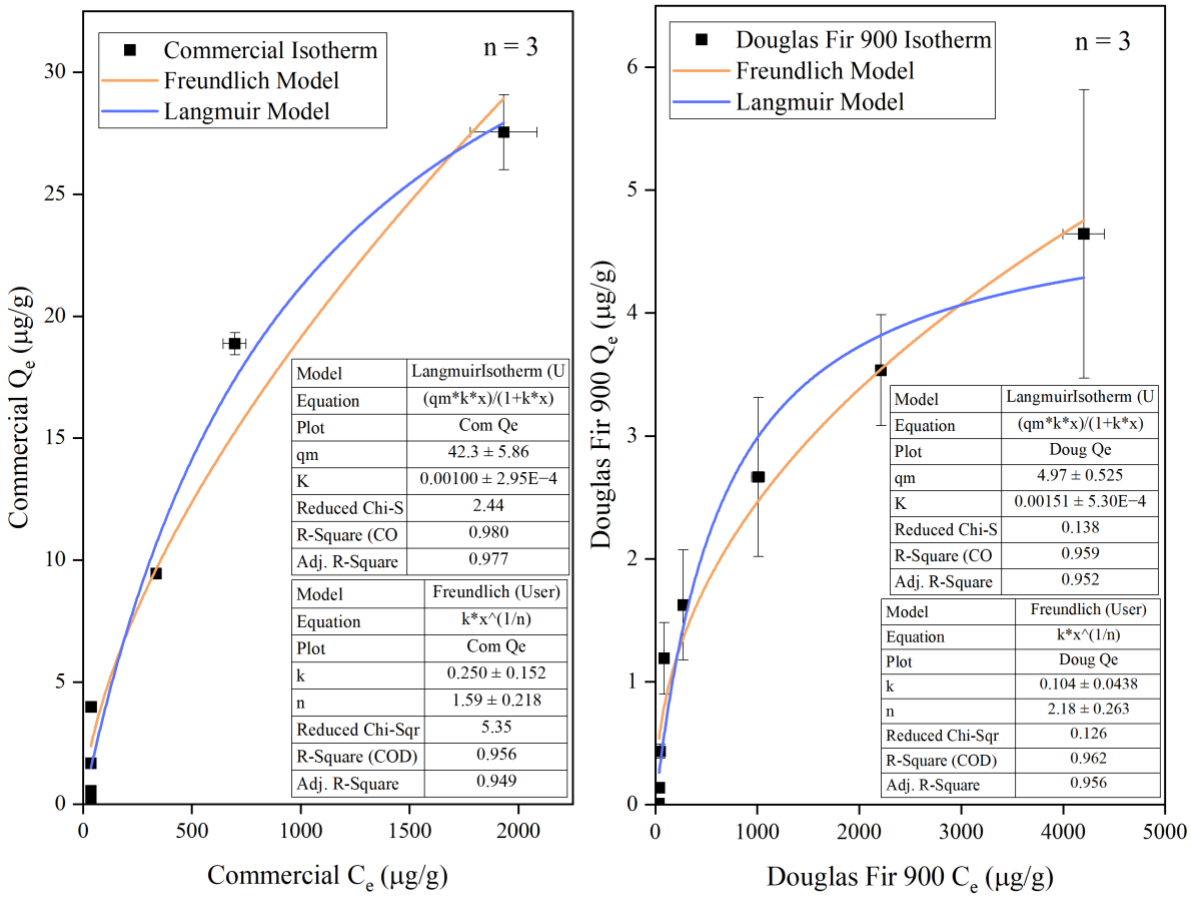

Fig. 3.4. Sorption Isotherm models for both Douglas Fir 900 and Commercial biochars. PFOS concentrations ranged from 10-4,000 µg/L, biochar concentration was 0.1 g/L and the background solution had 1 mM NaCl. All samples were allowed to equilibrate for 48 hrs.

The Freundlich model typically fits PFAS sorption data better, although the Langmuir model fitting performs better for other cases [94, 128, 170, 182]. Correlation coefficients are typically used to describe what type of sorption mechanism is occurring but visual inspection of the data indicates neither models are entirely clear (**Fig. 3.6**) [183]. Good fitting of both models suggests that PFOS was sorbed by binding onto biochars heterogeneous surface sites via different sorption mechanisms first, and then percolating into biochar pores when the surface is occupied [94, 182]. Values of $0 < 1/n < 1$ ($n = 0.63$ and 0.46 for commercial and Douglas Fir 900 biochars,

respectively) in the Freundlich model indicate favorable sorption to heterogeneous surface sites and confirm non-linear sorption [94, 179, 184]. This agrees with the findings from **Chapter 2** that biochars sorb PFAS from a variety of sorption mechanisms such as hydrophobic, electrostatic interactions with positively charged N containing functional groups, and the pore size trapping mechanisms. The Langmuir equation estimated that maximum monolayer sorption capacity (Q_m) was 42.3 and 4.97 µg/g for commercial and Douglas Fir 900 biochars, respectively. The Freundlich model estimated the k_f of 0.25 and 0.10 (µg/g)(L/µg)^n for commercial and Douglas Fir 900 biochars, respectively.

3.4.4 *Effect of pH gradient on PFOS sorption by biochar*

Solution pH was adjusted to 4-11 to assess how solution pH affects biochars ability for PFOS sorption. **Fig. 3.5** shows the commercial biochar was relatively unaffected under varying pH conditions, although sorptive performance did decrease slightly at solution pH above 8.19. It should be noted that the adjusted pH values were very unstable near the biochars original pH (pH = 8.60) before pH adjustment (**Table 2.2**). Even at a pH as high as 11, commercial biochar can still consistently remove over 90% of PFOS at an initial concentration of 500 µg/L. At extreme environmental pH of 4 or 11, commercial biochar was still likely to be a good sorbent. Linear models were used to assess the data for a significant change in sorption efficiency. For every 1 unit increase in pH, we observed a 0.93% (±0.29%; 95% C.I.) decrease in PFOS sorption ($p < 0.05$; $r^2 = 0.66$). However, the pH did not significantly impact sorption performance until it was above a pH of 8.19 ($p < 0.05$; $r^2 = 0.81$), based on the two points at pH 8.19 and 10.8 (**Fig. 3.5**).

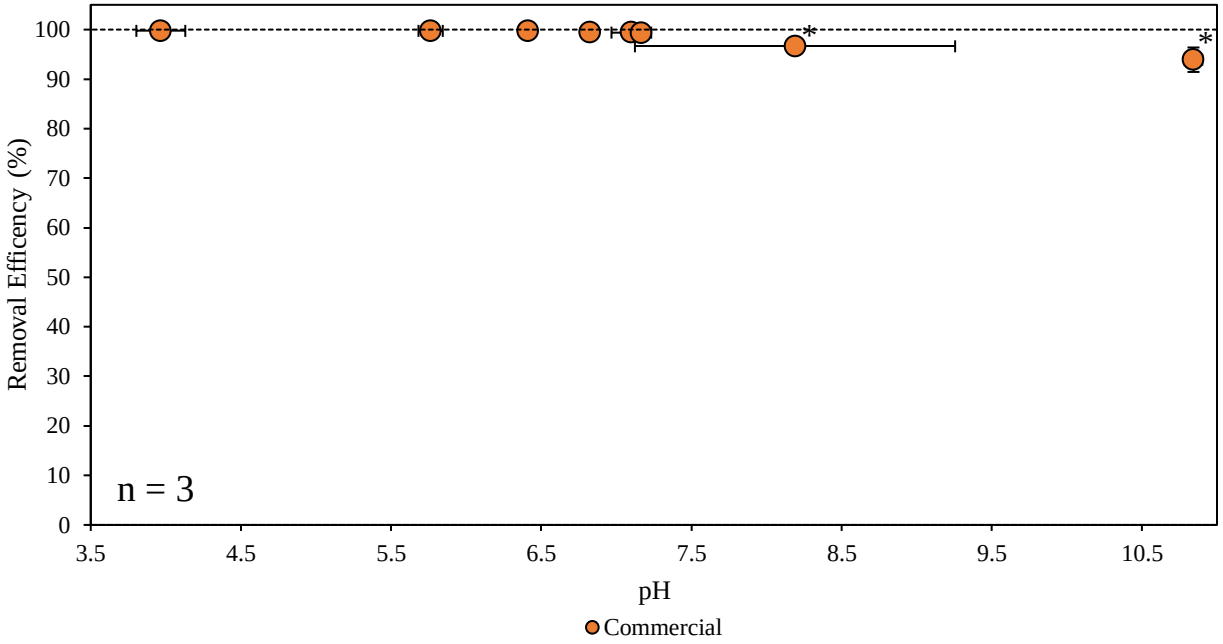

Fig. 3.5. PFOS removal by commercial biochar with a pH range of 4–11 and an initial PFOS concentration of 500 µg/L. The biochar concentration was 0.1 g/L under 1 mM NaCl. (*) indicates statistically significant difference from neutral pH at the p = 0.05 level.

3.4.5 Effect of salt type and concentration on PFOS sorption by biochar

Sodium chloride (NaCl) and calcium chloride ($CaCl_2$) were selected because of their omnipresence in natural waters [185]. Salt concentration gradients were made based on the ionic strength of the solution and the concentrations ranged from 1–10 mM for NaCl and 0.5–2.0 mM for $CaCl_2$, respectively. Both salts were found to increase sorption efficiency for the Douglas Fir 900 biochar and commercial biochar, although the commercial biochar removed over 99% of PFOS from all studied solutions (**Fig. 3.6**). Statistical analysis showed that commercial biochar removed about 0.30% (±0.14%; 95% C.I.) more PFOS across all concentrations of salts than the samples without salts ($p < 0.05$; $r^2 = 0.51$). Similar observations were shown for Douglas Fir 900, as Douglas Fir 900 biochar removed about 6.77% (±1.30%; 95% C.I.) more PFOS at all salt concentrations compared to samples without salts ($p < 0.05$, $r^2 = 0.63$). It was also observed that

commercial biochar removed about 3.93% (±1.34%; 95% C.I.) more PFOS than Douglas Fir 900 biochar across all salt concentrations ($p < 0.05$; $r^2 = 0.28$) (**Fig. 3.6**).

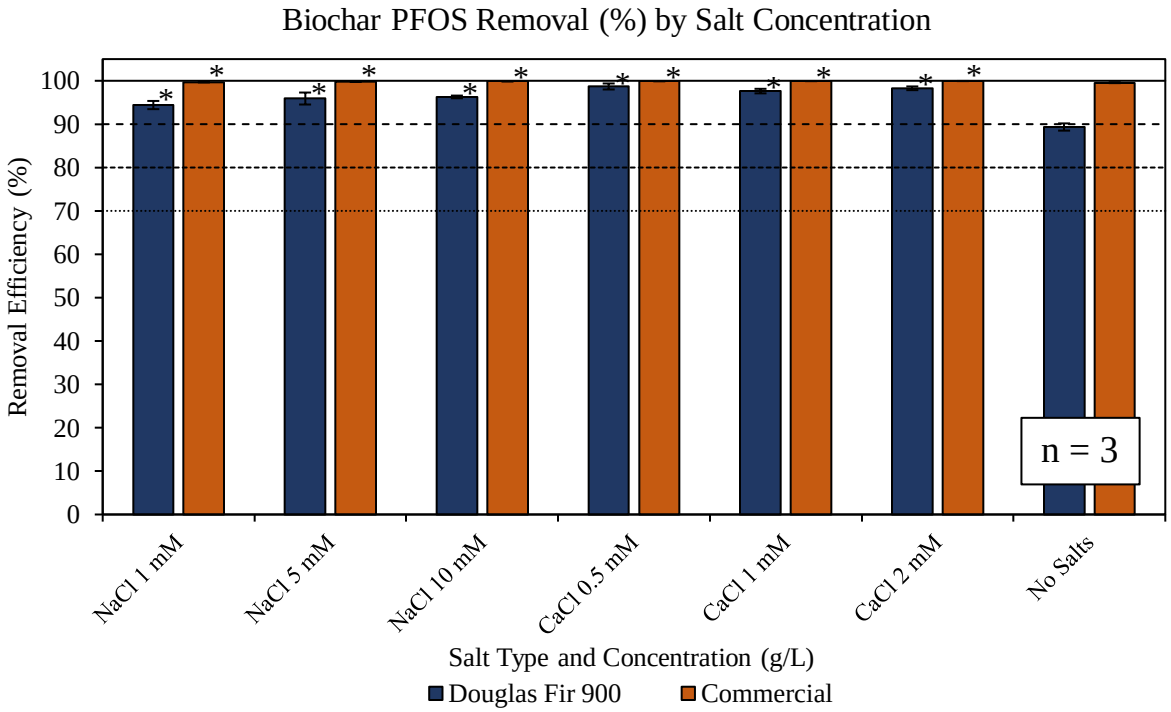

Fig 3.6. PFOS removal efficiency (%) under different NaCl (0–10 mM) and $CaCl_2$ (0–2 mM), respectively, at an initial PFOS concentration was 500 µg/L. (*) Indicates significantly higher sorption for respective salt concentrations compared to samples without salts at the $p = 0.05$ level.

One possible hypothesis is that PFOS solubility is reduced with the presence of salts already dissolved in the water, although it is unlikely to occur at the concentrations examined herein [171]. Alternatively, a more well documented scenario is that the double layer surface charge created by positively charged Na^+ and Ca^{2+} dissociates when they are dissolved [171, 186, 187]. This phenomenon creates a less negative surface charge on the biochar, allowing PFOS to sorb more readily onto the surface (**Fig. 3.7**). This was also reported in a review paper by Yang et at. (2020) who specifically studied the zeta potential change under different concentrations of NaCl

and CaCl2 [188]. Positively charged ions essentially bridge the gap between the negatively charged sulfonate groups and biochar surface.

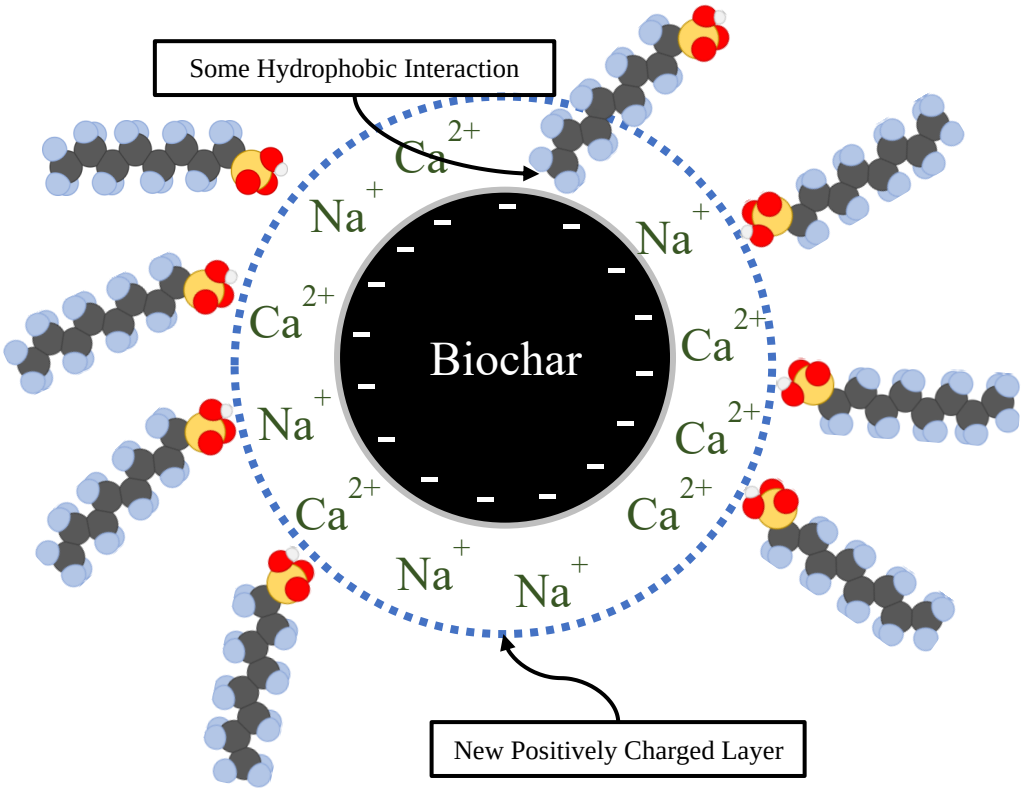

Fig. 3.7. Schematic showing PFOS sorption onto the proposed charge screening effect from positively charged ions in solution. It is assumed that some PFOS still sorb through hydrophobic interactions.

At high concentrations of PFAS and salts, dissolved ions have been shown to cause significant aggregation in solution and underreporting of PFAS (i.e., PFAS concentration detected by the instrument is lower than the actual PFAS concentration in solution) [171]. However, this effect is expected to be negligible at PFAS concentrations less than 5 mg/L, meaning PFAS aggregation was likely not occurring in this study [171]. Salts have also been shown to reduce the surface tension of water molecules, which may allow solutions to more easily wet the inner surface of biochar pores, thereby enhancing sorption efficiency [171].

3.4.6 Effect of Humic acid concentrations on PFOS sorption by biochar

Organic matter is seen as one of the greatest inhibiting factors for the sorptive removal of contaminants from natural waters. The large complex structure of organic matter is anticipated to clog pores and occupy a large amount of surface areas on sorbents like biochars. A humic acid gradient of 0–5 mg/L was used to test the effects of NOM on PFOS sorption by biochars. The sorptive performance of Douglas Fir 900 biochar was greatly inhibited by the addition of humic acid, while commercial biochar was less affected (**Fig. 3.8**). All the tested humic acid concentrations significantly decreased Douglas Fir 900 biochars sorptive performance. The sorptive performance of the Douglas Fir 900 biochar decreased by 13.1–46.7% (±7.30%; 95% C.I.), when the humic acid concentration was increased from 0.1 to 5 mg/L ($p < 0.05$; $r^2 = 0.87$). Humic acid also significantly affected commercial biochars performance at concentrations above 0.1 mg/L, ranging from a 0.22–2.02% (±0.17%; 95% C.I.) decrease in sorption performance ($p < 0.05$; $r^2 = 0.95$). At the highest humic acid concentration of 5 mg/L, the commercial biochar still removed over 97% of PFOS from solution (**Fig. 3.8**). Overall, commercial biochar removed significantly more PFOS at all the tested humic acid concentrations than Douglas Fir 900 biochar (**Fig. 3.8**). These findings indicate that the commercial biochar would be a good effective option for removing PFAS from water under environmentally relevant conditions.

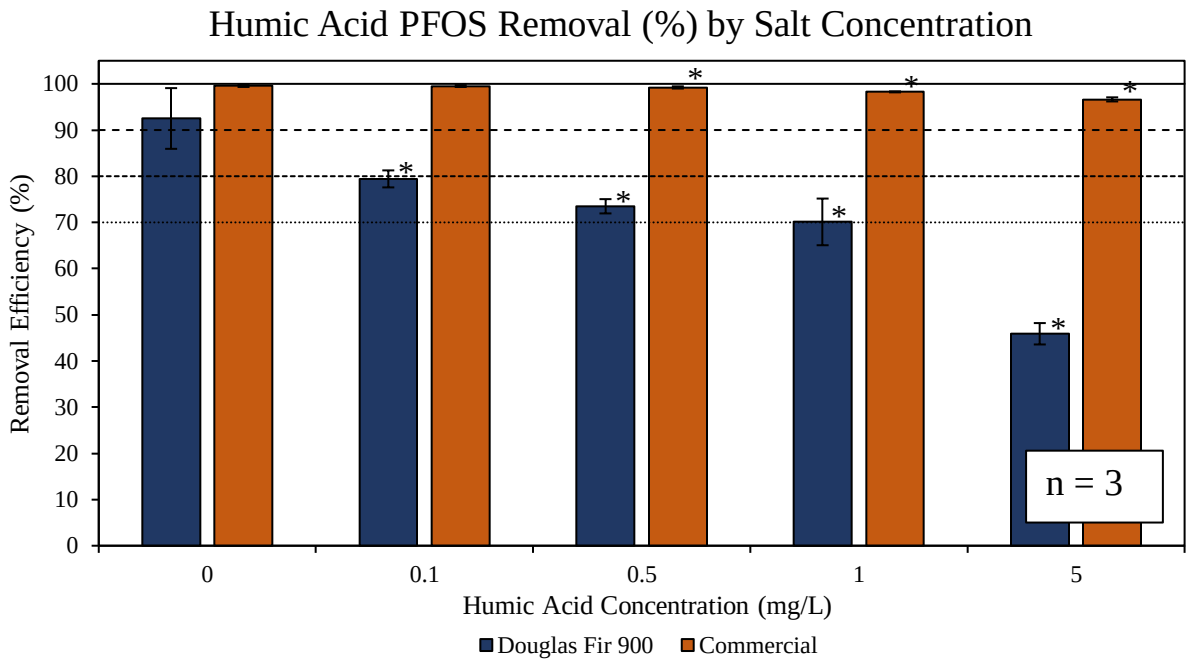

Fig. 3.8. Effect of humic acid concentration (0–5 mg/L) on the removal efficiency of PFOS (500 µg/L) by biochars under 1 mM NaCl. (*) indicates statistical significance from no humic acid samples at the p = 0.05 level.

3.4.7 Effect of artificial groundwater on C4-C8 sorption by biochar

The final set of experiments in this Chapter was to examine how biochar performs at removing all C4-C8 PFAS in an artificial groundwater solution. The gathered data can help us to predict the real performance of biochar for PFAS sorption in a real-world water treatment scenario. Shorter chain length PFAS were already removed at lower amounts than longer chain counterparts (**Fig. 3.1**), and there is little to no removal by both biochars for PFAS shorter than C5 (**Fig. 3.9**).

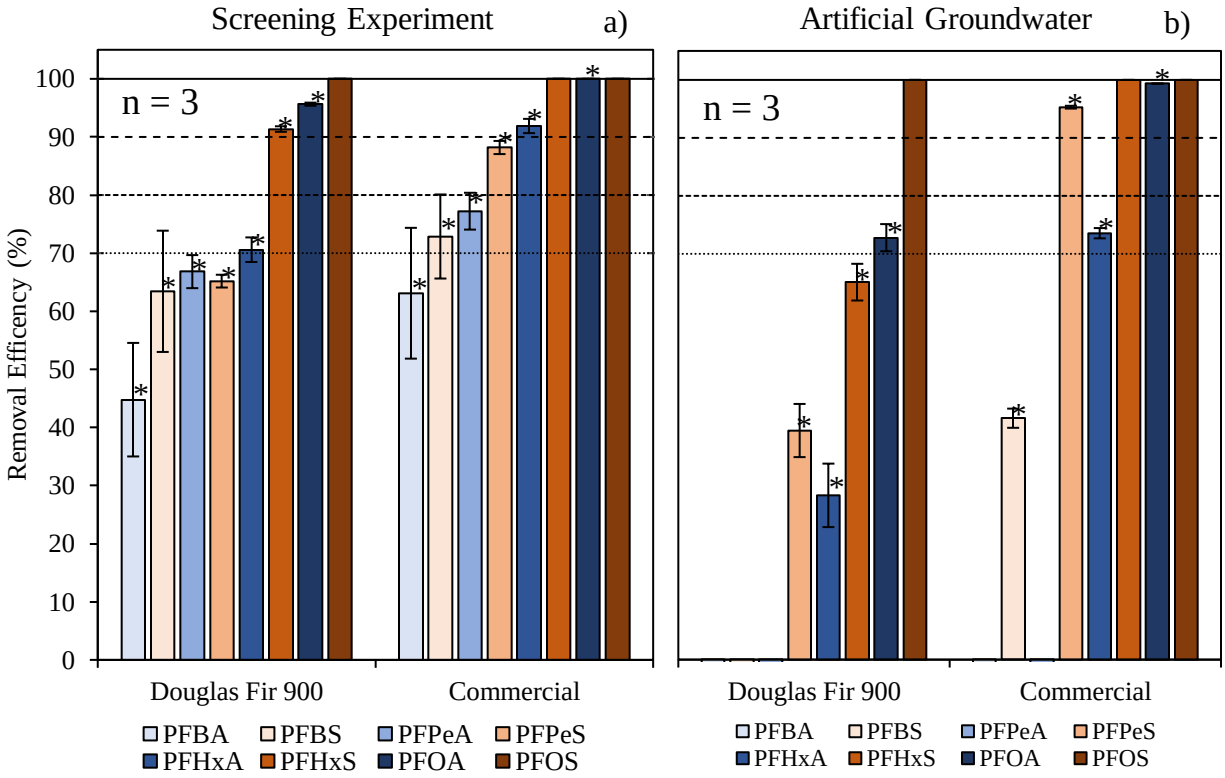

Fig. 3.9. Comparison of PFAS removal by biochars in a clean background solution **(a)** versus that in an artificial groundwater solution **(b)**. Biochar concentration was 0.1 g/L and concentration of each PFAS was 200 ng/L. The screening experiment had 1 mM NaCl, while the artificial groundwater experiment had $CaCl_2$, $MgSO_4$, and $NaHCO_3$, spiked at a concentration of 3.33 mM each for a total salt ionic strength of 10 mM with 1 mg/L of humic acid. All samples were run in triplicate and error bars represent the standard deviations between samples. (*) indicates PFAS that have significantly different sorption values between the screening experiment and artificial groundwater at the $p = 0.05$ level.

The sorptive performance of Douglas Fir 900 biochar was greatly inhibited in the artificial groundwater and only two PFAS removal efficiencies were over 70% (PFOA and PFOS) (**Fig. 3.9**). However, Douglas Fir 900 biochar can still remove PFOS to the levels below the detection limit of the instrument. Overall, Douglas Fir 900 biochar removed about 53.1% (±13.2%; 95% C.I.) less of each PFAS compound in artificial groundwater compared to the clean background solution ($p < 0.05$, $r^2 = 0.30$), and about 24.5% (±15.3%; 95% C.I.) more sulfonate PFAS than carboxylate PFAS ($p < 0.05$, $r^2 = 0.07$). We observed no removal for PFBA, PFBS, and PFPeA

in the artificial groundwater solution for both Douglas Fir 900 and commercial biochars. These compounds have shorter C-F chains giving them lower hydrophobicity, higher water solubility and thus making them less prone to sorption to the biochars surface.

Commercial biochar still performed well for longer chain PFAS, removing over 95% of PFHxA, PFHxS, PFOA, and PFOS, while still removing PFHxS and PFOS to levels below the detection limit. Surprisingly, PFPeS sorption increased by 7.11% (±4.18%; 95% C.I) in the artificial groundwater experiment ($p < 0.05$; $r^2 = 0.990$). Overall, commercial biochar removed about 32.6% (±13.7%; 95% C.I.) less of each compound in artificial groundwater compared to the clean background solution ($p < 0.05$; $r^2 = 0.13$), and sulfonate PFAS were removed about 32.6% (±13.7%; 95% C.I.) more than carboxylate PFAS across all solutions ($p < 0.05$; $r^2 = 0.13$). There was no removal observed for PFBA and PFPeA in the artificial groundwater solution due to their high water solubility and low hydrophobicity.

Overall, PFAS sorption performance of commercial biochar was much better than that of Douglas Fir 900 biochar. Both biochars were derived from pine feedstocks, but the commercial biochar had higher surface area and pyrolysis temperature, which could be responsible for its better sorption performance. Although the sorption efficiency (i.e., percent of PFAS sorbed) of both biochars was high, both commercial and Douglas Fir 900 biochars had relatively low sorption capacities (i.e., total amount of PFAS sorbed per gram of biochar). It is possible that ball milling may destroy surface structures that are critical for the sorption of PFOS [189]. Despite this, commercial biochar still performed well in artificial groundwater solutions at PFAS concentrations that are higher than most drinking water concentrations. The low sorption

capacity of these biochars may not be applicable to highly concentrated PFAS effluents in WWTPs, but perhaps there is a potential application for household water treatment systems. Many areas that do not have extremely high contamination levels from primary PFAS producers still have unsafe levels of PFAS that could be managed by these studied biochars. For example the Auburn water works drinking water plant reported a total C4-C8 PFAS concentration of 32 ng/L [39]. This concentration is well within the effective removal range of the commercial and Douglas Fir 900 biochars. These biochars possibly offer a cost-effective solution for people with relatively low incomes to clean their water for safe consumption at a household scale. Activated carbon costs have been reported at a cost of $5.60/kg, whereas this commercially produced biochar is only $2.00/kg. Short chain PFAS still pose a major issue for treatment due to their high water solubility and lower hydrophobicity.

3.5.0 Conclusion

PFAS sorption performance of both Douglas Fir 900 and commercial biochars is negatively affected by the environmental parameters that are tested in the artificial groundwater. Nonetheless, commercial biochar is still effective at removing PFHpS, PFHxS, PFOA, and PFOS under environmentally relevant conditions. Both biochars had a lower efficiency in removing carboxylate PFAS, compared to sulfonates, especially for these short chain carboxylate PFAS. There was almost no removal for PFBA or PFPeA under artificial groundwater conditions for both biochars. Still, data from this study showed that biochar made at a commercial scale is a viable solution to treat natural waters with long-chain PFAS contamination. Commercial biochar may be a good post water treatment option, such as a drinking water-based home carbon filter. However, more work is needed to draw conclusions on that hypothesis.

Chapter 4. Conclusion

The overarching goal of this thesis was to find out which biochars perform better for removing PFAS from water with two objectives. The first objective was to find what physiochemical properties are most important for PFOS sorption, and the second objective was to determine what environmental factors affect the sorptive performance of PFAS by biochars. Along the way, we were also able to determine what feedstock and production characteristics produce the best biochars for PFAS sorption. We found biochar properties such as pore diameter, pore diameter/pore volume ratio, contact angle, and nitrogen content are the most key factors controlling PFOS sorption. Wood feedstocks produce more efficient sorbents in general, but softwood feedstocks produce the best sorbents for C8 PFAS in a cocktail solution. Specifically, biochars that have pore diameters between 7.5 to 11 nm, pore diameter/pore volume ratios between 50 to 150 ($nm/cm^3/g$), large SSA, and high hydrophobicity have the favorable physiochemical properties for PFOS sorption. A high nitrogen content relative to the biochars feedstock type and other properties was found to be an important chemical property of biochars. We hypothesize that positively charged N-containing groups (e.g., amine groups) of biochars can strongly sorb negatively charged PFOS via electrostatic attractions, accounting for a higher removal efficiency of PFOS by biochars with higher N contents. It is important to note that although some biochar properties were determined to be more important than others, there is not one factor alone that is the sole driver for PFOS sorption. Ultimately, it is the combination of all biochar physiochemical properties that make an ideal sorbent.

The Douglas Fir 900 and commercial biochars were the two best biochars identified from this thesis for the removal of C4-C8 PFAS. Different environmental parameters were tested on Douglas Fir 900 and commercial biochars to investigate the effects of pH, salts, organic matter

and ultimately an artificial groundwater solution. PFOS sorption was not significantly impacted until the solution pH was above 8.19. Both NaCl and $CaCl_2$ were found to enhance PFAS sorption at all the tested concentrations. This phenomenon is likely due to a charge screening effect from dissociated cations in the solution. Organic matter negatively impacted sorption at all concentrations. However, even with the presence of 5 mg/L of humic acid, the commercial biochar was still able to remove more than 97% of PFOS from solution at an initial concentration of 500 µg/L. As expected, artificial groundwater impacted the sorption efficiency of both the Douglas Fir 900 and commercial biochars. However, both biochars still removed PFOS to the level below the detection limit of instrument (UPLC-MS/MS or UPLC-HRMS/MS) and commercial biochar also removed PFHxS to the levels below the detection limit. The Douglas Fir 900 biochar only removed two PFAS with a removal efficiency over 70% (PFOA and PFOS), while commercial biochar removed five PFAS at removal efficiency above 70% (PFPeS, PFHxA, PFHxS, PFOA, and PFOS) at an initial concentration of around 200 ng/L of each PFAS with 10 mM of salts and 1 mg/L of humic acid.

Overall, this thesis makes a good case for commercially produced biochar as a cost effective and environmentally friendly PFAS sorbent. This opens new areas of research for more effective biochar solutions. This research lays a solid foundation for further investigation into engineering the ideal biochar for PFAS sorption. There is enormous opportunity to further modify or "tune" the physicochemical properties of biochars to further promote sorption efficiency and capacity, as well as test more specific environmental parameters that pertain to PFAS contamination. Parameters such as pore diameter, pore diameter/pore volume ratio, contact angle, and nitrogen content should be paid more attention to, based on the findings from the structural equation

model. Future research is needed to test more biochar types that have ideal physiochemical properties for PFAS sorption, as well as implement biochar sorption in real world water treatment scenarios. A practical engineering flaw in this study is the small particle size of biochars. Although this does produce high surface areas ideal for sorbing contaminants, it undoubtably adds other hurdles to overcome for the practical application of the biochars. However, there are also possibilities to further improve biochar sorption abilities with surface modifications such as a positively charged biochar surface, or a magnetized surface. Biochar with a positively charged surface could possibly significantly increase PFAS affinity, while a magnetized surface could make colloidal biochar particles efficient to use in large scale water treatment scenarios. Significantly more future efforts are needed for these aspects toward better performance of PFAS removal by biochars. Furthermore, different experimental methods could be employed such as packed column experiments and biochar regeneration techniques to make it reusable for PFAS sorption. Biochar also has the potential for use in a larger synergistic system focusing on PFAS concentration and degradation. The blank slate of biochar has many possibilities and methods surrounding it that can be utilized to improve its characteristics towards PFAS sorption.

References

1. Institute, S.H. *Historical Biography: Roy J. Plunkett*. 2017 December 14 2017 [cited 2023 January 20, 2023]; Available from: https://www.sciencehistory.org/historical-profile/roy-j-plunkett.
2. Chemours. *The History of Teflon™ Fluoropolymers*. 2017 [cited 2023 January 20,2023]; Available from: https://www.teflon.com/en/news-events/history.
3. 3M, *The Science of Organic Fluorochemistry*. 1999.
4. Concawe, *Environmental fate and effects of polyand perfluoroalkyl substances (PFAS)* 2016.
5. Benskin, J.P., et al., *Manufacturing Origin of Perfluorooctanoate (PFOA) in Atlantic and Canadian Arctic Seawater*. Environmental Science & Technology, 2012. **46**(2): p. 677-685.
6. ITRC, *History and Use of Per- and Polyfluoroalkyl Substances (PFAS)*. 2020.
7. 3M, *Phase-out Plan for POSF-Based Products*. 2000.
8. Kissa, E., *Fluorinated Surfactants and Repellents*. second ed. 2005, New York, NY: Marcel Dekker Inc.
9. Prevedouros, K., et al., *Sources, Fate and Transport of Perfluorocarboxylates.* Environmental Science & Technology, 2006. **40**(1): p. 32-44.
10. 3M. *3M to Exit PFAS Manufacturing by the End of 2025*. 2022 [cited 2023 March 9, 2023]; Available from: https://news.3m.com/2022-12-20-3M-to-Exit-PFAS-Manufacturing-by-the-End-of-2025.
11. EWG. *What are PFAS chemicals?* 2023 [cited 2023 March 9, 2023]; Available from: https://www.ewg.org/what-are-pfas-chemicals#:~:text=Although%20the%20original%20PFAS%20chemical,fast%20food%20and%20bakery%20goods.
12. ITRC, *Naming Conventions for Per- and Polyfluoroalkyl Substances (PFAS)*. 2022: itrcweb.org.
13. Viticoski, R.L., et al., *Spatial distribution and mass transport of Perfluoroalkyl Substances (PFAS) in surface water: A statewide evaluation of PFAS occurrence and fate in Alabama.* Science of The Total Environment, 2022. **836**: p. 155524.
14. Giesy, J.P. and K. Kannan, *Global Distribution of Perfluorooctane Sulfonate in Wildlife.* Environmental Science & Technology, 2001. **35**(7): p. 1339-1342.
15. Buck, R.C., et al., *Perfluoroalkyl and polyfluoroalkyl substances in the environment: Terminology, classification, and origins.* Integrated Environmental Assessment and Management, 2011. **7**(4): p. 513-541.
16. Adamson, D.T., et al., *Characterization of relevant site-specific PFAS fate and transport processes at multiple AFFF sites.* Environmental Advances, 2022. **7**: p. 100167.
17. ITRC, *Aqueous Film-Forming Foam (AFFF)*. 2020.
18. Protection, M.D.o.E., *Advisory Information for Aqueous Film Forming Foam (AFFF) Containing Per- and Polyfluorinated Alkyl Substances (PFAS)*. 2021: mass.gov.
19. Gore-Tex. *Our History*. 2018 [cited 2023 January 20, 2023]; Available from: https://www.gore-tex.com/technology/history.
20. Podder, A., et al., *Per and poly-fluoroalkyl substances (PFAS) as a contaminant of emerging concern in surface water: A transboundary review of their occurrences and toxicity effects.* Journal of Hazardous Materials, 2021. **419**: p. 126361.

21. Glüge, J., et al., *An overview of the uses of per- and polyfluoroalkyl substances (PFAS).* Environmental Science: Processes & Impacts, 2020. **22**(12): p. 2345-2373.
22. Nakayama, S.F., et al., *Worldwide trends in tracing poly- and perfluoroalkyl substances (PFAS) in the environment.* TrAC Trends in Analytical Chemistry, 2019. **121**: p. 115410.
23. ITRC, *PFAS Releases to the Environment*. 2021.
24. Bečanová, J., et al., *Screening for perfluoroalkyl acids in consumer products, building materials and wastes.* Chemosphere, 2016. **164**: p. 322-329.
25. Kotthoff, M., et al., *Perfluoroalkyl and polyfluoroalkyl substances in consumer products.* Environmental Science and Pollution Research, 2015. **22**(19): p. 14546-14559.
26. Hekster, F.M., R.W. Laane, and P. de Voogt, *Environmental and toxicity effects of perfluoroalkylated substances.* Rev Environ Contam Toxicol, 2003. **179**: p. 99-121.
27. Poulsen, P.B., et al., *More environmentally friendly alternatives to PFOS-compounds and PFOA.* Environmental Project, 2005. **1013**: p. 2005.
28. Shin, H.-M., et al., *Environmental Fate and Transport Modeling for Perfluorooctanoic Acid Emitted from the Washington Works Facility in West Virginia.* Environmental Science & Technology, 2011. **45**(4): p. 1435-1442.
29. Davis, K.L., et al., *Transport of ammonium perfluorooctanoate in environmental media near a fluoropolymer manufacturing facility.* Chemosphere, 2007. **67**(10): p. 2011-2019.
30. Hu, X.C., et al., *Detection of Poly- and Perfluoroalkyl Substances (PFASs) in U.S. Drinking Water Linked to Industrial Sites, Military Fire Training Areas, and Wastewater Treatment Plants.* Environmental science & technology letters, 2016. **3**(10): p. 344-350.
31. Busch, J., et al., *Polyfluoroalkyl compounds in landfill leachates.* Environmental Pollution, 2010. **158**(5): p. 1467-1471.
32. Eggen, T., M. Moeder, and A. Arukwe, *Municipal landfill leachates: A significant source for new and emerging pollutants.* Science of The Total Environment, 2010. **408**(21): p. 5147-5157.
33. Ahrens, L., et al., *Wastewater Treatment Plant and Landfills as Sources of Polyfluoroalkyl Compounds to the Atmosphere.* Environmental Science & Technology, 2011. **45**(19): p. 8098-8105.
34. Hamid, H. and L. Li, *Role of wastewater treatment plant (WWTP) in environmental cycling of poly- and perfluoroalkyl (PFAS) compounds.* Ecocycles, 2016. **2**(2).
35. Higgins, C.P., et al., *Quantitative Determination of Perfluorochemicals in Sediments and Domestic Sludge.* Environmental Science & Technology, 2005. **39**(11): p. 3946-3956.
36. Yoo, H., et al., *Analysis of perfluorinated chemicals in sludge: Method development and initial results.* Journal of Chromatography A, 2009. **1216**(45): p. 7831-7839.
37. Lindstrom, A.B., et al., *Application of WWTP Biosolids and Resulting Perfluorinated Compound Contamination of Surface and Well Water in Decatur, Alabama, USA.* Environmental Science & Technology, 2011. **45**(19): p. 8015-8021.
38. Yoo, H., et al., *Quantitative Determination of Perfluorochemicals and Fluorotelomer Alcohols in Plants from Biosolid-Amended Fields using LC/MS/MS and GC/MS.* Environmental Science & Technology, 2011. **45**(19): p. 7985-7990.
39. ewg. *PFAS Contamination in the U.S. (June 8, 2022)*. 2022; Available from: https://www.ewg.org/interactive-maps/pfas_contamination/map/.
40. Domingo, J.L. and M. Nadal, *Human exposure to per- and polyfluoroalkyl substances (PFAS) through drinking water: A review of the recent scientific literature.* Environmental Research, 2019. **177**: p. 108648.

41. Barisci, S. and R. Suri, *Occurrence and removal of poly/perfluoroalkyl substances (PFAS) in municipal and industrial wastewater treatment plants.* Water Science and Technology, 2021. **84**(12): p. 3442-3468.
42. Lenka, S.P., M. Kah, and L.P. Padhye, *A review of the occurrence, transformation, and removal of poly- and perfluoroalkyl substances (PFAS) in wastewater treatment plants.* Water Research, 2021. **199**: p. 117187.
43. Lang, J.R., et al., *National Estimate of Per- and Polyfluoroalkyl Substance (PFAS) Release to U.S. Municipal Landfill Leachate.* Environmental Science & Technology, 2017. **51**(4): p. 2197-2205.
44. Høisæter, Å., A. Pfaff, and G.D. Breedveld, *Leaching and transport of PFAS from aqueous film-forming foam (AFFF) in the unsaturated soil at a firefighting training facility under cold climatic conditions.* Journal of Contaminant Hydrology, 2019. **222**: p. 112-122.
45. Antoniou, E., et al., *Immunomodulation and exposure to per- and polyfluoroalkyl substances: an overview of the current evidence from animal and human studies.* Archives of Toxicology, 2022. **96**(8): p. 2261-2285.
46. Boyd, R.I., et al., *Toward a Mechanistic Understanding of Poly- and Perfluoroalkylated Substances and Cancer.* Cancers, 2022. **14**(12): p. 2919.
47. Ubel, F.A., S.D. Sorenson, and D.E. Roach, *Health status of plant workers exposed to fluorochemicals - a preliminary report.* American Industrial Hygiene Association Journal, 1980. **41**(8): p. 584-589.
48. Hansen, K.J., et al., *Compound-Specific, Quantitative Characterization of Organic Fluorochemicals in Biological Matrices.* Environmental Science & Technology, 2001. **35**(4): p. 766-770.
49. Kannan, K., et al., *Perfluorooctanesulfonate and Related Fluorochemicals in Human Blood from Several Countries.* Environmental Science & Technology, 2004. **38**(17): p. 4489-4495.
50. Kärrman, A., et al., *Perfluorinated chemicals in relation to other persistent organic pollutants in human blood.* Chemosphere, 2006. **64**(9): p. 1582-1591.
51. Olsen, G.W., et al., *Perfluorooctanesulfonate and other fluorochemicals in the serum of American Red Cross adult blood donors.* Environmental Health Perspectives, 2003. **111**(16): p. 1892-1901.
52. Sunderland, E.M., et al., *A review of the pathways of human exposure to poly- and perfluoroalkyl substances (PFASs) and present understanding of health effects.* Journal of Exposure Science & Environmental Epidemiology, 2019. **29**(2): p. 131-147.
53. Barry, V., A. Winquist, and K. Steenland, *Perfluorooctanoic Acid (PFOA) Exposures and Incident Cancers among Adults Living Near a Chemical Plant.* Environmental Health Perspectives, 2013. **121**(11-12): p. 1313-1318.
54. Lopez-Espinosa, M.-J., et al., *Thyroid Function and Perfluoroalkyl Acids in Children Living Near a Chemical Plant.* Environmental Health Perspectives, 2012. **120**(7): p. 1036-1041.
55. Steenland, K., et al., *Ulcerative Colitis and Perfluorooctanoic Acid (PFOA) in a Highly Exposed Population of Community Residents and Workers in the Mid-Ohio Valley.* Environmental Health Perspectives, 2013. **121**(8): p. 900-905.

56. Darrow, L.A., C.R. Stein, and K. Steenland, *Serum Perfluorooctanoic Acid and Perfluorooctane Sulfonate Concentrations in Relation to Birth Outcomes in the Mid-Ohio Valley, 2005–2010.* Environmental Health Perspectives, 2013. **121**(10): p. 1207-1213.
57. Frisbee, S.J., et al., *The C8 Health Project: Design, Methods, and Participants.* Environmental Health Perspectives, 2009. **117**(12): p. 1873-1882.
58. Grandjean, P., et al., *Serum Vaccine Antibody Concentrations in Children Exposed to Perfluorinated Compounds.* JAMA, 2012. **307**(4): p. 391-397.
59. Grandjean, P. and E. Budtz-Jørgensen, *Immunotoxicity of perfluorinated alkylates: calculation of benchmark doses based on serum concentrations in children.* Environmental Health, 2013. **12**(1): p. 35.
60. ATSDR. *PFAS in the U.S. Population*. 2022 [cited 2023 March 27th, 2023]; Available from: https://www.atsdr.cdc.gov/pfas/health-effects/us-population.html.
61. USEPA, *FACT SHEET PFOA & PFOS Drinking Water HealthAdvisories*. 2016: U.S. Environmental Protection Agency (EPA).
62. USEPA. *Drinking Water Health Advisories for PFOA and PFOS*. U.S. Environmental Protection Agency (EPA) 2022; Available from: https://www.epa.gov/sdwa/drinking-water-health-advisories-pfoa-and-pfos.
63. USEPA. *Proposed PFAS National Primary Drinking Water Regulation*. 2023 [cited 2023 March 21st, 2023]; Available from: https://www.epa.gov/sdwa/and-polyfluoroalkyl-substances-pfas.
64. USEPA, *Understanding the PFAS National Primary Drinking Water Proposal Hazard Index*. 2023.
65. NCSL. *Per- and Polyfluoroalkyl Substances (PFAS) | State Legislation and Federal Action*. 2022 [cited 2023 February 27th, 2023]; Available from: https://www.ncsl.org/environment-and-natural-resources/per-and-polyfluoroalkyl-substances#:~:text=In%202021%2C%20state%20legislatures%20considered,%2C%20cosmetics%2C%20and%20other%20products.
66. Wanninayake, D.M., *Comparison of currently available PFAS remediation technologies in water: A review.* Journal of Environmental Management, 2021. **283**: p. 111977.
67. Birch, Q.T., et al., *Nano-enhanced treatment of per-fluorinated and poly-fluorinated alkyl substances (PFAS).* Current Opinion in Chemical Engineering, 2022. **35**: p. 100779.
68. Merino, N., et al., *Degradation and Removal Methods for Perfluoroalkyl and Polyfluoroalkyl Substances in Water.* Environmental Engineering Science, 2016. **33**(9): p. 615-649.
69. Horst, J., et al., *Water Treatment Technologies for PFAS: The Next Generation.* Groundwater Monitoring & Remediation, 2018. **38**(2): p. 13-23.
70. Ross, I., et al., *A review of emerging technologies for remediation of PFASs.* Remediation Journal, 2018. **28**(2): p. 101-126.
71. Ranjan, M., P.K. Singh, and A.L. Srivastav, *A review of bismuth-based sorptive materials for the removal of major contaminants from drinking water.* Environmental Science and Pollution Research, 2020. **27**(15): p. 17492-17504.
72. Zhang, D.Q., W.L. Zhang, and Y.N. Liang, *Adsorption of perfluoroalkyl and polyfluoroalkyl substances (PFASs) from aqueous solution - A review.* Science of The Total Environment, 2019. **694**: p. 133606.

73. Gao, Y., et al., *Adsorptive removal of emerging polyfluoroalky substances F-53B and PFOS by anion-exchange resin: A comparative study.* Journal of Hazardous Materials, 2017. **323**: p. 550-557.
74. Deng, S., et al., *Removal of perfluorooctane sulfonate from wastewater by anion exchange resins: Effects of resin properties and solution chemistry.* Water Research, 2010. **44**(18): p. 5188-5195.
75. Wu, T., et al., *Fabrication of Few-Layered Porous Graphite for Removing Fluorosurfactant from Aqueous Solution.* Langmuir, 2018. **34**(50): p. 15181-15188.
76. Chen, X., et al., *A comparative study on sorption of perfluorooctane sulfonate (PFOS) by chars, ash and carbon nanotubes.* Chemosphere, 2011. **83**(10): p. 1313-1319.
77. Yu, Q., S. Deng, and G. Yu, *Selective removal of perfluorooctane sulfonate from aqueous solution using chitosan-based molecularly imprinted polymer adsorbents.* Water Research, 2008. **42**(12): p. 3089-3097.
78. Cao, F., et al., *Synthesis of a perfluorooctanoic acid molecularly imprinted polymer for the selective removal of perfluorooctanoic acid in an aqueous environment.* Journal of Applied Polymer Science, 2016. **133**(15): p. n/a-n/a.
79. Pichon, V. and F. Chapuis-Hugon, *Role of molecularly imprinted polymers for selective determination of environmental pollutants—A review.* Analytica Chimica Acta, 2008. **622**(1): p. 48-61.
80. Liu, X., et al., *Installation of synergistic binding sites onto porous organic polymers for efficient removal of perfluorooctanoic acid.* Nature Communications, 2022. **13**(1).
81. Ochoa-Herrera, V. and R. Sierra-Alvarez, *Removal of perfluorinated surfactants by sorption onto granular activated carbon, zeolite and sludge.* Chemosphere, 2008. **72**(10): p. 1588-1593.
82. Zhou, Q., et al., *Sorption of perfluorooctane sulfonate on organo-montmorillonites.* Chemosphere, 2010. **78**(6): p. 688-694.
83. Bergaya, F. and G. Lagaly, *Surface modification of clay minerals.* Applied Clay Science, 2001. **19**(1): p. 1-3.
84. Ateia, M., et al., *Cationic polymer for selective removal of GenX and short-chain PFAS from surface waters and wastewaters at ng/L levels.* Water Research, 2019. **163**: p. 114874.
85. Silvani, L., et al., *Can biochar and designer biochar be used to remediate per- and polyfluorinated alkyl substances (PFAS) and lead and antimony contaminated soils?* Science of The Total Environment, 2019. **694**: p. 133693.
86. Liu, G., et al., *Novel Fluorinated Nitrogen-Rich Porous Organic Polymer for Efficient Removal of Perfluorooctanoic Acid from Water.* Water, 2022. **14**(7): p. 1010.
87. Quinlivan, P.A., L. Li, and D.R.U. Knappe, *Effects of activated carbon characteristics on the simultaneous adsorption of aqueous organic micropollutants and natural organic matter.* Water Research, 2005. **39**(8): p. 1663-1673.
88. Ioannidou, O. and A. Zabaniotou, *Agricultural residues as precursors for activated carbon production—A review.* Renewable and Sustainable Energy Reviews, 2007. **11**(9): p. 1966-2005.
89. Thompson, K.A., et al., *Environmental Comparison of Biochar and Activated Carbon for Tertiary Wastewater Treatment.* Environmental Science & Technology, 2016. **50**(20): p. 11253-11262.

90. Bubanale, S. and M. Shivashankar, *History, method of production, structure and applications of activated carbon.* Int. J. Eng. Res, 2017. **6**(06): p. 495-498.
91. Jjagwe, J., et al., *Synthesis and application of Granular activated carbon from biomass waste materials for water treatment: A review.* Journal of Bioresources and Bioproducts, 2021. **6**(4): p. 292-322.
92. Du, Z., et al., *Removal of perfluorinated carboxylates from washing wastewater of perfluorooctanesulfonyl fluoride using activated carbons and resins.* Journal of Hazardous Materials, 2015. **286**: p. 136-143.
93. Yu, Q., et al., *Sorption of perfluorooctane sulfonate and perfluorooctanoate on activated carbons and resin: Kinetic and isotherm study.* Water Research, 2009. **43**(4): p. 1150-1158.
94. Yu, J., et al., *Effect of effluent organic matter on the adsorption of perfluorinated compounds onto activated carbon.* Journal of Hazardous Materials, 2012. **225-226**: p. 99-106.
95. McDonough, J.T., et al., *Field-Scale Demonstration of PFAS Leachability Following In Situ Soil Stabilization.* ACS Omega, 2022. **7**(1): p. 419-429.
96. Sörengård, M., D.B. Kleja, and L. Ahrens, *Stabilization and solidification remediation of soil contaminated with poly- and perfluoroalkyl substances (PFASs).* Journal of Hazardous Materials, 2019. **367**: p. 639-646.
97. Niarchos, G., et al., *Per- and polyfluoroalkyl substance (PFAS) retention by colloidal activated carbon (CAC) using dynamic column experiments.* Environmental Pollution, 2022. **308**: p. 119667.
98. Xing, W., et al., *Adsorption and bioadsorption of granular activated carbon (GAC) for dissolved organic carbon (DOC) removal in wastewater.* Bioresource Technology, 2008. **99**(18): p. 8674-8678.
99. Choe, H.-S., et al., *Parallel study on removal efficiency of pharmaceuticals and PFASs in advanced water treatment processes: Ozonation, GAC adsorption, and RO processes.* Environmental Engineering Research, 2022. **27**(1): p. 200509-0.
100. Sagbo, O., et al., *Effect of PAC addition on MBR process for drinking water treatment.* Separation and Purification Technology, 2008. **58**(3): p. 320-327.
101. Oh, H., et al., *Evaluation of PAC behavior and fouling formation in an integrated PAC–UF membrane for surface water treatment.* Desalination, 2006. **192**(1): p. 54-62.
102. Suffet, I.H., *An Evaluation of Activated Carbon for Drinking Water Treatment: A National Academy of Science Report.* Journal AWWA, 1980. **72**(1): p. 41-50.
103. Heijman, S.G.J. and R. Hopman, *Activated carbon filtration in drinking water production: model prediction and new concepts.* Colloids and Surfaces A: Physicochemical and Engineering Aspects, 1999. **151**(1): p. 303-310.
104. Appleman, T.D., et al., *Treatment of poly- and perfluoroalkyl substances in U.S. full-scale water treatment systems.* Water Research, 2014. **51**: p. 246-255.
105. Biochar, I., *Standardized Product Definition and Product Testing Guidelines for Biochar That Is Used in Soil| International Biochar Initiative. International Biochar Initiative, 47 pp.* www. biochar-international. org/characterizationstandard, 2012.
106. Ceyhan, A.A., et al., *A novel thermal process for activated carbon production from the vetch biomass with air at low temperature by two-stage procedure.* Journal of Analytical and Applied Pyrolysis, 2013. **104**: p. 170-175.

107. Daud, W.M.A.W. and W.S.W. Ali, *Comparison on pore development of activated carbon produced from palm shell and coconut shell.* Bioresource Technology, 2004. **93**(1): p. 63-69.
108. Hunt, J., et al., *The basics of biochar: A natural soil amendment.* Soil and Crop Management, 2010. **30**(7): p. 1-6.
109. Kamarudin, N.S., et al., *Biochar: A review of its history, characteristics, factors that influence its yield, methods of production, application in wastewater treatment and recent development.* Biointerface Res. Appl. Chem, 2022. **12**: p. 7914-7926.
110. Lehmann, J., *Terra Preta Nova – Where to from Here?*, in *Amazonian Dark Earths: Wim Sombroek's Vision*, W.I. Woods, et al., Editors. 2009, Springer Netherlands: Dordrecht. p. 473-486.
111. Matovic, D., *Biochar as a viable carbon sequestration option: Global and Canadian perspective.* Energy, 2011. **36**(4).
112. Puettmann, M., et al., *Life cycle assessment of biochar produced from forest residues using portable systems.* Journal of Cleaner Production, 2020. **250**: p. 119564.
113. Allohverdi, T., et al., *A Review on Current Status of Biochar Uses in Agriculture.* Molecules, 2021. **26**(18): p. 5584.
114. Han, C., et al., *Development of Preparation Method and Application of*

Biochar. International Journal of Emerging Technology and Advanced Engineering, 2020. **10**(09): p. 6-13.
115. Legan, M., A.Ž. Gotvajn, and K. Zupan, *Potential of biochar use in building materials.* Journal of Environmental Management, 2022. **309**: p. 114704.
116. Oliveira, F.R., et al., *Environmental application of biochar: Current status and perspectives.* Bioresource Technology, 2017. **246**: p. 110-122.
117. Gwenzi, W., et al., *Biochar-based water treatment systems as a potential low-cost and sustainable technology for clean water provision.* Journal of Environmental Management, 2017. **197**: p. 732-749.
118. Ahmad, M., et al., *Biochar as a sorbent for contaminant management in soil and water: A review.* Chemosphere, 2014. **99**: p. 19-33.
119. Xiang, W., et al., *Biochar technology in wastewater treatment: A critical review.* Chemosphere, 2020. **252**: p. 126539.
120. Enaime, G., et al., *Biochar for Wastewater Treatment—Conversion Technologies and Applications.* Applied Sciences, 2020. **10**(10): p. 3492.
121. Jayakumar, A., et al., *New directions and challenges in engineering biologically-enhanced biochar for biological water treatment.* Science of The Total Environment, 2021. **796**: p. 148977.
122. Xiaoqing Wang, Z.G., Zhen Hu, Jian Zhang, *Recent advances in biochar application for water and wastewater treatment: a review.* PeerJ, 2022. **8:e9164**.
123. Han, Y., et al., *Heavy metal and phenol adsorptive properties of biochars from pyrolyzed switchgrass and woody biomass in correlation with surface properties.* Journal of Environmental Management, 2013. **118**: p. 196-204.
124. Valdés, H., et al., *Effect of Ozone Treatment on Surface Properties of Activated Carbon.* Langmuir, 2002. **18**(6): p. 2111-2116.
125. Alhashimi, H.A. and C.B. Aktas, *Life cycle environmental and economic performance of biochar compared with activated carbon: A meta-analysis.* Resources, Conservation and Recycling, 2017. **118**: p. 13-26.

126. Dalahmeh, S.S., N. Alziq, and L. Ahrens, *Potential of biochar filters for onsite wastewater treatment: Effects of active and inactive biofilms on adsorption of per- and polyfluoroalkyl substances in laboratory column experiments.* Environmental Pollution, 2019. **247**: p. 155-164.
127. Fabregat-Palau, J., M. Vidal, and A. Rigol, *Examining sorption of perfluoroalkyl substances (PFAS) in biochars and other carbon-rich materials.* Chemosphere, 2022. **302**: p. 134733.
128. Liu, N., et al., *Efficient adsorptive removal of short-chain perfluoroalkyl acids using reed straw-derived biochar (RESCA).* Science of The Total Environment, 2021. **798**: p. 149191.
129. Vo, H.N.P., et al., *Biochar sorption of perfluoroalkyl substances (PFASs) in aqueous film-forming foams-impacted groundwater: Effects of PFASs properties and groundwater chemistry.* Chemosphere, 2022. **286**: p. 131622.
130. Zhang, D., et al., *Sorption of perfluoroalkylated substances (PFASs) onto granular activated carbon and biochar.* Environ Technol, 2021. **42**(12): p. 1798-1809.
131. Cordner, A., et al., *The True Cost of PFAS and the Benefits of Acting Now.* Environmental Science & Technology, 2021. **55**(14): p. 9630-9633.
132. Li, X., et al., *Preparation and application of magnetic biochar in water treatment: A critical review.* Science of The Total Environment, 2020. **711**: p. 134847.
133. Beesley, L. and M. Marmiroli, *The immobilisation and retention of soluble arsenic, cadmium and zinc by biochar.* Environmental Pollution, 2011. **159**(2): p. 474-480.
134. Regmi, P., et al., *Removal of copper and cadmium from aqueous solution using switchgrass biochar produced via hydrothermal carbonization process.* Journal of Environmental Management, 2012. **109**: p. 61-69.
135. Yuan, J.-H., R.-K. Xu, and H. Zhang, *The forms of alkalis in the biochar produced from crop residues at different temperatures.* Bioresource Technology, 2011. **102**(3): p. 3488-3497.
136. ASTM, *Standard Test Methods for Instrumental Determination of Carbon, Hydrogen, and Nitrogen in Laboratory Samples of Coal and Coke (ASTM D5373-21).* ASTM International, 2021.
137. Bardestani, R., G.S. Patience, and S. Kaliaguine, *Experimental methods in chemical engineering: specific surface area and pore size distribution measurements—BET, BJH, and DFT.* The Canadian Journal of Chemical Engineering, 2019. **97**(11): p. 2781-2791.
138. Navarathna, C.M., et al., *Biochar Adsorbents with Enhanced Hydrophobicity for Oil Spill Removal.* ACS Applied Materials & Interfaces, 2020. **12**(8): p. 9248-9260.
139. Team, R.C., *R: A Language and Environment for Statistical Computing*. 2022, R Foundation for Statistical Computing: Vienna, Austria.
140. Byrnes, J.F.a.Z.N.a.J., *sem: Structural Equation Models*. 2022. p. R package version 3.1-15.
141. Karels, T.J., et al., *ORIGINAL ARTICLE: The biogeography of avian extinctions on oceanic islands.* Journal of Biogeography, 2008. **35**(6): p. 1106-1111.
142. Chen, F., et al., *Effects of periodic drying-wetting on microbial dynamics and activity of nitrite/nitrate-dependent anaerobic methane oxidizers in intertidal wetland sediments.* Water Research, 2023. **229**: p. 119436.

143. Tarka, P., *An overview of structural equation modeling: its beginnings, historical development, usefulness and controversies in the social sciences.* Quality & Quantity, 2018. **52**(1): p. 313-354.
144. Bransby, D.I., S.B. McLaughlin, and D.J. Parrish, *A review of carbon and nitrogen balances in switchgrass grown for energy.* Biomass and Bioenergy, 1998. **14**(4): p. 379-384.
145. Özcan, Y., E. Makineci, and E. Özdemir, *Biomass, carbon and nitrogen in single tree components of grey poplar (Populus × canescens) in an uncultivated habitat in Van, Turkey.* Environmental Monitoring and Assessment, 2020. **192**(6).
146. Wang, P., et al., *Enhancement of biogas production from wastewater sludge via anaerobic digestion assisted with biochar amendment.* Bioresource Technology, 2020. **309**: p. 123368.
147. Gray, M., et al., *Water uptake in biochars: The roles of porosity and hydrophobicity.* Biomass and Bioenergy, 2014. **61**: p. 196-205.
148. Das, O. and A.K. Sarmah, *The love–hate relationship of pyrolysis biochar and water: A perspective.* Science of The Total Environment, 2015. **512-513**: p. 682-685.
149. Ojeda, G., et al., *Are soil–water functions affected by biochar application?* Geoderma, 2015. **249-250**: p. 1-11.
150. Hassan, M., et al., *Influences of feedstock sources and pyrolysis temperature on the properties of biochar and functionality as adsorbents: A meta-analysis.* Science of The Total Environment, 2020. **744**: p. 140714.
151. Wiersma, W., et al., *No effect of pyrolysis temperature and feedstock type on hydraulic properties of biochar and amended sandy soil.* Geoderma, 2020. **364**: p. 114209.
152. Adhikari, S., W. Timms, and M.A.P. Mahmud, *Optimising water holding capacity and hydrophobicity of biochar for soil amendment – A review.* Science of The Total Environment, 2022. **851**: p. 158043.
153. Lyu, X., et al., *Per- and polyfluoroalkyl substances (PFAS) in subsurface environments: Occurrence, fate, transport, and research prospect.* Reviews of Geophysics, 2022. **60**(3): p. e2021RG000765.
154. Keiluweit, M., et al., *Dynamic Molecular Structure of Plant Biomass-Derived Black Carbon (Biochar).* Environmental Science & Technology, 2010. **44**(4): p. 1247-1253.
155. Chia, C.H., et al., *Imaging of mineral-enriched biochar by FTIR, Raman and SEM–EDX.* Vibrational Spectroscopy, 2012. **62**: p. 248-257.
156. Janu, R., et al., *Biochar surface functional groups as affected by biomass feedstock, biochar composition and pyrolysis temperature.* Carbon Resources Conversion, 2021. **4**: p. 36-46.
157. Orgchemboulder. *IR Spectroscopy Tutorial: Amines*. [cited 2023; Available from: https://www.orgchemboulder.com/Spectroscopy/irtutor/aminesir.shtml#:~:text=IR%20Spectroscopy%20Tutorial%3A%20Amines,appear%20in%20the%20same%20region.
158. Smith, D.M. and A.R. Chughtai, *The surface structure and reactivity of black carbon.* Colloids and Surfaces A: Physicochemical and Engineering Aspects, 1995. **105**(1): p. 47-77.
159. Lin-Vien, D., et al., *The Handbook of Infrared and Raman Characteristic Frequencies of Organic Molecules*. 1991: Elsevier Science.

160. Chen, B., et al., *Sorption of Polar and Nonpolar Aromatic Organic Contaminants by Plant Cuticular Materials: Role of Polarity and Accessibility.* Environmental Science & Technology, 2005. **39**(16): p. 6138-6146.
161. Chen, B., D. Zhou, and L. Zhu, *Transitional Adsorption and Partition of Nonpolar and Polar Aromatic Contaminants by Biochars of Pine Needles with Different Pyrolytic Temperatures.* Environmental Science & Technology, 2008. **42**(14): p. 5137-5143.
162. Koch, A., et al., *A study of carbonaceous char oxidation in air by semi-quantitative FTIR spectroscopy.* Fuel, 1998. **77**(6): p. 563-569.
163. Pradhan, B.K. and N.K. Sandle, *Effect of different oxidizing agent treatments on the surface properties of activated carbons.* Carbon, 1999. **37**(8): p. 1323-1332.
164. Pasquali, C.E.L. and H. Herrera, *Pyrolysis of lignin and IR analysis of residues.* Thermochimica Acta, 1997. **293**(1): p. 39-46.
165. Bustin, R.M. and Y. Guo, *Abrupt changes (jumps) in reflectance values and chemical compositions of artificial charcoals and inertinite in coals.* International Journal of Coal Geology, 1999. **38**(3): p. 237-260.
166. Haberhauer, G., et al., *Comparison of the composition of forest soil litter derived from three different sites at various decompositional stages using FTIR spectroscopy.* Geoderma, 1998. **83**(3): p. 331-342.
167. Zhang, K., et al., *Characterization of biochar derived from rice husks and its potential in chlorobenzene degradation.* Carbon, 2018. **130**: p. 730-740.
168. Rong, X., et al., *The magnetic biochar derived from banana peels as a persulfate activator for organic contaminants degradation.* Chemical Engineering Journal, 2019. **372**: p. 294-303.
169. Hsiao, M.-C., et al., *Preparation of Covalently Functionalized Graphene Using Residual Oxygen-Containing Functional Groups.* ACS Applied Materials & Interfaces, 2010. **2**(11): p. 3092-3099.
170. Hassan, M., et al., *Magnetic biochar for removal of perfluorooctane sulphonate (PFOS): Interfacial interaction and adsorption mechanism.* Environmental Technology & Innovation, 2022. **28**: p. 102593.
171. Steffens, S.D., et al., *Under-reporting Potential of Perfluorooctanesulfonic Acid (PFOS) under High-Ionic Strength Conditions.* Environmental Science & Technology Letters, 2021. **8**(12): p. 1032-1037.
172. Carlson, G.L. and S. Tupper, *Ski wax use contributes to environmental contamination by per- and polyfluoroalkyl substances.* Chemosphere, 2020. **261**: p. 128078.
173. Huset, C.A. and K. M. Barry, *Quantitative determination of perfluoroalkyl substances (PFAS) in soil, water, and home garden produce.* MethodsX, 2018. **5**: p. 697-704.
174. Guo, W., et al., *Adsorption of perfluorooctane sulfonate (PFOS) on corn straw-derived biochar prepared at different pyrolytic temperatures.* Journal of the Taiwan Institute of Chemical Engineers, 2017. **78**: p. 265-271.
175. Xiao, X., et al., *Sorption of Poly- and Perfluoroalkyl Substances (PFASs) Relevant to Aqueous Film-Forming Foam (AFFF)-Impacted Groundwater by Biochars and Activated Carbon.* Environmental Science & Technology, 2017. **51**(11): p. 6342-6351.
176. Ho, Y.S. and G. McKay, *Pseudo-second order model for sorption processes.* Process Biochemistry, 1999. **34**(5): p. 451-465.

177. Plazinski, W., W. Rudzinski, and A. Plazinska, *Theoretical models of sorption kinetics including a surface reaction mechanism: A review.* Advances in Colloid and Interface Science, 2009. **152**(1): p. 2-13.
178. Zhang, Y., et al., *Enhanced Removal of Polyfluoroalkyl Substances by Simple Modified Biochar: Adsorption Performance and Theoretical Calculation.* ACS ES&T Water, 2023.
179. Kalam, S., et al., *Surfactant Adsorption Isotherms: A Review.* ACS Omega, 2021. **6**(48): p. 32342-32348.
180. Freundlich, H., *Über die Adsorption in Lösungen.* Zeitschrift für Physikalische Chemie, 1907. **57U**(1): p. 385-470.
181. Langmuir, I., *The adsorption of gases on plane surfaces of glass, mica and platinum.* Journal of the American Chemical society, 1918. **40**(9): p. 1361-1403.
182. Inyang, M. and E.R.V. Dickenson, *The use of carbon adsorbents for the removal of perfluoroalkyl acids from potable reuse systems.* Chemosphere, 2017. **184**: p. 168-175.
183. Steigerwald, J.M. and J.R. Ray, *Adsorption behavior of perfluorooctanesulfonate (PFOS) onto activated spent coffee grounds biochar in synthetic wastewater effluent.* Journal of Hazardous Materials Letters, 2021. **2**: p. 100025.
184. Kupryianchyk, D., et al., *Treatment of sites contaminated with perfluorinated compounds using biochar amendment.* Chemosphere, 2016. **142**: p. 35-40.
185. John R. Mullaney, D.L.L., and Alan D. Arntson, *Chloride in Groundwater and Surface Water in Areas Underlain by the Glacial Aquifer System, Northern United States*. 2009, USGS.
186. Borthakur, P., et al., *Experimental and Molecular Dynamics Simulation Study of Specific Ion Effect on the Graphene Oxide Surface and Investigation of the Influence on Reactive Extraction of Model Dye Molecule at Water–Organic Interface.* The Journal of Physical Chemistry C, 2016. **120**(26): p. 14088-14100.
187. Borthakur, P., et al., *Computational and experimental assessment of pH and specific ions on the solute solvent interactions of clay-biochar composites towards tetracycline adsorption: Implications on wastewater treatment.* Journal of Environmental Management, 2021. **283**: p. 111989.
188. Yang, W., et al., *Surface and colloid properties of biochar and implications for transport in porous media.* Critical Reviews in Environmental Science and Technology, 2020. **50**(23): p. 2484-2522.
189. Wang, W., et al., *Adsorption behaviour and mechanism of the PFOS substitute OBS (sodium p-perfluorous nonenoxybenzene sulfonate) on activated carbon.* Royal Society Open Science, 2019. **6**(9): p. 191069.